Calhoun: The NPS Institutional Archive

DSpace Repository

Theses and Dissertations	1. Thesis and Dissertation Collection, all items

1984-12

Underwater shock-induced responses of stiffened flat plates : an investigation into predictive capabilities of the USA-STAGS code.

King, Nelson R.

http://hdl.handle.net/10945/19601

This publication is a work of the U.S. Government as defined in Title 17, United States Code, Section 101. Copyright protection is not available for this work in the United States.

Downloaded from NPS Archive: Calhoun

http://www.nps.edu/library

Calhoun is the Naval Postgraduate School's public access digital repository for research materials and institutional publications created by the NPS community. Calhoun is named for Professor of Mathematics Guy K. Calhoun, NPS's first appointed -- and published -- scholarly author.

Dudley Knox Library / Naval Postgraduate School
411 Dyer Road / 1 University Circle
Monterey, California USA 93943

DUDLEY KNOX LIBRARY
NAVAL POSTGRADUATE SCHOOL
MONTEREY, CALIFORNIA 93943

NAVAL POSTGRADUATE SCHOOL
Monterey, California

THESIS

UNDERWATER SHOCK-INDUCED RESPONSES OF STIFFENED FLAT PLATES: AN INVESTIGATION INTO THE PREDICTIVE CAPABILITIES OF THE USA-STAGS CODE

by

Nelson R. King

December 1984

Thesis Advisor: Young S. Shin

Approved for public release; distribution unlimited

T224033

SECURITY CLASSIFICATION OF THIS PAGE (When Data Entered)

REPORT DOCUMENTATION PAGE

READ INSTRUCTIONS BEFORE COMPLETING FORM

1. REPORT NUMBER	2. GOVT ACCESSION NO. / 3. RECIPIENT'S CATALOG NUMBER
4. TITLE (and Subtitle): Underwater Shock-Induced Responses of Stiffened Flat Plates: An Investigation into the Predictive Capabilities of the USA-STAGS Code	5. TYPE OF REPORT & PERIOD COVERED: Master's Thesis, December 1984 / 6. PERFORMING ORG. REPORT NUMBER
7. AUTHOR(s): Nelson R. King	8. CONTRACT OR GRANT NUMBER(s)
9. PERFORMING ORGANIZATION NAME AND ADDRESS: Naval Postgraduate School, Monterey, California 93943	10. PROGRAM ELEMENT, PROJECT, TASK AREA & WORK UNIT NUMBERS
11. CONTROLLING OFFICE NAME AND ADDRESS: Naval Postgraduate School, Monterey, California 93943	12. REPORT DATE: December 1984 / 13. NUMBER OF PAGES: 181
14. MONITORING AGENCY NAME & ADDRESS (if different from Controlling Office)	15. SECURITY CLASS. (of this report): Unclassified / 15a. DECLASSIFICATION/DOWNGRADING SCHEDULE

16. DISTRIBUTION STATEMENT (of this Report)

Approved for public release; distribution unlimited

17. DISTRIBUTION STATEMENT (of the abstract entered in Block 20, if different from Report)

18. SUPPLEMENTARY NOTES

19. KEY WORDS (Continue on reverse side if necessary and identify by block number)

Finite Elements
Flat Plate
Underwater Explosion
Stiffener Tripping
Fluid Structure Interaction
Submerged Structure

20. ABSTRACT (Continue on reverse side if necessary and identify by block number)

An experimental investigation was conducted to determine the dynamic responses of stiffened flat plates to impulsive loading by underwater shock waves. Air-backed flat plates with machined external stiffeners and clamped boundary conditions were subjected to shock loadings from TNT charges detonated underwater. The plates were instrumented to measure transient strains and free field pressures. Test results were compared to preshot

DD FORM 1 JAN 73 1473 EDITION OF 1 NOV 65 IS OBSOLETE

S N 0102-LF-014-6601

SECURITY CLASSIFICATION OF THIS PAGE (When Data Entered)

20. ABSTRACT (Continued)

calculations done using the USA-STAGS code. Particular emphasis was placed upon the code's ability to predict stiffener tripping and shear at plate boundaries.

Approved for public release; distribution unlimited

Underwater Shock-Induced Responses of Stiffened Flat Plates: An Investigation into the Predictive Capabilities of the USA-STAGS Code

by

Nelson R. King
Lieutenant, United States Navy
B.A., Reed College, 1973

Submitted in partial fulfillment of the
requirements for the degree of

MASTER OF SCIENCE IN MECHANICAL ENGINEERING

from the

NAVAL POSTGRADUATE SCHOOL
December 1984

ABSTRACT

An experimental investigation was conducted to determine the dynamic responses of stiffened flat plates to impulsive loading by underwater shock waves. Air-backed flat plates with machined external stiffeners and clamped boundary conditions were subjected to shock loadings from TNT charges detonated underwater. The plates were instrumented to measure transient strains and free field pressures. Test results were compared to preshot calculations done using the USA-STAGS code. Particular emphasis was placed upon the code's ability to predict stiffener tripping and shear at plate boundaries.

TABLE OF CONTENTS

I. INTRODUCTION 11

A. BACKGROUND AND HISTORY 11

B. OBJECTIVES 15

II. UNDERWATER EXPLOSION THEORY 18

A. THE PRESSURE PULSE 18

B. SURFACE CUTOFF AND BOTTOM REFLECTION 21

C. BUBBLE EFFECT 28

D. APPLICATIONS OF THEORY TO EXPERIMENT DESIGN . 31

III. THE FLAT PLATE MODEL 36

IV. THE USA-STAGS CODE 51

A. GENERAL 51

B. THEORY 52

C. ORGANIZATION 57

1. The Structural Preprocessor 58

2. The Fluid Mass Preprocessor 59

3. The Augmented Matrix Preprocessor 59

4. The Time Integration Processor 59

5. The Data Postprocessor 60

D. USING THE CODE 60

E. DISCRETIZING THE MODEL 76

V. TESTING THE CODE 85

A. MODAL TESTING 85

B. UNDERWATER SHOCK TESTING 88
1. The Test Platform 90
2. Instrumentation 92
C. DATA RETRIEVAL 103
VI. RESULTS AND CONCLUSIONS 110
A. MODAL COMPARISONS 110
B. COMPARISONS WITH UNDERWATER TEST RESULTS . . . 115
C. CONCLUSIONS AND SUGGESTIONS FOR FUTURE STUDY . 138
APPENDIX A: SOURCE DATA 143
APPENDIX B: BASIC SHELL TYPES FOR USE WITH STAGS 150
APPENDIX C: USA-STAGS INPUT FILES 156
LIST OF REFERENCES 178
BIBLIOGRAPHY 180
INITIAL DISTRIBUTION LIST 181

LIST OF TABLES

I. Explosive Constants I 21

II. Explosive Constants II 30

III. Calibration Data for Tee-Stiffened Plate 109

IV. Modal Comparisons for Tee-Stiffened Plate 112

V. Modal Comparisons for Rectangular-Stiffened Plate 113

LIST OF FIGURES

2.1 Simple Exponential Approximation of Incident Shock Wave 19

2.2 Exponential Approximation with Surface Cutoff . . 23

2.3 Complex Shock Wave Pattern 25

2.4 Three Image Presentation of Shock Waves 26

2.5 Multiple Expansions of the Hot Gas Bubble 29

2.6 Region of Bulk Cavitation 33

3.1 Test Panel with Transverse Rectangular Stiffeners 39

3.2 Test Panel with Transverse Tee Stiffeners 40

3.3 Plastic Modulus of Tee-Stiffened Plate 42

3.4 Effective Cross Section of Tee-Stiffened Plate . . 43

3.5 Explosion Damage to Tee-Stiffened Plate 46

3.6 Test Panel with Longitudinal Rectangular Stiffener 48

3.7 Stiffener Deflections 49

3.8 Plate Deflections 50

4.1 Range of Problem Types to which STAGS is Applicable 55

4.2 Shell Units for Tee-Stiffened Plate 77

4.3 Quarter Model of Tee-Stiffened Plate 79

4.4 Shell Units for Rectangular-Stiffened Plate . . . 80

4.5 Half Model of Rectangular-Stiffened Plate 81

5.1 Typical Modal Test Plot 89

5.2 Test Plate and Backing Structure 91

5.3 Test Platform 93

5.4 Location of Free Field Pressure Gage 95

5.5 Strain Gage Placement on Tee-Stiffened Plate . . 98

5.6 Strain Gage Placement on Rectangular-Stiffened Plate 99

5.7 Jig Used to Measure Plate Deflections 104

5.8 Flow Chart for Electronics Set-Up at WCSF 105

6.1 Freefield Pressure for Tee-Stiffened Plate . . . 117

6.2 Untranslated Strain Output for Tee-Stiffened Plate 123

6.3 Untranslated Strain Output, Rectangular-Stiffened Plate 124

6.4 Tee-Stiffened Plate, Gage 2 (USA-STAGS) 127

6.5 Tee-Stiffened Plate, Gage 2 127

6.6 Tee-Stiffened Plate, Gage 8 (USA-STAGS) 128

6.7 Tee-Stiffened Plate, Gage 8 128

6.8 Tee-Stiffened Plate, Gage 11 (USA-STAGS) 129

6.9 Tee-Stiffened Plate, Gage 11 129

6.10 Rectangular-Stiffened Plate Gage 1 (USA-STAGS) . 130

6.11 Rectangular-Stiffened Plate, Gage 1 130

6.12 Rectangular-Stiffened Plate, Gage 15 (USA-STAGS) 131

6.13 Rectangular-Stiffened Plate, Gage 15 131

6.14 Rectangular-Stiffened Plate, Gage 18 (USA-STAGS) 132

6.15 Rectangular-Stiffened Plate, Gage 18 132

6.16 POSTPR Predicted Fluid Pressures for Tee-Plate . 134

6.17 POSTPR Predicted Fluid Pressures for Rectangular-Stiffened Plate 135

ACKNOWLEDGMENTS

This thesis has not been the effort of a single person or time. Rather, it has been a small part of an evolutionary process in which many have been involved. The actual list of those who have contributed is too long to recount here. Especial note must be made, however, of the select few without whose inputs no thesis would have been possible. To Charles Crow, Thomas Christian, and Thomas McCord from the Mechanical Engineering Shop facility at the Naval Postgraduate School; Dr's. John DeRuntz and Charles Rankin from Lockheed Research, Palo Alto; and to all of the people in the NPS Computer Science Department who operate the VAX system; sincerest thanks are extended. A final expression of deepest gratitude is required to Dr. Young S. Shin for his understanding, his support, and his judicious use of both the carrot and the big stick.

I. INTRODUCTION

A. BACKGROUND AND HISTORY

Sergei Gorshkov, Admiral of the Soviet Fleet, has observed that the end of World War Two marked, "... the start of a military-technical revolution which in scope and depth transcended all the reforms and transmissions which had previously occurred in the armies and fleets of the world." [Ref. 1]

Much has been made of the tactical and geo-political implications of that revolution. Less popularly publicized, but equally radical are the changes that the developments in technology have spawned in the processes of ship design and construction.

Throughout most of history, war at sea has been a process of trying to set one's opponent afire, board him, or hurl chunks of stone or metal at him across relatively short distances. All of these methods had the distinguishing characteristic of being essentially disabling tactics, unless a ship was burned or perforated to the point of sinking (and they often were not), damage was generally largely superficial and the ship could be refitted to see service again. Witness the many vessels that have been fought on both sides of a conflict and the tradition of

expecting naval personnel to supplement their pay with prize money.

Two events occurred at or around the beginning of the twentieth century to change all of that: the invention of high explosives and the advent of the submarine.

Initially, the submarine was primarily a commerce raider. It was too small to carry a prize crew and too lightly armed to effectively combat a conventional warship. During World War One, most battles between submarines and conventional ships were fought on the surface. Submarines would use their stealth to sneak-up upon unsuspecting merchantmen, surface and then attempt to sink them with their deck cannons. Torpedoes were largely unreliable and the submarines themselves were at risk if fast armed vessels were present. Convoying the merchants with small, agile men-of-war was, briefly, an effective means of countering the submarine threat. However, as torpedoes became more effective so, too, did the submarine. For the convoy escort vessels it was no longer sufficient to have to wait for a submarine to surface in order to attack it. An effective standoff weapon was needed.

That standoff weapon was the depth charge. First introduced in World War One, the depth charge came of age in the Second World War; and with it a new era in ship design was ushered into existence. For the principle of this new weapon was not one of punching a hole in a ship's hull and then exploding internally; rather, high explosives permitted

generation of intense pressure waves in the sea that could break a vessel's back or rupture hull fittings whether the vessel's skin was punctured or not. Simply increasing the thickness of plating in discrete areas of vulnerability was no longer sufficient. Design for strength and resiliency under unequal pressure loadings was required. Moreover, this requirement applied to attacker as well as attacked. Although the attacking surface vessel had the advantage of being able to run from the immediate scene of the explosion and the effects were not compounded by as great a pre-existing static head of water, these weapons were not directional and could be expected to damage all within their sphere.

The issue of a vessel's ability to withstand an underwater explosion, be it submarine or surface ship, became more pressing as the explosive devices became increasingly powerful and sophisticated. Not only did depth charges become lethal over a wider area, but the advancing technology permitted mines, too, to grow from essentially contact weapons to devices that could endanger all types of shipping from considerable depths. The issue has become particularly crucial with the development of nuclear weapons which are so powerful that no device need contact a ship or group of ships to cause rampant destruction.

The response of the U.S. Navy was to require that ships and their critical components be designed and built to

withstand specified levels of shock loading. These requirements included (and continue to include) actual shock testing of the first ship of a class and many crucial systems on the component level.

During the immediate post-World War Two period, many of these requirements were largely tentative and experimental. By the early 1960's, however, sufficient experience had been gained to allow design requirements to be set forth [Ref. 2]. These specifications established specific guidelines for contractors to meet based upon type of equipment, type of vessel in which the equipment was to be used, and location and method of mounting within the vessel. As with the ships themselves, actual shock testing of the item was the primary means of establishing compliance; as it remains today.

Performing a shock test upon production end products; particularly when those items are as large as an aircraft carrier can have some obvious drawbacks: it is costly, it is dangerous, and the results can be embarrassing. Moreover, there can be longterm structural damage which is neither immediately apparent nor correctable, but which does not by itself constitute non-compliance of contract terms. Moreover, some items simply do not lend themselves to shock testing.

What has been needed is a method of analyzing the design itself in order to achieve a numerical approximation of the end product's response to shock.

This need has coalesced into the development of two computer codes; EPSA (Elasto Plastic Shell Analysis), produced by Weidlinger Associates, and USA-STAGS (Underwater Shock Analysis--Structural Analysis of General Shells) produced by Lockheed Missiles and Spacecraft, Inc.

B. OBJECTIVES

This study is the second in an ongoing series sponsored by the Defense Nuclear Agency (DNA) into the effects of underwater explosions upon ship hulls. The intent of these studies has been to test the applicability of the two previously mentioned structural response, underwater shock analysis computer codes to naval design and analysis requirements. Under the umbrella of general applicability, focus has been placed upon two defined goals:

1. Use of the codes to gain insights into large deflection elastic-plastic responses of a submerged structure subjected to transient acoustic shock loading; with especial emphasis upon stiffener tripping phenomena.

2. Performance of underwater explosion testing of the structure to validate the results predicted by the code.

To achieve these goals, flat plate models geometrically similar to a ship's stiffened hull structure have been studied. These plates were air backed to simulate general

conditions that could be expected in a ship's plating; and were subjected to shock loadings that produced deformations well into the plastic regime in order to ensure stiffener tripping. Existing information concerning underwater explosion phenomena was employed in an attempt to reduce experimental uncertainties.

The first study in this series was that conducted by LT Thomas Rentz, USN in fulfillment of thesis requirements at the Naval Postgraduate School [Ref. 3] and [Ref. 4]. In that study he developed the following experimental strategy to study the EPSA code:

An attempt to validate the code was conducted in two phases: Using pressure approximations based upon empirically determined formulae, the code was first used as a pre-test predictor of test results. Once the underwater explosion testing had been conducted, pressure histories derived from that testing were input into the code. The plate strains predicted by the code in both its preshot and post-shot capacities were then compared to actual strain histories from testing. Plate deformations and boundary stresses predicted by the code were compared to observed physical responses.

In this study, the code to be tested is USA-STAGS. In an effort to maintain continuity with the earlier study in the series, the same experimental strategy will be followed. The test geometry and flat plate model will also be

retained. Conclusions regarding the ability of USA-STAGS to predict the responses of a simple model to underwater explosions will be drawn; and, perhaps of even greater importance, guidelines will be established for using the USA-STAGS code and conducting underwater explosion testing for future studies.

II. UNDERWATER EXPLOSION THEORY

A. THE PRESSURE PULSE

Any conversion of matter, whether chemical or nuclear, which results in the very rapid production of large quantities of gas at very high temperature can be categorized within the broad species "explosion." Typically, for military high explosives such as TNT the pressure and temperature within the gases produced by an explosion are on the order of 50,000 atmospheres and 3000 degrees Celsius [Ref. 5: p. 3]. For nuclear explosions the initial temperature is on the order of a million degrees Celsius and the pressure, which is dependent upon the yield is similarly orders of magnitude higher than that for a conventional explosive [Ref. 6].

Clearly, temperatures and pressures of the levels described must dissipate high levels of energy through any surrounding medium. In the case of water, the initial manifestation of this disturbance is an intense compression created pressure wave propagating radially outward from the charge; followed nearly instantaneously by a displacement of the fluid. In the immediate vicinity of the charge, the velocity of propagation of the pressure wave is several times the speed of sound (about 5000 feet per second in water) but approaches the value almost immediately and

therefore may be apprehended as an essentially acoustic phenomenon. As the water begins to be displaced, the gas bubble created by the explosion expands; thereby decreasing its internal pressure and correspondingly the pressure on the constraining fluid. Viewed on a pressure-time curve the initial rise in pressure is so nearly vertical as to appear discontinuous, while the pressure relief is characterized by an approximately exponential decay (Fig. 2.1) [Ref. 5: pp. 4-7].

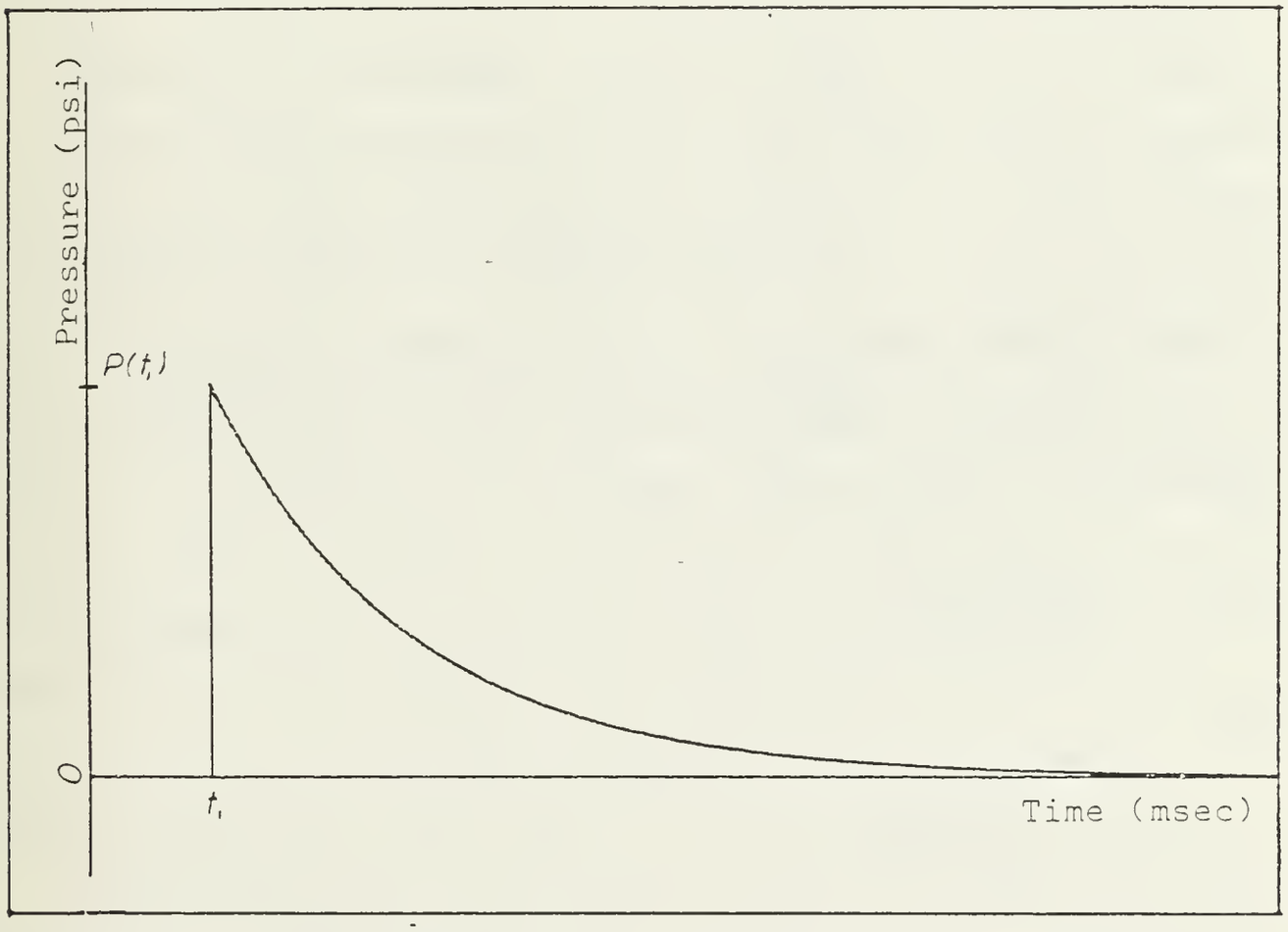

Figure 2.1 Simple Exponential Approximation of Incident Shock Wave

The actual magnitudes of the pressure pulses and the rate of exponential decay have been found through experiment to be

functions of the type of explosive, the charge weight, and the standoff distance.[1] The equations for the pressure and decay constant were originally determined by Robert H. Cole and were presented in his work, Underwater Explosions [Ref. 5]. These have since been simplified to use a series of empirically derived coefficients developed by R. S. Price [Ref. 7].

The pressure profile can be expressed by the equation

$$P(t) = P_o \exp \frac{t_1 - t}{\theta} \qquad \text{(eqn 2.1)}$$

where P_o is the initial (greatest) pressure of the shock wave, θ is the decay constant describing the exponential decay, and $t - t_1$ is the time elapsed from the arrival of the shock front.

The initial pressure, P_o, and the decay constant, θ, are dependent largely upon the type of explosive and the weight of the charge. These may be expressed

$$P_o = K_1 \left(\frac{W^{1/3}}{R} \right)^{A_2} \qquad \text{(eqn 2.2)}$$

and,

$$\theta = K_2 W^{1/3} \left(\frac{W^{1/3}}{R} \right)^{A_2} \qquad \text{(eqn 2.3)}$$

---

[1]The standoff distance is defined as the distance from the charge to the nearest point on the target.

where P_o is in pounds per square inch and θ in milliseconds. K_1, K_2, A_1, A_2 are the explosive dependent values (Table I). W and R are the charge weight (in pounds) and standoff distance (in feet), respectively.

Table I

Explosive Constants I

Explosive	TNT	HBX-1	PENTOLITE
K_1	22505	22347.6	24589
A_1	1.18	1.144	1.194
K_2	.058	.056	.052
A_2	-.185	-.247	-.257

B. SURFACE CUTOFF AND BOTTOM REFLECTION

Shock waves propagate radially from the charge. Thus, for a point source in an infinite medium, the wave could be expected to travel as an ever expanding sphere until damped by the fluid. For small to moderately sized charges detonated well below the surface in great depths of water, this is a satisfactory analogy. For explosions nearer the surface or in shoal water, however, there are secondary effects for which there must be an accounting.

When a shock wave reaches the surface of the water, the adjoining air is of sufficiently lesser density to be incapable of supporting the shock wave. The result is that the effective pressure at the interface must be zero in

compliance with the laws of continuity. This implies that a negative shock wave of magnitude equal to the original incident wave must be propagated downward through the medium to satisfy equilibrium conditions. This negative wave will travel through the water at an angle to the surface that is equal to that of the incident wave; much as the negative reflection image from a mirror continues at an angle equal to the angle of incidence.

Remembering that these waves are radiating spherically outward from the point of inception, it is clear that both the incident wave and the generated surface wave will eventually reach the ship, submarine, or other target object. It is likewise clear that, with its longer path, the surface wave must reach the target at some time later than the incident; which travels only the shortest, or standoff, distance between charge and target. The net effect is additive. When the surface wave reaches the target, the initial shock front will have passed and the incident wave will be at some point in its exponential decay. The negative surface wave will then "chop off" the tail of the incident wave. If the spatial geometry of the shot is such that the magnitude of the surface wave is greater than the remaining magnitude of the incident wave, a region of negative pressure will be created (Fig. 2.2). If this negative is less than the pressure required to keep the fluid in a liquid state, the fluid will "flash" into vapor. This chopping effect is

referred to as surface cutoff, and the negative pressure as bulk cavitation.

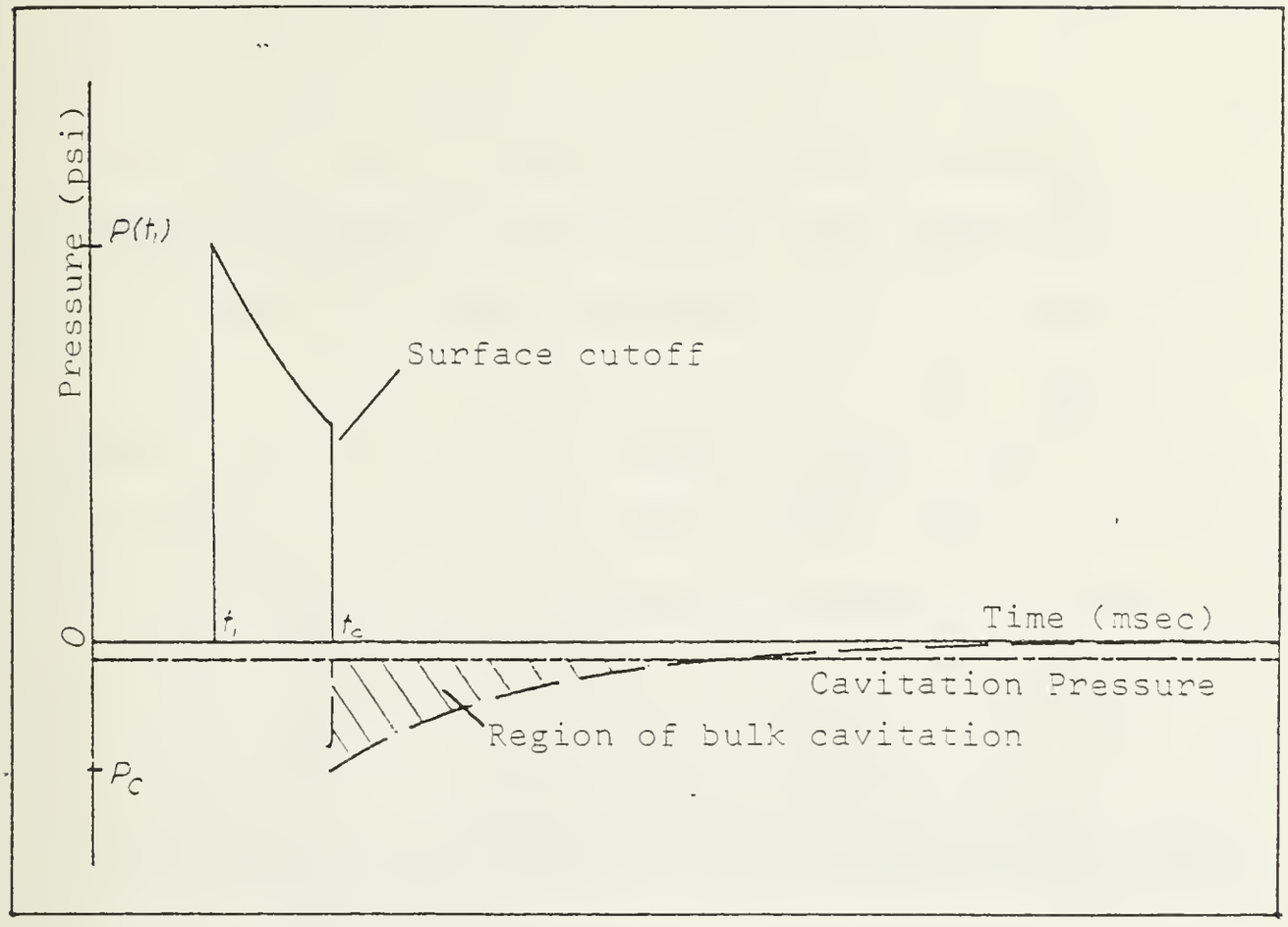

Figure 2.2 Exponential Approximation with Surface Cutoff

The direct effect of bulk cavitation is, by itself, not particularly harmful. The structure simply experiences essentially no pressure while it is in the cavitated region. When, however, the static head of water above the region overcomes the cavitation forces, the region closes suddenly to generate a destructive reloading upon the structure.

To further complicate matters, if the shot occurs in shoal waters or at depths near the bottom a second boundary is also present. Unlike the surface, in this case the

incident wave is impinging upon a medium of greater density than the fluid. The reflected wave will therefore be positive. The actual magnitude of this wave depends upon the physical characteristics of the bottom material. The effects of this bottom reflected wave are also additive and will generally reach the target at some time after the initial shock front has passed; although the actual time of arrival of this secondary front will once again be dependent upon the bottom conditions and the speed at which the wave travels through the bottom medium. Additionally, in shoal waters, that same bottom reflected wave will reach the surface; creating its own surface cutoff.

The net effect upon the target is thus one of an incident shock wave; which, if the charge and target are sufficiently near the surface, will be cutoff by the negative surface wave. This, in turn, is followed by the bottom reflected wave which also experiences an exponential decay, and which may also be cutoff by its own generated surface wave (Fig. 2.3).

Analytically, the easiest way to model the effects of incident, surface, and bottom waves upon the target is as has been represented in Figure 2.4, with three separate images.

The incident and surface images are relatively easy to depict. The incident image, M_i, of course represents the charge itself and occupies the same location in the spatial

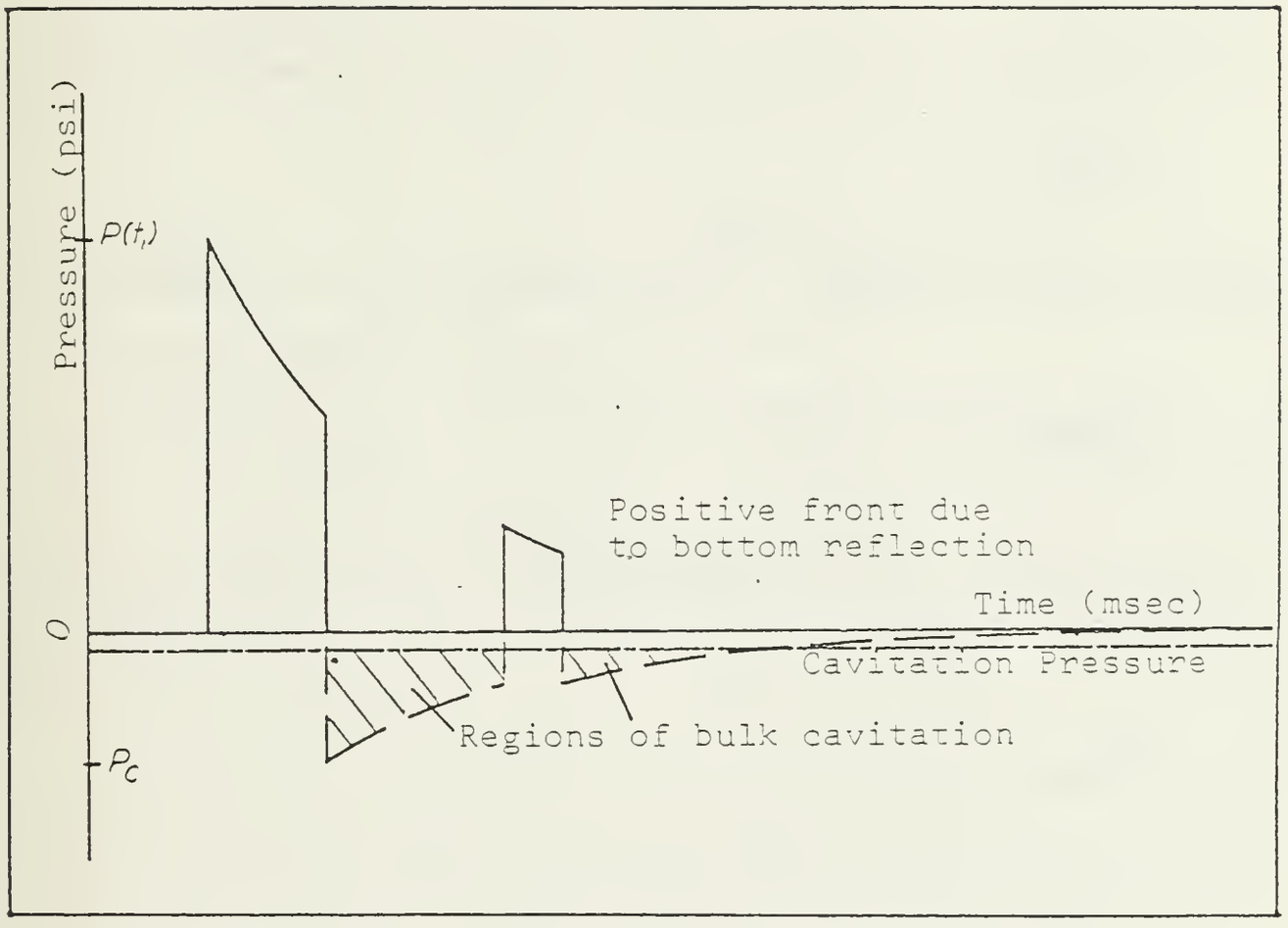

Figure 2.3 Complex Shock Wave Pattern

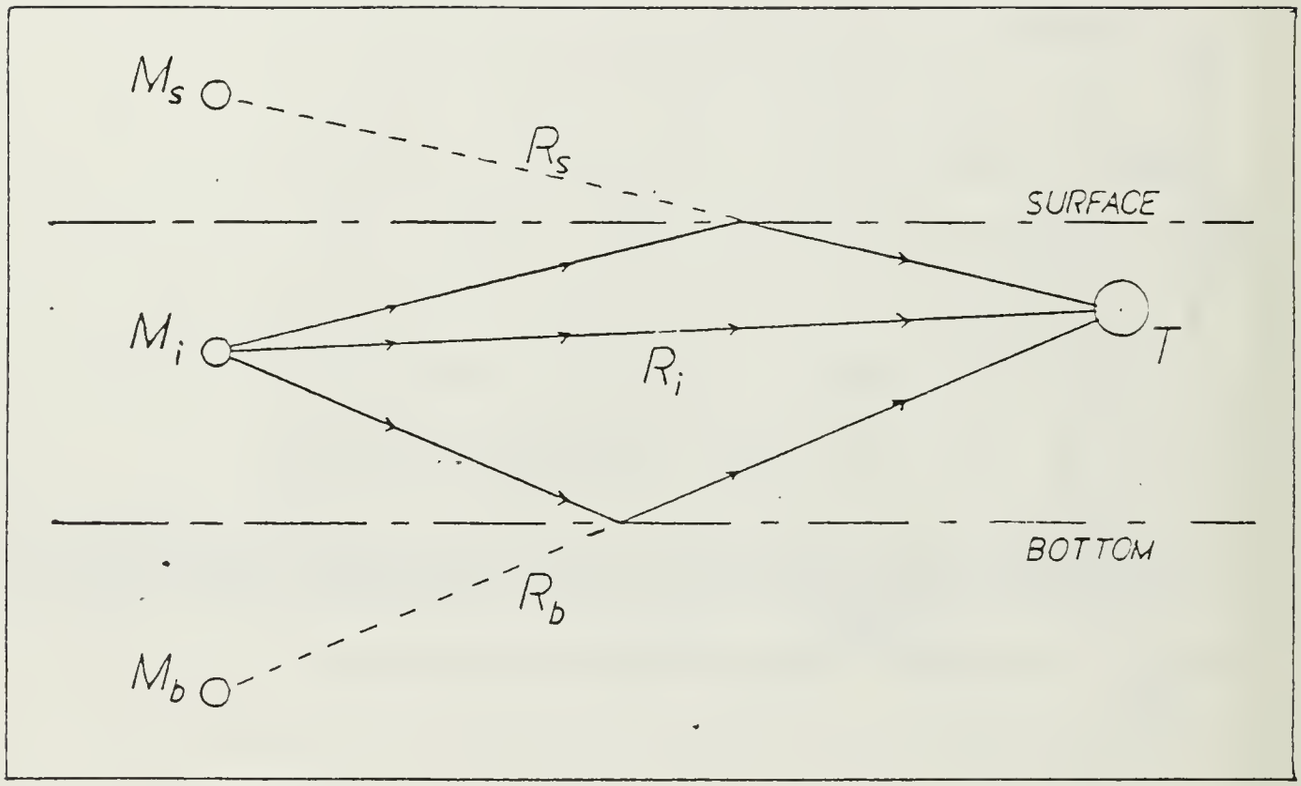

Figure 2.4 Three Image Presentation of Shock Waves

geometry. The surface image, M_s, is of the same magnitude as the incident image but of an opposite sign. It lies on a line drawn vertically through the charge at a distance above the surface equal to the depth of the charge below.

The surface cutoff pressure may therefore be computed

$$P_c = -K_1\left(\frac{W^{1/3}}{R_s}\right)^{A_1} \qquad \text{(eqn 2.4)}$$

where R_s is now the distance from the surface image to the target. The time of cutoff after the passage of the initial shock front is thus the time difference for the wave to cover the greater distance, or

$$t_c = \frac{R_s - R_i}{c} \qquad \text{(eqn 2.5)}$$

where c is the speed of sound in the fluid. The cutoff pressure will then decay in the same exponential manner as the incident pressure.

As may be conceived from the preceding discussion of the bottom reflection; the location of the bottom image is not so straightforward. It may be viewed as initiating along the same vertical line as do the incident and surface images, and at a depth below the fluid-bottom interface equal to the distance of the charge above. Here, however, the similarities to the surface image end. The bottom image cannot be considered a point charge because of the tendency of the pressure wave to "smear" across the bottom. The magnitude and speed of the wave, too, are dependent upon

bottom characteristics. A muddy bottom, for instance, will tend to reflect a diffuse, low magnitude wave travelling at or about the speed of sound in water. A rock bottom on the other hand will produce sharp, high magnitude pulses which will tend to radiate over a distance due to the higher speed of travel of the shock wave in the bottom medium than in the fluid. Due to this dependence upon bottom conditions, determination of bottom reflection effects do not lend themselves to general predictive studies and are often disregarded, although they can be significant.

C. BUBBLE EFFECT

The foregoing discussion of the development of the pressure wave and its impact upon the target assumes that a single, clean wavefront is produced by the explosion. In point of fact, such is rarely the case. When the charge explodes, it first creates a high intensity shock front which is the initial incident shock wave. It also produces a bubble of very hot gasses at very high pressure.

The bubble expands until it reaches pressure equilibrium with the surrounding water. When it does so, a portion of the energy within the bubble is released as a new shock front. This release of energy then permits the momentum of the water displaced to assert itself and the bubble is collapsed, compressing the gases within. The displaced water can be conceived as attempting to regain its original

pre-bubble condition. As the water rushes in, it compresses the gases beyond the equilibrium condition and the bubble again expands, again releasing a portion of its energy as a shock wave, albeit a smaller one than the preceding (Fig. 2.5). This process has been known to produce as many as ten significant pulses [Ref. 5: pp. 8, 9], which, though weaker than the initial shock front, can still have a pronounced effect upon a structure which has already been loaded by the earlier pulses.

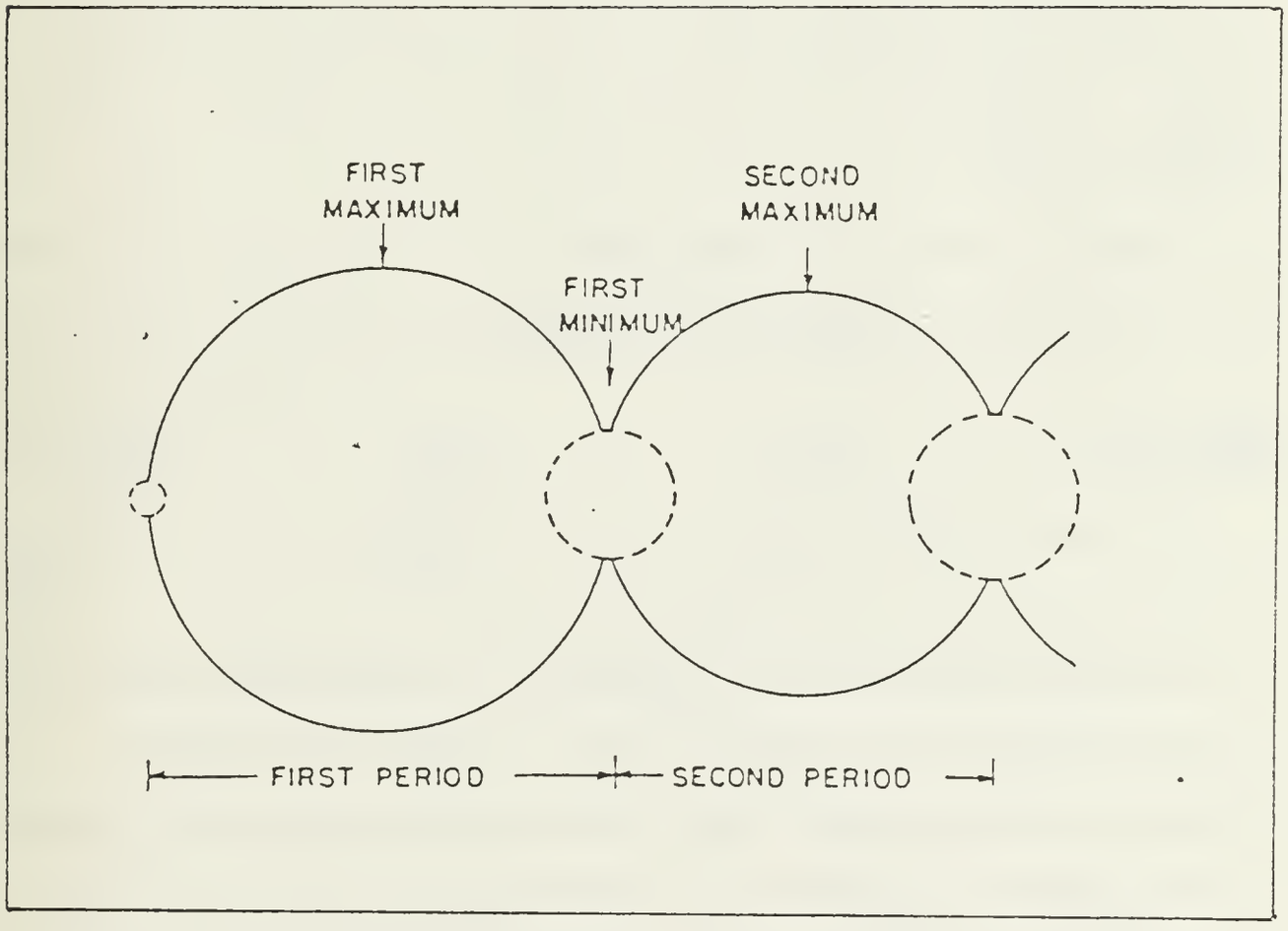

Figure 2.5 Multiple Expansions of the Hot Gas Bubble [Ref. 5: p. 7]

The time and radius of the bubble at the first pulse has, again, been determined empirically, the maximum radius as

$$A_{max} = K_3\left(\frac{W^{1/3}}{(D + 33)^{1/3}}\right) \qquad \text{(eqn 2.6)}$$

at time,

$$t = K_4\left(\frac{W^{1/3}}{(D + 33)^{5/6}}\right) \qquad \text{(eqn 2.7)}$$

where A_{max} is expressed in feet and t in seconds. W is once more the weight of the charge, K_3 and K_4 are explosive dependent constants (Table II), and D is the depth of the charge in feet.

Table II

Explosive Constants II

Explosive	HBX-1	TNT	PENTOLITE
K_3	14.14	12.67	12.88
K_4	4.761	4.268	4.339

A second and distinct phenomenon is bubble migration; so called because of the tendency of the bubble to migrate toward any nearby mass. When the bubble contacts the mass, it collapses and begins a series of rapid pulsations. The net effect is similar to that of the already described bubble pulse; a series of reloadings upon the structure. The rapidity of the pulsations of the collapsed bubble and

their increased localization tend, however, to magnify their severity.

D. APPLICATIONS OF THEORY TO EXPERIMENT DESIGN

Developing a basic understanding of the primary phenomena involved in underwater explosion theory is crucial to developing a successful underwater test program for many reasons. Two are of particular interest here, however:

First, and most obviously, equations 2.1 through 2.3 allow initial estimates of the peak pressure and pressure history to which a test structure is to be exposed. These are then input to the computer code so that preshot approximations of the structural responses may be made; thereby creating guidelines for calibrating gages, determining charge weights, etc.

Second, the design of the test itself is a direct consequence of the phenomena being observed. As is readily apparent from the earlier sections of this chapter, the loadings imposed upon a structure by an underwater explosion can be extremely complex. The incident wave may be a simple exponential decay dependent only upon charge and standoff, but the many secondary effects are subject to variables which cannot be readily controlled experimentally.

The contributions of the secondary effects are significant and must eventually be studied. However, during these early phases of investigation into underwater explosion

effects a determined effort has been made to simplify the problem as much as possible.

It has therefore been required that:

1. The model to be studied be as basic as is consistent with stated objectives.
2. Study be limited only to the incident shock wave.

These two requirements are interrelated and are tied intrinsically to the nature of underwater explosion phenomena. As has been seen earlier, the incident shock may be approximated as a plane wave emanating from the charge and striking the panel. In the absence of secondary effects, the responses being studied here may thus be limited to those of the test panel alone. If, on the other hand, secondary effects are included, more than a single point source is involved and the interactions of any support or backing structures with the fluid medium must also be considered.

Fortunately, for the purposes of this study, surface cutoff and bottom reflection are later time responses which can be neglected if study is confined to the first few milliseconds after detonation. Bubble and cavitation effects can be reduced greatly or eliminated through careful attention to the test geometry.

If an explosion occurs sufficiently near the surface that the initial bubble radius is greater than the charge depth, the hot gases forming the bubble will vent into the

atmosphere and be dissipated. This venting is instantaneous and, if occurring at the proper depths, prevents any further bubble pulsation or migration.

Bulk cavitation, too, is dependent upon the test geometry. The region of cavitation tends to expand horizontally away from the line drawn between source and surface images (Fig. 2.6). The actual shape and dimensions of the cavitation region will vary with charge size, type, and depth, but the area at depths below the charge can generally be expected to remain free of cavitation effects.

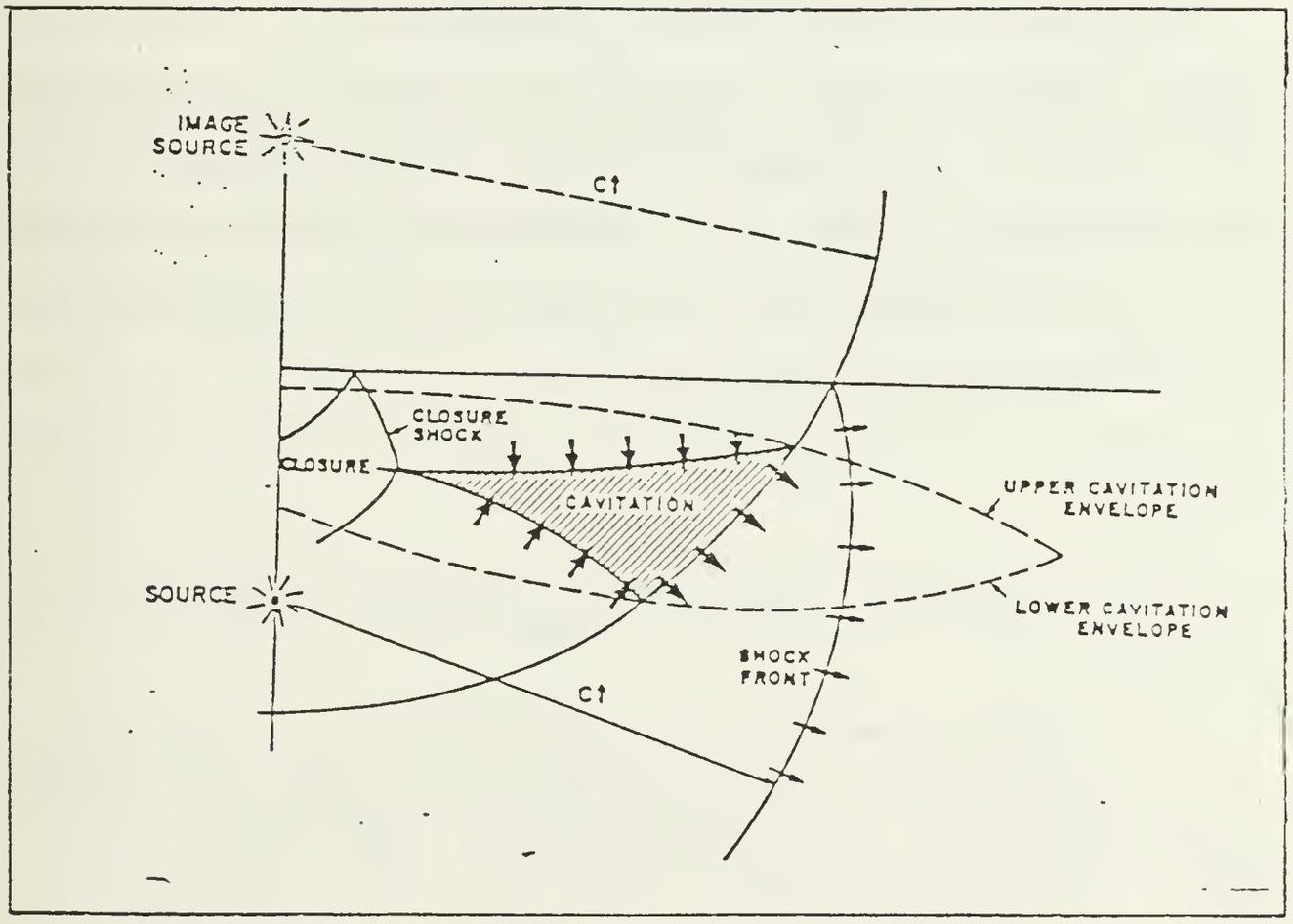

Figure 2.6 Region of Bulk Cavitation
(From Weidlinger Associates CUE Code.)

Bulk cavitation and bubble effects can therefore be reduced significantly or eliminated entirely if the test geometry is such that the charge is located directly above the plate at a depth to cause bubble venting.

In designing the test platform [Ref. 3: pp. 19-28] a series of iterations were run using the EPSA code to determine a charge weight and standoff distance that would produce maximum test panel deflections of approximately four plate thicknesses.[2] From these runs it was determined that the ideal charge weight and standoff were 8 pounds of TNT at 9 feet.

The maximum bubble radius is expressed as a function of charge weight and depth (Eqn. 2.6). Since it has been found that bubble venting occurs when the ratio of charge depth to maximum radius is less than 0.75,[3] choosing a charge depth is a fairly straightforward procedure once a determination of the desired ratio has been made.

---

[2]This value was recommended by Weidlinger Associates as one which experience indicated would ensure stiffener tripping.

[3]Any ratio below 0.75 will cause venting. Venting by its very nature will duct a portion of the explosion energy into the atmosphere, thereby decreasing the maximum pressure of the shock wave. As a rule of thumb, this decrease in usually considered negligible until the ratio drops below 0.50.

By selecting a depth to radius ratio of 0.50 it was readily determined that a charge depth of four feet was appropriate. Applying this to Eqn. 2.6 yields

$$A_{max} = (12.67)\left(\frac{8^{1/3}}{(4 + 33)^{1/3}}\right)$$

$$= 7.60 \text{ ft}$$

$$\frac{4 \text{ ft}}{7.60 \text{ ft}} = 0.526$$

which assures venting.

From the foregoing it can be seen that a test configuration that will have the desired consequences of reducing bubble and bulk cavitation effects can be designed. For an eight pound TNT charge, this platform will have the charge centered vertically at a standoff distance of nine feet above the plate. The charge itself will be located at a depth of four feet below that surface. The actual design of the test platform will be discussed more fully in Chapter V.

III. THE FLAT PLATE MODEL

As stated in the introduction, the objective of this study has been to test the applicability of a computer code, USA-STAGS, to predicting the effects of an underwater explosion upon ships' hulls. To do this, it is clearly necessary that some basis for modelling simple sections of a typical ship's grillage[4] be established.

The scaling laws used here and in the earlier work of this series [Ref. 3] were those developed by Dr. Raymond P. Daddazio of Weidlinger Associates, Inc.

In his work [Ref. 8], Dr. Daddazio has established two dimensionless parameters, β and λ, which he refers to as the "plate slenderness ratio," and the "longitudinal stiffener slenderness ratio," respectively. These are defined

$$\beta = \frac{b}{t} \frac{\sigma_y}{E} \qquad \text{(eqn 3.1)}$$

and

$$\lambda = \frac{a}{k\pi} \frac{\sigma_y}{E} \qquad \text{(eqn 3.2)}$$

---

[4]The ship's hull or superstructural plating and associated stiffeners.

where

σ_y = material yield strength

E = Young's modulus

a = spacing between transverse frames

b = spacing between longitudinal stiffeners

t = plate thickness

k = radius of gyration of the longitudinal stiffener acting with an assumed effective width of plating b_e where,

$$b_e = b\left(\frac{2}{\beta} - \frac{1}{\beta^2}\right)$$

Through sampling a variety of ship types, Dr. Daddazio found that typical values for ships' grillage fall into the range:

$$1.0 \leq \beta \leq 4.5$$

and,

$$0.15 \leq \lambda \leq 0.9$$

The intent of this series of studies has been to use one basic model but with a variety of stiffener types so that the responses of different stiffener geometries could be studied.

The model established in Ref. 3 was a 3/16 inch thick test panel 18 inches long by 12 inches wide milled into the center of a two inch thick 6061-T6 aluminum blank measuring

33 inches by 27 inches. Two stiffeners with rectangular cross sections, 3/16 inch thick by one inch deep were mounted transversely across the test panel in such a manner as to be symmetric to both the transverse and longitudinal axes (Fig. 3.1). The entire assembly was machined as a single unit to avoid the inconsistencies of welding. A radius was cut at all corners and the whole polished to avoid stress concentration points.

To apply Equation 3.1 and Equation 3.2 the two milled stiffeners were considered to be longitudinal stiffening members and the longer boundaries of the panel to be transverse frame members. Thus, the dimensions of the plate are, a = 12 inches, b = 6 inches, and t = 3/16 inches. Using the standard reference values for 6061-T6 aluminum, it was found that, for this original plate: [Ref. 3]

$$\beta = 2.02$$

and

$$\lambda = 0.9$$

which fall within the acceptable ranges.

The initial plate used in this study was identical to that used in Ref. 3 with the exception that the stiffener cross section used was a tee rather than a rectangle (Fig. 3.2).

Since the spacing of the stiffeners in this tee-stiffened plate was identical to that in the original plate,

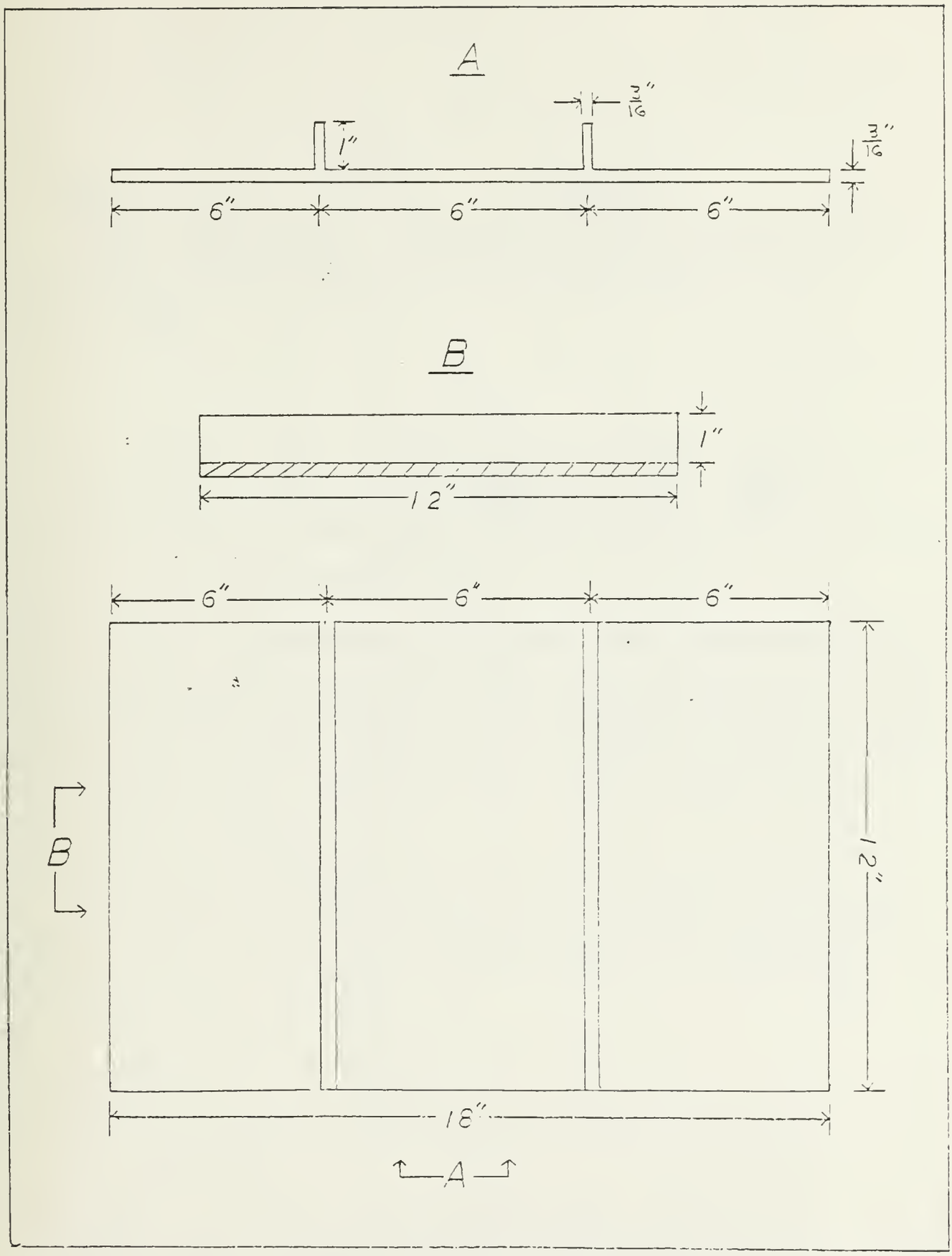

Figure 3.1 Test Panel with Transverse Rectangular Stiffeners [Ref. 3: p. 13]

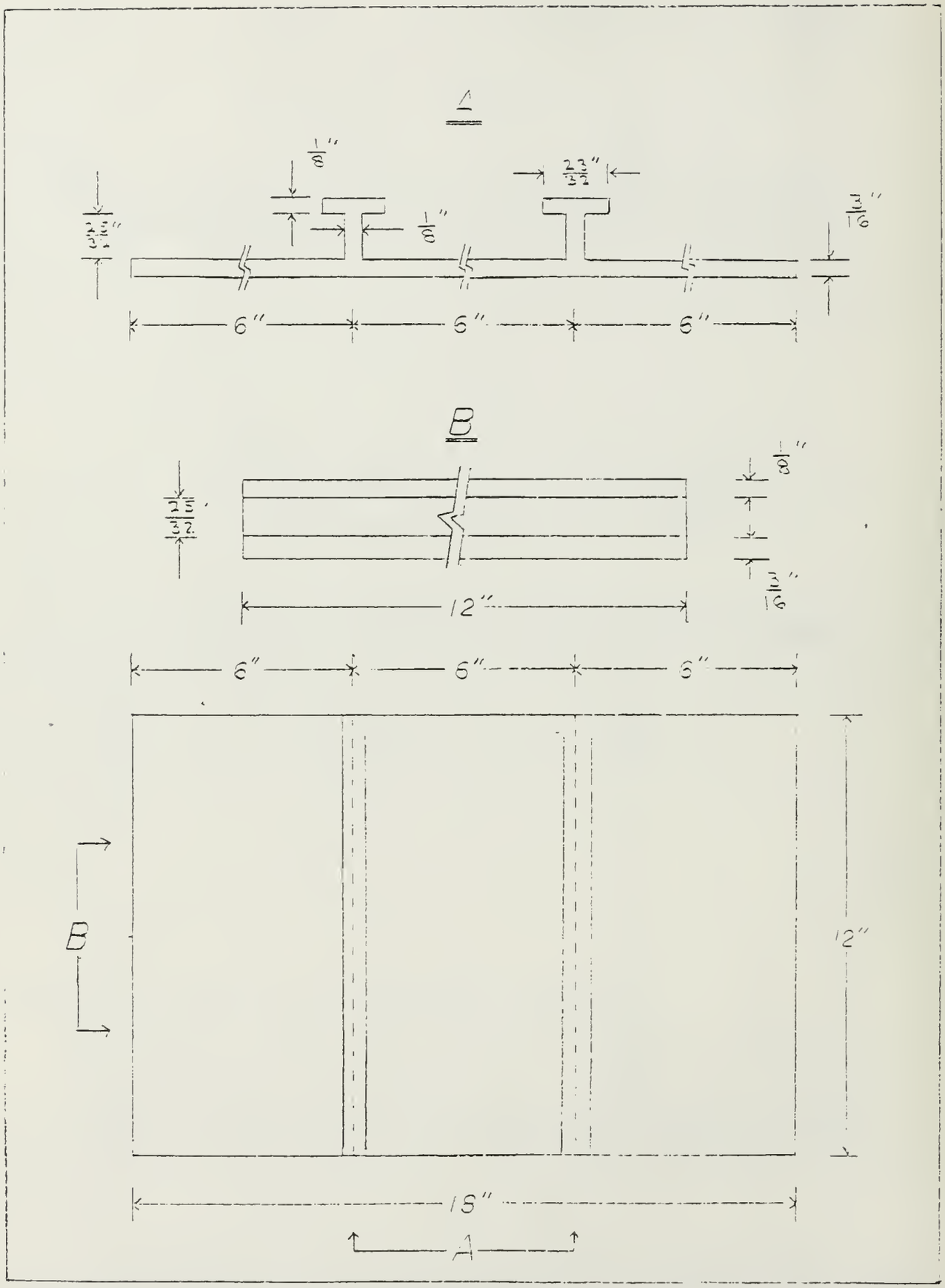

Figure 3.2 Test Panel with Transverse Tee Stiffeners

clearly the 3 values remained invariant. Given the changed geometry of the stiffener the effective radius of gyration of the plate/stiffener assembly (k) could be expected to change, and with it the value of λ.

Before that value λ could be determined, however, the dimensions of the stiffener itself first had to be established.

In an effort to ensure that stiffener responses were a function of stiffener design alone, the plastic moduli, Z_p, of the two stiffener cross sections were set as close as possible to equal. For the original, rectangular-stiffened plate, Z_p equaled 0.046875 in^3.

By a process of iteration, a tee-stiffener with flange dimensions 23/32 inch by 1/8 inch, and web dimensions 25/32 inch by 1/8 inch was fixed upon as giving an elastic modulus, Z_p = 0.046170 in^3, which is within 1.5% of that for the rectangular stiffener (Fig. 3.3).

Now, applying these dimensions to the grillage parameter, λ, we find that the neutral axis of the effective stiffener (Fig. 3.4) is:

$$\bar{y} = \frac{\Sigma A_i y_i}{A_T}$$

$$= 0.2220 \text{ in}$$

The moment of inertia of the effective stiffener is:

$$I_{ZZ} = \Sigma I_i + \Sigma A_i d_i^2$$

$$= 0.092562 \text{ in}^4$$

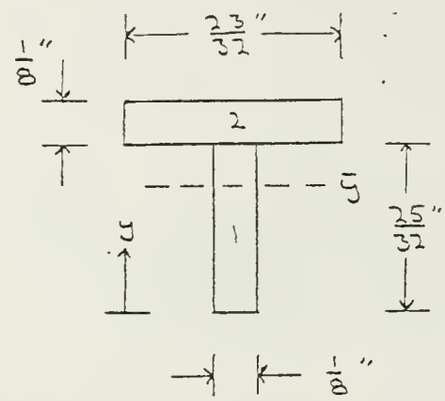

Neutral Axis:

$$\bar{y} = \frac{\Sigma A_i y_i}{A_T}$$

$$= \frac{\frac{25}{32}\ \frac{1}{8}\ \frac{25}{64} + \frac{23}{32}\ \frac{1}{8}\ \frac{25}{32} + \frac{1}{16}}{\frac{25}{32}\ \frac{1}{8} + \frac{23}{32}\ \frac{1}{8}}$$

$$= 0.607747 \text{ in.}$$

Plastic Section Modulus:

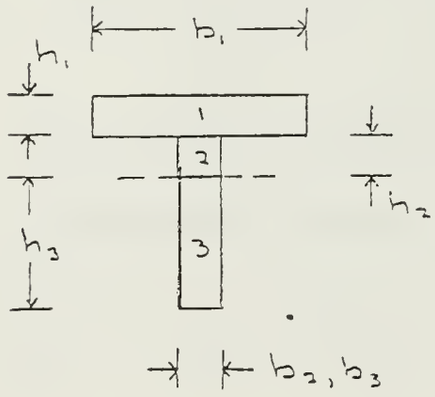

Z_p = Sum of the moments about the neutral axis of the cross sections above and below the axis

$$Z_p = (b_1 h_1)(h_2 + \tfrac{1}{2}h_1)$$

$h_1 = 1/8$ in. $= 0.125000$ in.

$b_1 = \frac{23}{32}$ in. $= 0.718750$ in.

$h_2 = \frac{25}{32} - 0.607747$

$= 0.173503$ in.

$h_3 = 0.607747$ in.

$b_2 = b_3 = \frac{1}{8}$ in. $= 0.125000$ in.

$$Z_p = (0.718750)(0.125)(0.173503 + \tfrac{1}{2} - 0.125)$$
$$+ \tfrac{1}{2}(0.125)(0.173503)^2$$
$$+ \tfrac{1}{2}(0.125)(0.607747)^2$$
$$= 0.046170 \text{ in}^3$$

Figure 3.3 Plastic Modulus of Tee-Stiffened Plate

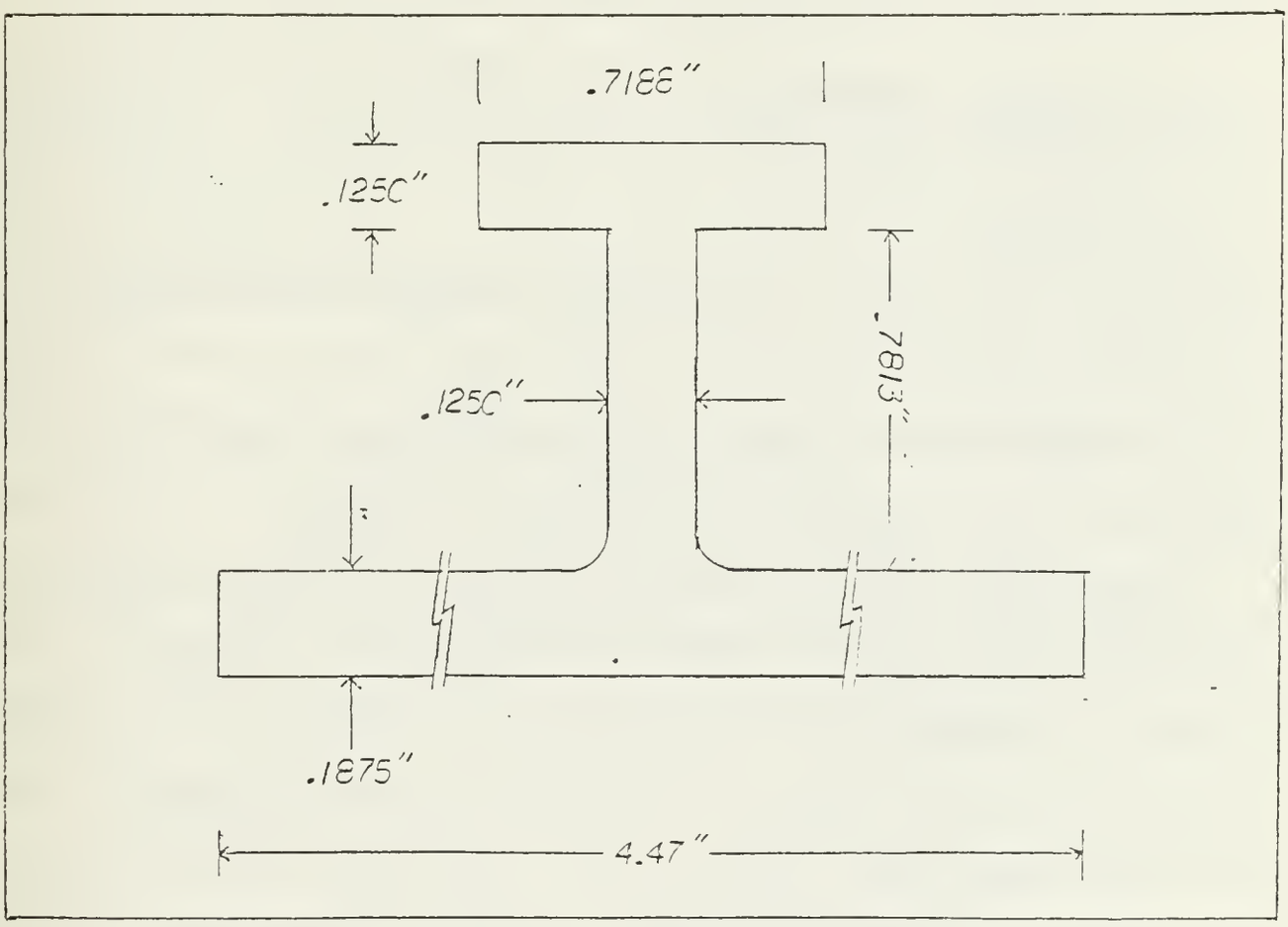

Figure 3.4 Effective Cross Section of Tee-Stiffend Plate

which gives a radius of curvature:

$$k = \frac{I_{ZZ}}{A}$$

$$= [0.092562 \text{ in}^4/1.0256 \text{ in}^2]^{\frac{1}{2}}$$

$$= 0.300419 \text{ in}$$

Thus, for the tee-stiffened plate,

$$\lambda = \frac{12}{.300419\pi} \quad \frac{40000}{10 \times 10^6}^{\frac{1}{2}}$$

$$= 0.804144$$

which is well within the parameter range required for modelling ships' grillage.

The second requirement levied upon these test plates was the ability to demonstrate stiffener tripping.

Stiffener tripping has been identified as the lateral-torsional instability of the stiffener as it becomes suddenly unstable and fails under load. It is identified by a characteristic warping and buckling of the stiffener. It is significant that the continued resistance of a stiffened structure to deformation under loading is dramatically reduced after the stiffeners have tripped. In earlier studies of impulsive loadings upon ships' grillage, tripping has been identified as ". . . a primary ductile failure mode for ship structure." [Ref. 9: p. 2].

Previous observations have indicated that tripping is most readily initiated when an axially compressive loading

is applied to the top fibers of the stiffener. Recognizing that a flat plate will tend to deform away from the source of an explosion, the plates in this series of studies have been oriented with the stiffener sides outward into the fluid medium.[5]

As stated earlier in this chapter, the original intent in this series of studies was to maintain an essentially fixed plate model, varying only the stiffener geometries. Unfortunately, the results of the first two explosion tests (on the original rectangular-stiffened plate [Ref. 3], and on the tee-stiffened plate here) were not satisfactory in view of the stated objectives. The two transversely mounted stiffeners were too short and the entire assembly too rigid to effectively demonstrate the desired stiffener tripping. The shock wave essentially "punched" through the panel material, shearing it at the fixed boundaries and at the base of the stiffeners[6] (Fig. 3.5).

The results of the two initial tests indicated that a design change was in order. The third plate of the series (the second of this study) was a simplified model to permit

---

[5]This is hardly the expected orientation on a surface vessel, but is common on many submarine pressure hulls.

[6]Although not easy to see in Figure 3.5, not all of the damage to the tee-stiffened plate was done by the incident shock wave. Apparently, when the bottom reflection hit the plate and its backing structure, it was forced upward into its own supporting cables. Much of the damage to the stiffeners in particular seems to have been caused by the actions of that cable.

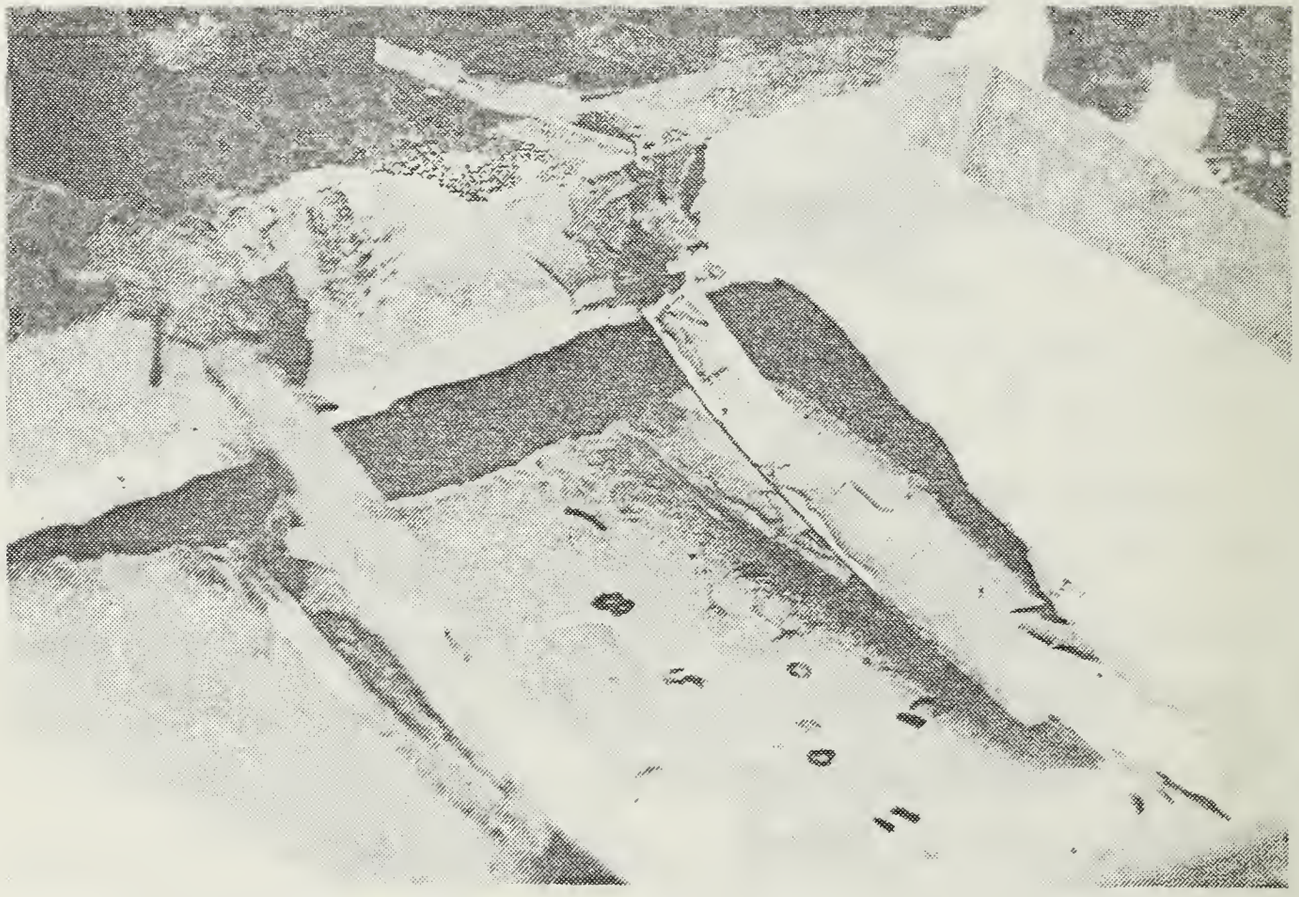

Figure 3.5 Explosion Damage to Tee-Stiffened Plate

closer investigation of the shock effects themselves, without attempting either to retain a set plastic modulus or to approximate ships' grillage.

The result of this simplification was a thickening of the base panel to $\frac{1}{4}$ inch to increase resistance to shear. The stiffener was restored to the original rectangular configuration but the thickness was increased to $\frac{1}{4}$ inch and the depth to $1\frac{1}{4}$ inches.[7] Most important, in this attempt, a single, longitudinally oriented stiffener was used rather than the two transverse stiffeners in an effort to provide greater flexibility along the length of the stiffener (Fig. 3.6).

Although the charge used to test the rectangular stiffened plate was small ($\frac{1}{2}$ pound of TNT), and the corresponding plate deflections were far too slight for any firm conclusions to be drawn, it can be seen in Figures 3.7 and 3.8 that tripping action appears to have begun to manifest itself. The single, longitudinally oriented stiffener seems to be the superior model; and, while further testing is required at larger charge weights, its employment is tentatively recommended for future studies.

---

[7] This decision was made somewhat arbitrarily. Dimensions were chosen, in part, to reduce the cost and simplify machining the plate. It is interesting to note, however, that, with $\beta = 1.52$ and $\lambda = 1.1$, this plate is not far outside the acceptable grillage range.

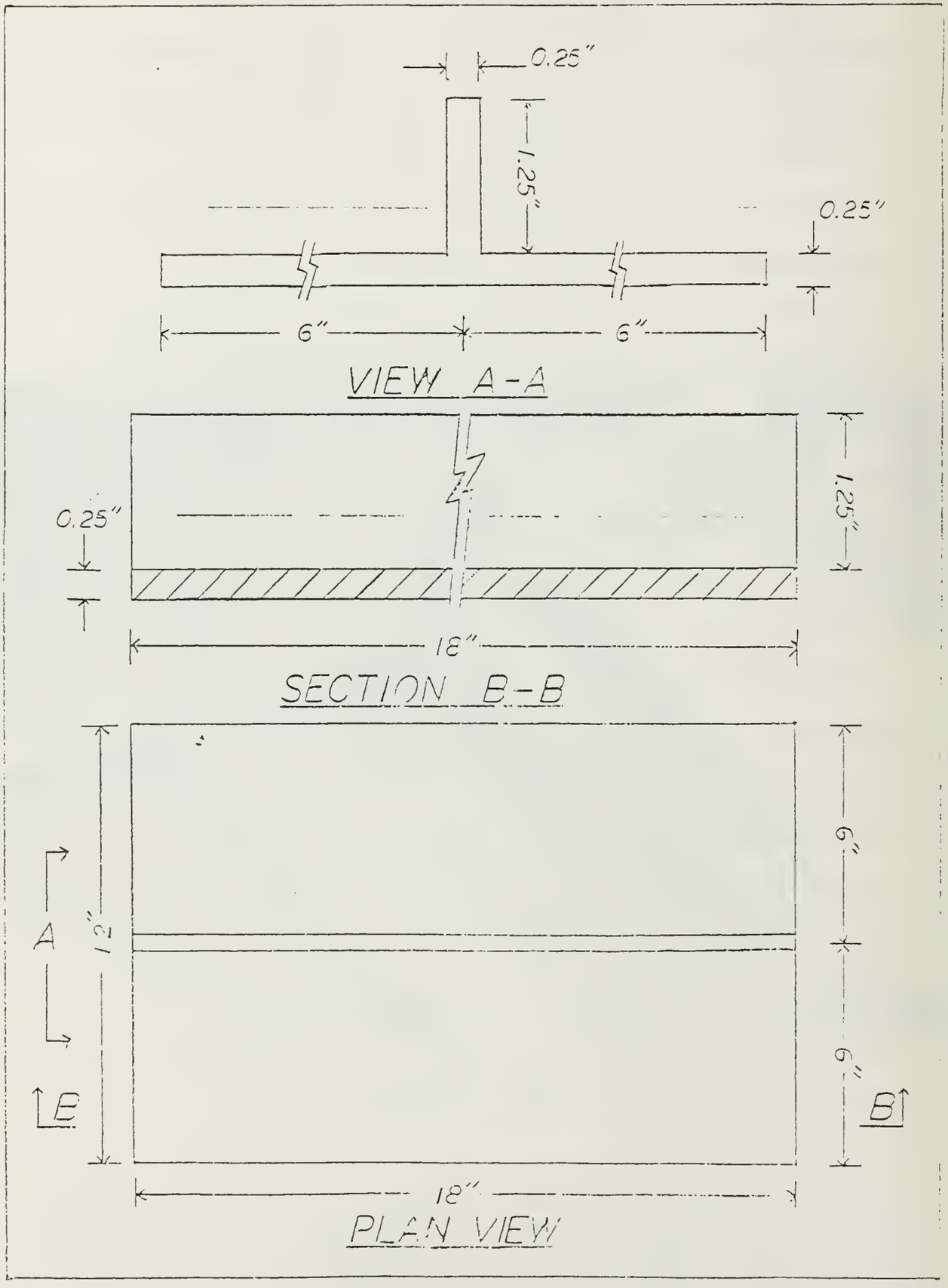

Figure 3.6 Test Panel with Longitudinal Rectangular Stiffener

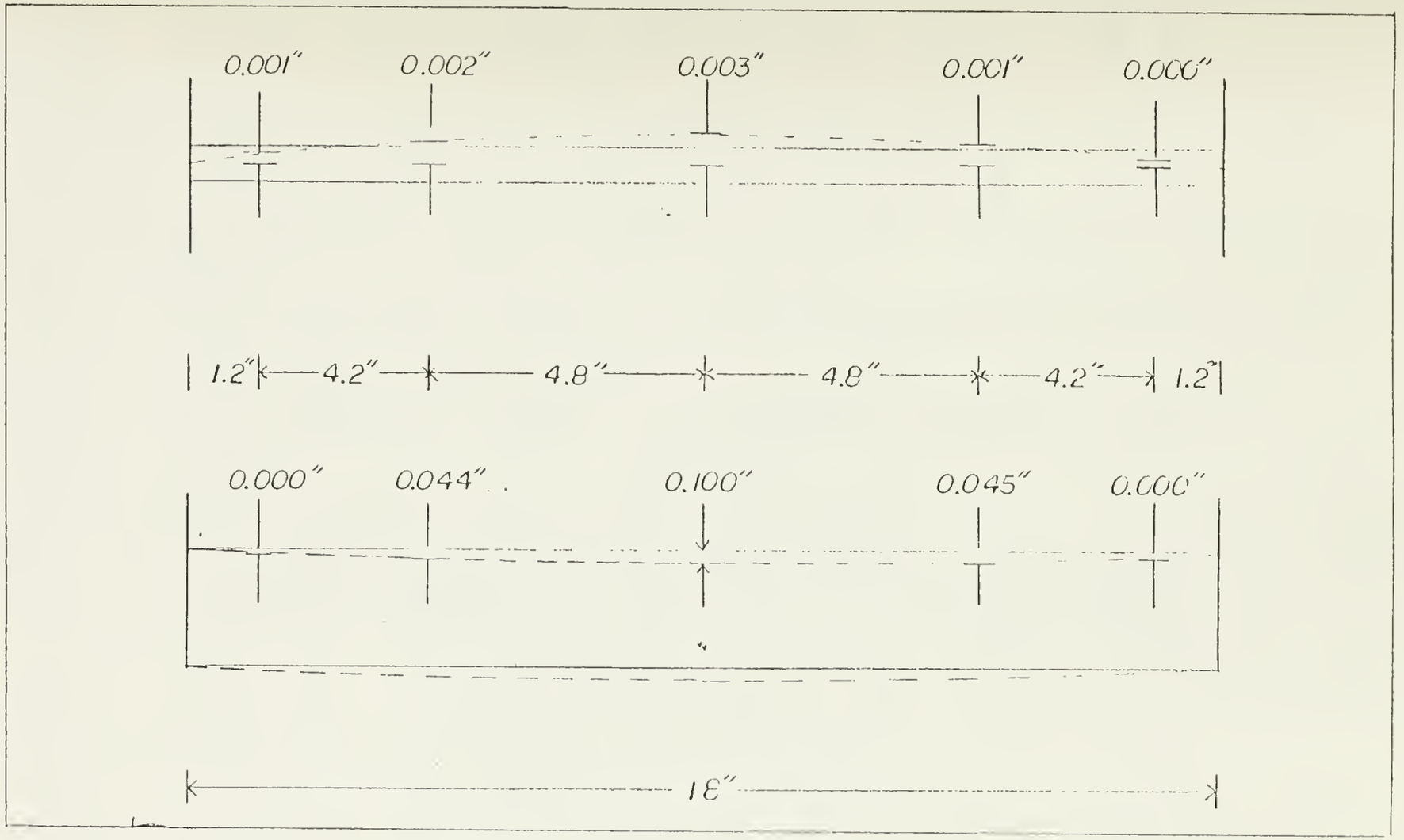

Figure 3.7 Stiffener Deflections

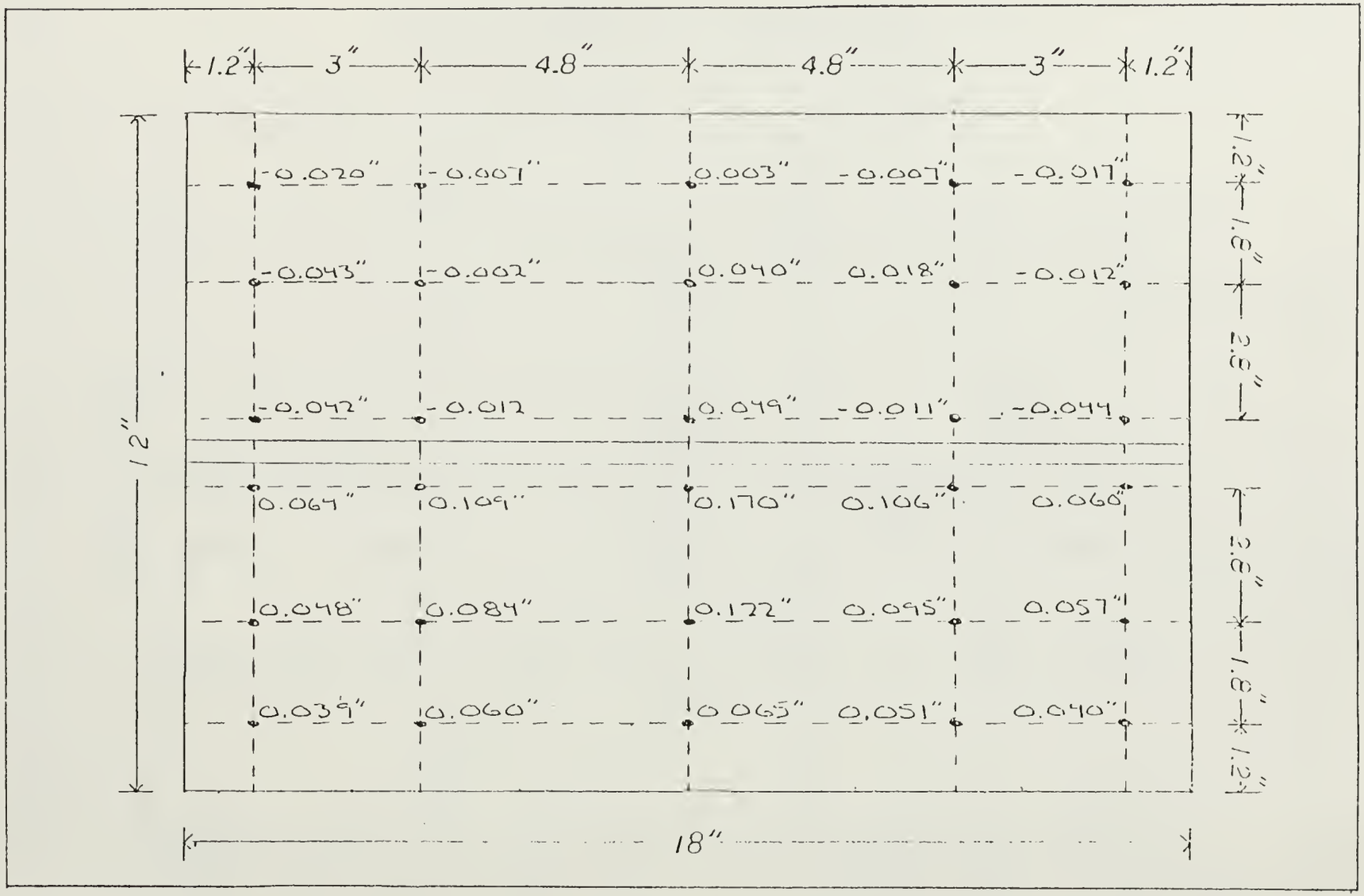

Figure 3.8 Plate Deflections

IV. THE USA-STAGS CODE

A. GENERAL

Structural Analysis of General Shells (STAGS) is the finite element code first developed by Lockheed Missiles and Space Company, Inc. during the 1960's in response to an initial tasking by the Navy and the Air Force plus an internally perceived need for a general structural analysis program.

The current version of STAGS is STAGS C-1, a dynamic analysis code with broad applications to the aerospace industry which has also found application in ship design and engineering. A new version, STAGS 2000, is now under development which will have an entirely changed data manager concept from that used in the C-1 version. This change should make the new code both easier to use and far more economical of the user's time. STAGS 2000 will appear initially as a static analysis code, but will eventually exceed STAGS C-1's capabilities.

STAGS C-1 is supported by Computer Software Management and Information Center (COSMIC) under the sponsorship of the National Aeronautics and Space Administration (NASA).

The USA-STAGS code is an extension of the basic STAGS routine to permit evaluation of impulsive loadings upon design structures in a fluid medium. As such, Underwater

Shock Analysis (USA) is a multimodule routine which is inserted as an intermediary and adjunct to the program pre-analyzer (STAGS1) and analyzer (STAGS2). The STAGS1, STAGS2 combination can stand alone for some types of general structural analysis. As a result of its add-on nature, the USA code cannot be used in a stand alone mode, but it is not STAGS dependent. Versions have been created for use with other finite element structural analysis codes.[8]

B. THEORY

The characteristics which make USA-STAGS unique lie in its applicability to a wide variety of problems and, particularly, in the individual techniques used to solve those problems. The broad, underlying theory behind those solutions is in itself common to most finite element codes.

Briefly, the technique used by codes of this genre is to solve the differential equations of motion for a structure in order to determine its responses to its environment [Ref. 10: pp. 2-1 through 2-14]. By then applying the constitutive equations (Hooke's law generalized to include anisotropic materials), the stresses in the governing equations of motion may be expressed in terms of strains. These strains may in turn be expressed as the first partials of the displacements with respect to the spatial coordinates

---

[8]As of this writing, USA has been linked to NASTRAN, GENSAM, SPAR, and DIAL.

through application of the kinematic relationships. An equivalency can be drawn between the motions of the structure between any two instants in time t_0 and t_1 and the extrema of the energy functional $\int_{t_0}^{t_1}(U - K)dt$ with respect to all admissible variations of the strain energy U and the kinetic energy K which satisfy the geometric boundary conditions and continuity conditions. The equilibrium equations can then be derived from the first variation of the energy functional through partial integration with respect to time and the spatial variables.

The variational approach provides a particularly effective means for analyzing continuous systems because of the way in which it generates and accounts for natural boundary conditions [Ref. 11]. The disadvantage of the method is that it is limited to conservative systems. However, by applying the principle of virtual work STAGS is able to greatly extend the classes of problems to which it can be applied.

In the second case; where inelastic deformations such as plastic strains or thermal expansions are encountered, STAGS treats them as "pseudo-loads." In this manner, by applying these pseudo-load terms to the force side of the equation, an initial estimate of the inelastic deformation values can be made and, if convergence is obtained, the nonconservative problem can be solved by iteration upon a series of

conservative problems [Ref. 10: pp. 2-7, 2-8]. The range of cases to which STAGS may now be applied is shown in Figure 4.1.

After being reduced to functions of displacement only, the governing equations of motion for a discretized system may be expressed in the form:

$$M_S \ddot{\underset{\sim}{\chi}} + D_S(\dot{\underset{\sim}{\chi}}) + B_S(\underset{\sim}{\chi}) + K_S(\underset{\sim}{\chi}) = \underset{\sim}{f}$$

where $\underset{\sim}{\chi}$ is the vector of displacement components, M_S is the structural mass matrix, $\underset{\sim}{f}$ is the vector of external forces, and K_S is the (generally nonlinear) structural stiffness operator. The operators B_S and D_S include forces that are functions of structural deformation and deformation velocity, respectively.

Equation 4.1 is the matrix equation that STAGS must solve to find structural displacements. For fluid/structural interactions the generalized force vector becomes a much more complex entity [Ref. 12: pp. 2-1 through 2-12].

For submerged structures excited by an acoustic wave, the exciting forces are given by:

$$\underset{\sim}{f} = -GA_f(\underset{\sim}{P}_I + \underset{\sim}{P}_S) \qquad \text{(eqn 4.2)}$$

where $\underset{\sim}{P}_I$ and $\underset{\sim}{P}_S$ are the incident and scattered nodal pressure vectors acting upon the surface of the structure at the fluid-structural interface. A_f is the diagonal area matrix associated with elements in the fluid mesh, and G is the

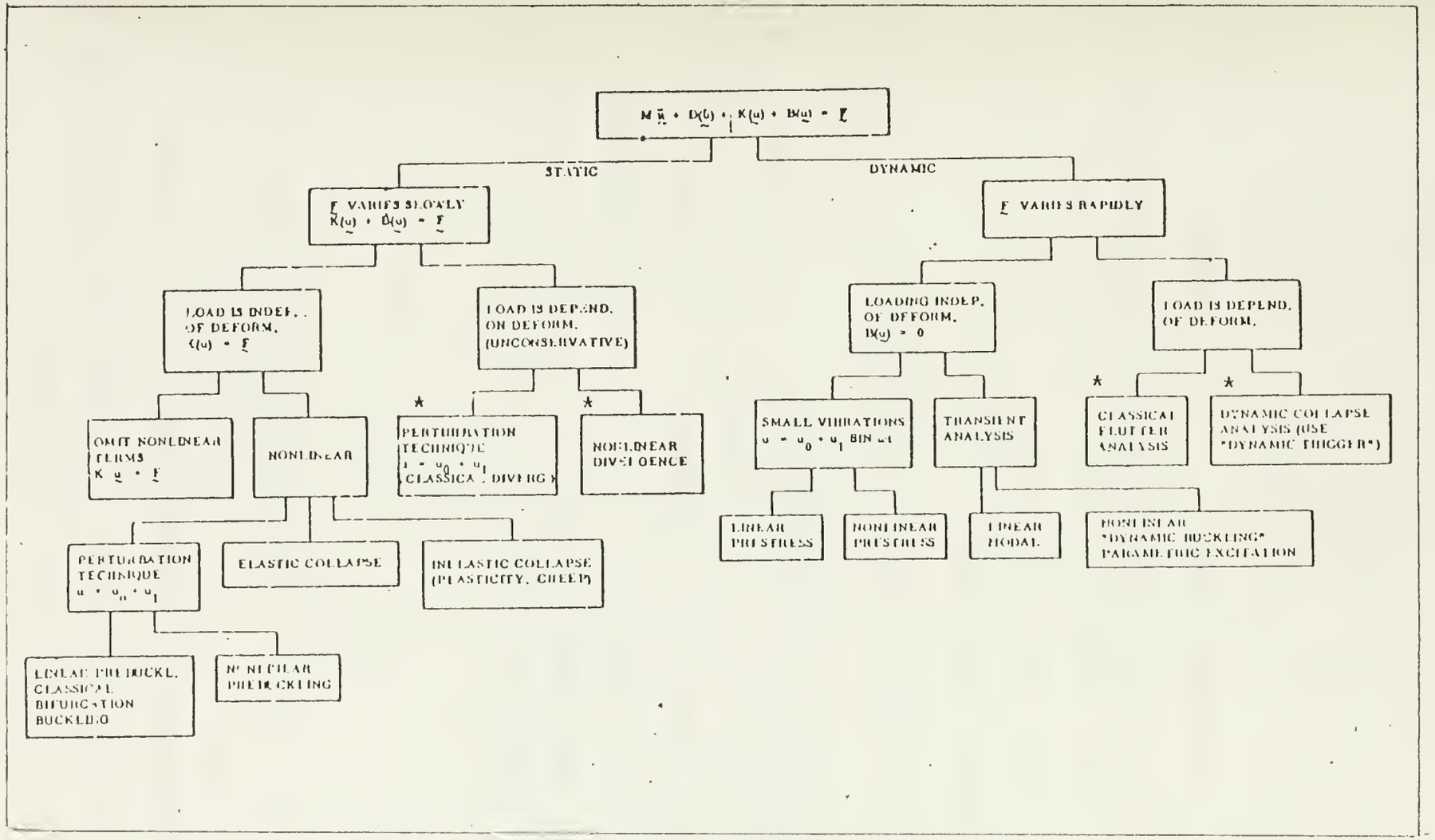

Figure 4.1 Range of Problem Types to which STAGS is Applicable [Ref. 10: p. 2-12]

matrix which relates the structural and fluid surface forces. It can be seen from the development of the pressure characteristics of an underwater shock wave in Chapter 1, that for an underwater explosion the incident pressure vector $\underset{\sim}{P}_I$ is known. The scattered pressure vector $\underset{\sim}{P}_S$ on the other hand is dependent upon the configuration of the structural surface and is therefore not only not immediately known but is also changing as the structure deforms.

It is to solve this computational dilemma and thereby solve the combined equation of motion:

$$M_S\underset{\sim}{\ddot{\chi}} + D_S(\underset{\sim}{\dot{\chi}}) + B_S(\underset{\sim}{\chi}) + K_S(\underset{\sim}{\chi}) = -GA_f(\underset{\sim}{P}_S + \underset{\sim}{P}_S) \qquad \text{(eqn 4.3)}$$

that the USA code was created.

The USA code finds $\underset{\sim}{P}_S$ by utilizing the Doubly Asymptotic Approximation (DAA) and a staggered solution procedure.

The DAA is an approximate relation which approaches exactness at both the high-frequency (early-time) and low-frequency (late-time) limits to the passage of the shock front. It may be written:

$$M_f\underset{\sim}{\dot{P}}_S + \rho cA_f\underset{\sim}{P}_S = \rho cM_f\underset{\sim}{\dot{v}}_S \qquad \text{(eqn 4.4)}$$

where $\underset{\sim}{v}_S$ is the vector of scattered-wave fluid-particle velocities normal to the structural surface at the fluid-structural interface. M_f is the fluid mass matrix for the fluid mesh at the interface, and ρ and c are the density and sound velocity of the fluid, respectively.

When fluid and structure are excited by an acoustic wave, the incident and scattered fluid particle velocities ($\underset{\sim}{v}_I$ and $\underset{\sim}{v}_S$) may be related to the structural response by the kinematic compatability relation:

$$G^T \dot{\underset{\sim}{\chi}} = \underset{\sim}{v}_I + \underset{\sim}{v}_S \qquad \text{(eqn 4.5)}$$

Solving for $\underset{\sim}{v}_S$ and substituting the resultant into equation 4.4 yields

$$M_f \dot{\underset{\sim}{P}}_S + \rho c A_f \underset{\sim}{P}_S = \rho c M_f (G^T \ddot{\underset{\sim}{\chi}} - \dot{\underset{\sim}{v}}_I) \qquad \text{(eqn 4.6)}$$

Equations 4.3 and 4.6 are now each expressed in terms of the single unknown $\underset{\sim}{P}_S$ and a solution may be obtained by a staggered iteration process between the two equations for each time step.

C. ORGANIZATION

As has already been stated, USA-STAGS is a modular code. Functionally, it may be divided into five basic components.

1. The structural preprocessor
2. The fluid mass preprocessor
3. The augmented matrix preprocessor
4. The time integration processor
5. The data postprocessor

Each of these components is run individually in sequence utilizing the outputs from the previous modules.

1. The Structural Preprocessor

The structural preprocessor is the unit that assembles the structural mass and stiffness matrices, creates the finite element mesh, and otherwise provides an encoded description of the structure's internal and external degrees of freedom [Ref. 12: pp. 3-3, 3-4].

For USA-STAGS, the structural preprocessor is the STAGS1 portion of the STAGS code itself.

Input for STAGS is made to each of ten functional subdivisions which correspond to the types of input that go into each. These subdivisions are:

- Summary and Control Parameters
- Computational Strategy Parameters
- Data Tables
- Geometry and Material
- Discretization
- Discrete Stiffeners*
- Boundary Conditions
- Loads*
- Output Control
- Finite Element Units*

(Subdirectories designated with * are not required with all models.)

Input to each subdirectory is in the form of a series of data records consisting of real and integer

numerical data fields. This will be discussed in greater detail in the following section.

2. The Fluid Mass Preprocessor

The fluid mass preprocessor (FLUMAS) constructs the fluid mass matrix for a structure submerged in a fluid. Inputs include [Ref. 12: pp. 3-4, 3-5] the global coordinates for the structural geometry (input from the structural preprocessor), plus

- Fluid wet-surface mesh
- Element definitions
- Material properties of the fluid
- Location of free surface
- Model symmetries

3. The Augmented Matrix Preprocessor

The augmented matrix preprocessor (AUGMAT) receives the output from the structural and fluid mass processors to create the matrices required for solution of the augmented equations 4.3 and 4.6.

4. The Time Integration Processor

The functional heart of the USA-STAGS system, the time integrator processor (TIMINT) links back to and supplements the structural processor STAGS2 to implement the staggered solution technique; creating the solution data files over the time range specified. Input includes the data passed from AUGMAT plus

- Spatial geometry of charge and target
- Initial incident pressure and pressure wave decay characteristics
- Time integration information
- Restart data

TIMINT includes an internal postprocessing capability. Generally, however, this function is left to the following module.

5. The Data Postprocessor

USA-STAGS Provides a selection of three possible postprocessors: POSTP, POSTPR, and STAPL. Their uses will be discussed in the following section.

D. USING THE CODE

As has already been stated, the STAGS code is extensive in its concept; attempting to cover in a single code as many approaches to problem solution as can be linked in a single contextual framework.

It is beyond the scope of this work to cover all possible aspects of the code; indeed within the stated capabilities of STAGS this approach may seem peripheral, being limited as it is to those aspects clearly related to underwater shock analysis of flat plate models.

STAGS is designed to be used for any one of six types of analysis [Ref. 13: p. 2-1].

- Linear stress analysis
- Geometrically nonlinear elastic stress analysis

- Inelastic stress analysis, geometrically linear or nonlinear
- Bifurcation buckling analysis with linear or geometrically nonlinear stress state (elastic)
- Small vibration analysis based on linear or geometrically nonlinear stress state (elastic)
- Transient response analysis, linear or geometrically nonlinear, elastic or inelastic

In this study, only two of those capabilities were used: (a) Small vibrations (in a stress free state), and (b) Geometrically nonlinear transient response analysis. Of these, the second alone is truly applicable to USA-STAGS. The small vibration analysis was used as a check on the code and input data. Since the actual inputs for the two analyses vary but slightly, both shall be addressed together.

Before that can be done, however, the codes must somehow be brought into some semblance of conformity; for they are not normally provided as a single unit.

Both codes are provided in tape form: STAGS from COSMIC, and USA directly from Lockheed. These are designed to be loaded onto the VAX 11/780 computer using the standard MOUNT MF: command.[9]

It is suggested that, at least during the early stages of processing, each tape be assigned to a separate directory, for many of the source files will be culled as the

---

[9] See Appendix A.

executable files (*.EXE)[10] are created. The source files supplied with each code are specific to the code until the final linkage, and their sheer number can cause confusion if not approached methodically.

The STAGS tape as provided contains all the necessary ingredients for the functioning codes except the executables themselves. These are left to be linked on the individual computer. The link commands for creation of these executables are provided with the tape on the INFO.VAX file, which also contains a full listing of the tape's contents. The commands that are of immediate interest are LSTAGS1.COM, LSTAGS2.COM, LPOSTP.COM, and LSTAPL.COM. These should be copied into the file and executed in the normal manner for a program run from the terminal.[11] The result will be the executable files for the respective module.

Executables are provided with the USA tape; however, since relinking may be required to adapt the code to local filenames, link command files are also provided.[12] The

---

[10]On the VAX, the asterisk represents a "wildcard" which may be substituted for any filename, filetype, or version number (the complete listing for a file is: filename, filetype, version number) whenever a general category is desired or the listing is to be repeated.

[11]This is done by simply typing "@ command filename" and hitting the return key.

[12]The USA tape also includes another particularly nice feature, the complete user's manual for each of the modules. This ensures that the most current version is available; and, more important, the version of the manual that is pertinent to that tape. A vital accompaniment since the tapes are continually being updated.

command files to be used in constructing the USA executables are LINKFLU.COM, LINKAUG.COM, LINKUSAS.COM, and LINKPOS.COM. It is the LINKUSAS.COM file which actually performs the marriage between the codes; allowing the integration/ structural analysis functions of STAGS to be coupled with the USA fluid processor.

Once all of the executable files have been created and tested in a full run of the combined code; all files but the executables may be deleted, thus realizing a considerable increase in computational space.[13]

The basic strategy that will be followed here shall be to address USA-STAGS as a single code broken into five different modules (see preceding section); each of which can be run independently in stepping stone fashion once necessary input from earlier modules has been obtained.

The first module to be run is STAGS1. The actual input for this includes all information needed for both STAGS1 and STAGS2 execution in a single entry file.

The first five data records: A-1, B-1, B-2, B-3, and C-1 are common to all STAGS runs. The inputs as set forth in the COSMIC STAGS users guide [Ref. 13: pp. 3-1 through 3-11] are largely self-explanatory but a few points should be noted.

---

[13]Total space required for the executables alone is less than 4000 blocks; compared to the almost 13000 blocks for the executables plus source codes.

First, IPOST0, IPOST1, and IPOST2 are applicable only to the STAGS postprocessors POSTP, and STAPL. If the user is interested only in the nodal displacements resulting from underwater shock these may be derived directly from either of the USA modules TIMINT or POSTPR. Thus IPOST0, IPOST1, and IPOST2 may be set to zero thereby suppressing creation of model and solution data files (*.MOD and FOR022.DAT) and realizing some savings in computer space. It is suggested that this be done in any case during early model development and while testing code inputs (as with the small vibrations analysis). If, however, strains are required; these are computed only within the STAGS postprocessors and IPOST0 must be set to 1. Considerable amounts of computer time and space can be used in processing a large model; time which would be wasted if this is not done. Similarly, IPOST1 and IPOST2 should be set to a non-zero value if displacement and stress plots are desired at the IPOST1st and IPOST2nd load steps.[14]

Second, it should also be noted well that IFLU must be set to 1 if underwater shock analysis using USA is to be undertaken. This will cause the FOR003.DAT and FOR004.DAT files required for USA to be created. These files are not

---

[14]This is required only when using STAPL. POSTP is capable of calculating displacements and stresses internally.

unduly lengthy, but for the sake of economy should be suppressed for non-USA runs.

The C-1 data record is meaningless for small vibration analysis and transient response analysis but must be included. A value of 0. should be entered.[15]

The only true variation in data record sequence between small vibration analysis and transient response analysis comes in the next group of cards. The proper sequencing for small vibrations is D-2, D-3, F-1; while for transient analysis it is D-1, E-1, E-2, F-1. These are the Strategy Parameters and the difference lies in the need for integration over time in the transient model. The D-1 record sets tolerances, limits the amount of CPU time, allows restarts, etc.; while the E records control the actual time integration itself.[16]

---

[15] This must be a real number. STAGS is often blind to data not submitted in the proper format. It will not record an error, but will simply pass over the improperly input data until finding some in the format it seeks. This can lead to sometimes dangerous distortions of the input records.

[16] At the time that this study was initiated it was understood that implicit integration using K. C. Park's formula (IMPL = 0, METHOD = 4 on the E-2 record) was the only form of integration that should be used with USA. As of this writing, however, Lockheed informs that USA may now also be used with explicit integration. It has been suggested that this might provide a faster and more economical solution. Due to time limitations that has not been tested here.

The D-2 and D-3 records are specific to modal analysis and deal with the number and range of eigenvalues to be calculated.

Data records F through P pertain to the model itself. The records F through L provide information general to the entire model and are listed in normal alphabetical sequence once through only, although specific cards may be repeated within the sequence. M through P, plus Q and R are specific to the individual shell and beam components and are repeated in sequence once for each component (see examples in the appendix).

The F-1 and F-2 records provide grid point and stiffener summaries, respectively. The information in F-1 controls generation of the finite element mesh. Inputs are simply the number of nodal rows and columns for each shell. Actual choice of which shell direction shall consist of rows and which columns is unimportant as long as that choice remains consistent for the local X and Y coordinates across the entire model (rows are lines of consistent X, columns are lines of consistent Y). Entry is made sequentially; number of rows(I), number of columns(I) for each shell in order of input. The mesh created forms the master elements which will then be fitted into the structural geometry by the information contained in the M records.

The F-2 record is a summary of shell stiffeners. Use of this record could be extremely useful in determining

generalized responses on large scale models, but was inconsistent with the purposes of this study because of the inherent assumption that stiffeners do not deform.

Record G-1 establishes the compatibility conditions for the various shells. The instructions listed in the COSMIC-STAGS user's manual are straightforward, but reference to Appendix B may prove helpful for establishing proper linkages. It will be noted that in each case, for a flat plate, side 1 is that nearest and parallel to the global Y axis while side 4 has a similar correspondence to the global X axis.

Records I, J, K, and L constitute the Data Table section of STAGS. Again the user's manual is self-explanatory and will not be explicated except to note that the Material Record, I-1; the Material Property Record, I-2; and the Plasticity Record I-3 (if used); are listed in sequence once for each of the materials enumerated in the B-3 record.

If plastic behavior is expected in the model and the White-Besseling theory of plasticity is chosen (IPLST options 0 or 1 on the I-1 record) especial note should be made of the user's manual's warnings concerning the slope of the line connecting points submitted for the discretized stress-strain curve in the I-3 record. The change in slope at each point must be negative. Another point not mentioned in the user's manual, but which should definitely be noted, is that the first stress-strain data entry on the I-3 record

must be consistent with the elastic modulus entered on the I-2 record. That is, the slope of a line drawn from the origin to that first data entry should be the elastic modulus. Also, while specifying plastic behavior may actually decrease the run time for the TIMINT module by reducing the number of iterations required for each time step, it can increase the required computer space by more than 100%.[17]

If plasticity is to be included in the model, there are also some changes that should be made in the K records.

STAGS determines the plastic responses of the shell by integrating through the thickness. The input NLIP in the K-2 record establishes the number of integration points through each material layer. Since Simpson's rule is used, this number must be odd. NLIP may lie between 0 and 9 (inclusive), but some care must be exercised in the choice, since the larger numbers will add to the length of the

---

[17] A normal run for a model with about 300 nodes seems to be on the order of about two to two-and-a-half hours of CPU time for strictly elastic behavior. If the elastic range is exceeded but plastic behavior is not specified, these runs can easily continue for 15 to 20 hours as the code attempts repeated iterations for each time step (the user can control this somewhat by specifying the maximum allowable time for any iteration), and the full number of specified time steps may not be attainable. Inclusion of plasticity will again reduce the run time to roughly three to four hours. Output of stresses beyond the yield point of the material, however, requires much larger solution data (FOR022.DAT) files for both the TIMINT and POSTP runs. Typically, these have been on the order of 45,000 and 35,000 blocks respectively for the pressure levels used here.

TIMINT run; which, as has already been mentioned, is not insignificant for the plastic case. The default value for plasticity is 3. This may be acceptable for models where the membrane stress governs, but will not be so if there is marked bending stress.

Another change that should be made for runs including plastic responses is to enter a value of 1 or 2 for the LSO entry of the K-2 record. If this is not done the USA-STAGS code will successfully complete an entire run, but the post-processor, POSTP, will not print stress or strain data.[18]

The sequence of records M through R defines the properties and loads on the shell units. As is noted most explicitly in the user's manual, these records are read sequentially for each unit. All data in the sequence will be read before the M-1 record for the next unit is read.

The individual shell geometries and the defining parameters by which they are to be connected to other shells (that is the means by which they are to be oriented to the global geometry) are specified in record M-1. IGLOBE option 0 is useful if the local coordinates of the unit already correspond precisely to the global coordinates. Option 1 is

---

[18] Actually, this may not be entirely true. In order to get any useful response whatsoever out of POSTP, it has been necessary to "trick" the code into producing the desired stresses and strains by running the module with an FOR002.DAT file created by a STAGS1 run for the elastic case. This has been true whether or not LSO has been flagged, with no noticable difference in the results.

similarly intended to be a labor saving device. A caveat should be observed, however, that option 1 should only be used if the side connecting two shells is uniquely defined (i.e., no straight lines). It is strongly recommended that options 2 or 3, which allow more user control by specifying boundaries through specific global reference points, be used in preference to option 1.

An option not listed in the user's manual, but which could conceivably be useful for construction of cylindrical models is option 4. This allows the user to specify the location of a unit origin in the global coordinate system and then define the boundary in terms of one translation and one rotation about the reference point.

It should also be noted that STAGS will permit introduction of shell geometries not included in the eleven which are indigenous to the program. This is done through a user written subroutine which may be specified by choosing ISHELL option 1 on the M-1 record.

If the ISHELL = 1 option is chosen, the shell geometric properties normally input in record M-2 will be input in the user-written subroutine LAME as stated above. Otherwise, shell geometries are chosen from those provided by the code. Property values for these geometries should be input as specified in the figures of Appendix B. If plastic deformations are expected, particular attention must be paid to inputs to the M-5 record. First, since Gaussian quadrature

is used to integrate across the mesh, STAGS will give erroneous results (or none at all) if that mesh is not located on the midplane of the shell thickness. ECZ must correspondingly be set to 0, and IPLAST set equal to 1. No further inputs need be made on this record unless one of the shell units is located on a plane of symmetry. If that is the case, STAGS will not compute lateral deformations without further information about how the shell is to respond. This information is provided in the form of minute randomly generated displacements or "random imperfections" of the shell nodes from the midplane. To trigger input of these imperfections, IRAMP should be set equal to 1, and the appropriate entries made on the M-6 and M-7A records.

The user's manual's instructions and flow patterns for records N through R are clear and it is believed that, with possible references to the input files in Appendix C, the user should have no difficulty completing the STAGS input deck.

As stated in the section on organization of the code, USA is divided into four modules. Each of these may be run independently once the needed data files have been produced by the previous module. Except for the required access to those generated data files, each module is run entirely in stand-alone fashion. Since modular input information is brief and error statements are generally good, this permits debugging without affecting earlier inputs and generates a high degree of confidence in the modular output.

It has already been mentioned that setting the IFLU switch equal to 1 on the B-1 record of the STAGS1 run will generate two data files FOR003.DAT and FOR004.DAT which are specific to USA. These are produced in addition to the FOR002.DAT and output files which are normally generated by a STAGS1 run.

Each of the three data files FOR002.DAT, FOR003.DAT, and FOR004.DAT must be renamed after the STAGS1 run for use in USA. The first, FOR002.DAT, should simply be renamed for the file subdirectory containing the USA files (e.g., (*.USA)FOR002.DAT). FOR003.DAT and FOR004.DAT must be renamed to correspond to the GRDNAM and MASNAM files specified in the FLUMAS and AUGMAT modules, respectively. This may be done by entering a simple RENAME command on the VAX. The user will then be queried regarding the name from which and to which they are being changed.

The GRDNAM file (the renamed FOR003.DAT file) contains the global coordinates of the structural grid points generated for the model by STAGS1. The FLUMAS module then uses this information to construct a fluid mass matrix (FLUNAM) as well as generate the fluid mesh data (GEONAM) and transformation coordinates that relate the structural and fluid degrees of freedom on the wetted surface. The FLUNAM and GEONAM data files will then be used in the AUGMAT module to create a final augmented mass matrix.

The module AUGMAT is the component of USA which assembles the data from the FLUMAS module and from STAGS1 into the specific constants and arrays required for the staggered solution process. The input deck for this module is very short and experience indicates that problems with the module will generally be caused by input errors to either STAGS1 or FLUMAS.

USA's time integrator module, TIMINT, links the results of the AUGMAT module which are stored in the data file PRENAM back to STAGS2 and then unites with STAGS2 to conduct a step-by-step numerical time integration of the governing equations for submerged structures exposed to shock waves. The time integration information input to TIMINT will overwrite earlier entries to the STAGS deck. It is suggested, however, that these entries should be made consistent.

Input to TIMINT includes not only time integration information but also the spatial coordinates for the charge and for the point on the structure closest to the charge (the standoff). These distances are made in reference to the origin of the global structural coordinate as defined in the STAGS input. One point of caution: The surface-cutoff provision in FLUMAS assumes a horizontal separation between charge and target. As the charge approaches a point vertically above the target, some of the computed values will go to infinity, causing the module to fail. The surface-cutoff function does not automatically turn itself off and the

FLUMAS input must be changed accordingly if a vertical aspect is required.

Provision has also been made in TIMINT to print nodal displacements without recourse to a post-processor. It is recommended that this option not be exercised. A run for any of the other USA-STAGS modules can be made in a matter of minutes. Running TIMINT can easily consume several hours of CPU time for a moderately sized model. It is therefore not time or cost effective to run TIMINT each time a new set of displacements is needed.

The solution data file, POSNAM, output by TIMINT is specific to the USA post-processor, POSTPR. If nodal displacements only are desired this is by far the easiest and most economical route to follow. It is not, however, the only option. USA-STAGS provides a selection of three possible post-processors. As mentioned, POSTPR is internal to USA and may be used to provide either data listings or graphical displays of nodal displacements. The other two, POSTP and STAPL, are a part of the STAGS package. A second solution data file in STAGS format,[19] FOR022.DAT, is created

---

[19] It is actually created by STAGS2 during the TIMINT run.

and may be renamed to the STAGS subdirectory for use in either of these.[20]

Both POSTP and STAPL have been designed to provide not only displacements but also stresses and strains; POSTP in tabular form and STAPL in graphical on a CALCOMP plotter. At the time of this writing, the Naval Postgraduate School did not have a graphical capability on VAX/VMS so neither the POSTPR-graphical nor STAPL options were run at the Naval Postgraduate School.[21]

In accordance with common usage on the VAX, the sequence of commands required to execute any module have been entered into command files (*.COM). Examples are given in Appendix A.

Once the appropriate file names have been entered into the command file for the module to be run, the command file may be executed by entering "@ command filename" for runs from the terminal; or "SUBMIT filename" for batch runs. A file definition statement (SET DEF [*.*]) is required for batch runs but is not necessary for runs from the terminal.

---

[20]It should be noted that the TIMINT entry, NSAVER, is the frequency with which responses are saved for the USA postprocessor only. The frequency with which data is saved for the POSTP and STAPL postprocessors is actually tied to the restart data in NRESET. If stress and strain information is required at each timestep, NRESET should therefore be set to 1.

[21]POSTPR and STAPL plots shown in later sections of this work were done by Lockheed.

E. DISCRETIZING THE MODEL

As its name implies, the primary building unit in the STAGS code is the shell element. These elements may be constructed into shapes which are warped through almost any conceivable configuration in three-space and beam elements may be added, but the basic unit remains two-dimensional.

The flat plate models constructed for this study, then, were ideally suited for discretization using such elements. Each plate with its associated stiffeners was capable of being divided into several flat shell units composed of square or nearly square elements. Additionally, the even spacing of the stiffeners allowed advantage to be taken of the plate symmetries to reduce the overall size of the model and corresponding length of the computer run.

The transverse tee-stiffened plate established symmetry in two directions permitting a quarter model to be used. That quarter model was then divided into five shells; two for the base plate, and three for the stiffener. These shells were numbered beginning with the two shells comprising the base upward through the stiffener (Fig. 4.2). This was done to permit changes to be made to the code input by simply adding or deleting shells. As long as the basic plate dimensions and symmetries remained the same,

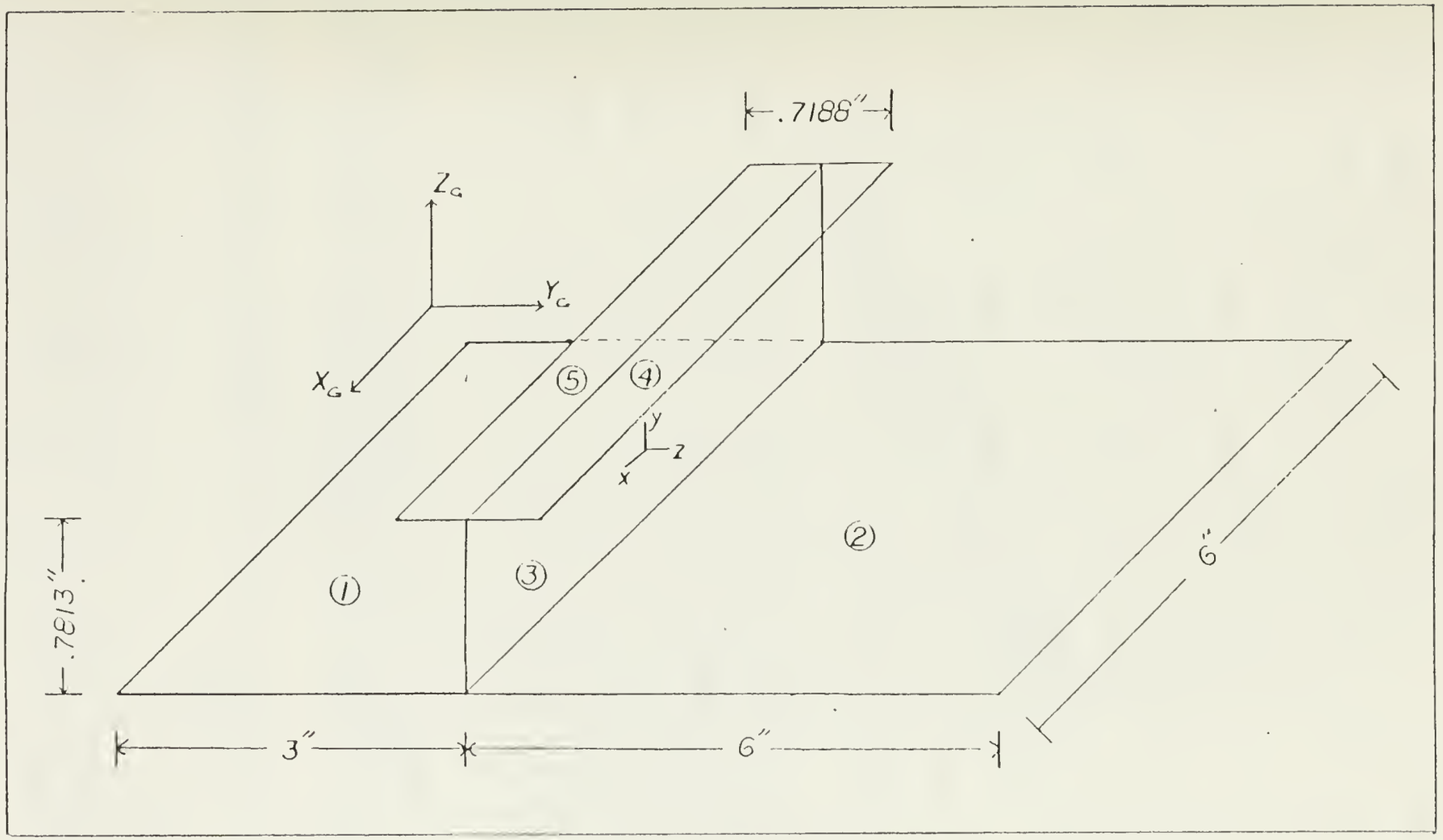

Figure 4.2 Shell Units for Tee-Stiffened Plate

extensive rewriting could be avoided throughout the USA-STAGS modules.[22]

The STAGS code will generate the finite element mesh. The user need only specify the number of nodal rows and columns. In the case of the tee stiffened plate, an element 0.6 inches by 0.6 inches was chosen in order to keep the mesh as fine as possible and yet be able to place the active filaments of the strain gages used during the underwater explosion testing entirely within the element.[23] This corresponded to 11 nodal rows and 6 nodal columns in shell unit 1, 11 rows and 11 columns in shell unit 2, and 11 rows and 3 columns in each of the three stiffener shells (Figure 4.3).

Since the stiffener used on the second test plate was rectangular, three shell units sufficed to model it (Fig. 4.4). At the time that this plate stiffener was discretized, the limit set upon the number fluid mesh elements by the FLUMAS module was 171.[24] The increased surface area

---

[22]Unfortunately, it was not possible to carry through with this plan since the plate with the longitudinal rectangular stiffener completely changed material dimensions and permitted only one axis of symmetry.

[23]STAGS computes stresses and strains at the geometric centroids of the elements. Strain gages should therefore be centered on the element.

[24]It turns out that this is relatively easy to change, but it involves technical considerations that are beyond the scope of this work. Questions about such modification should be directed to Lockheed. The limit on most accounts has recently been increased to 400.

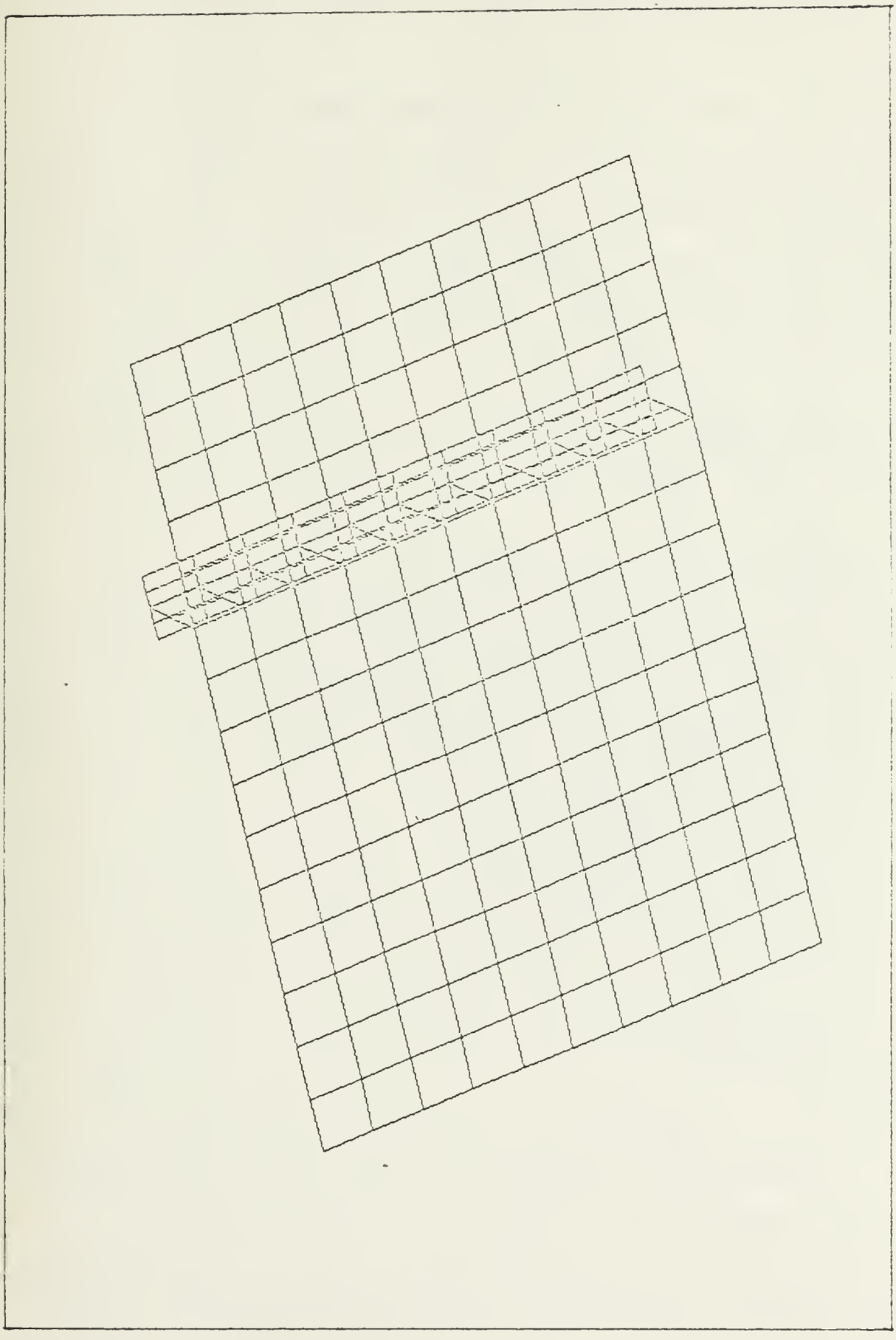

Figure 4.3 Quarter Model of Tee-Stiffened Plate

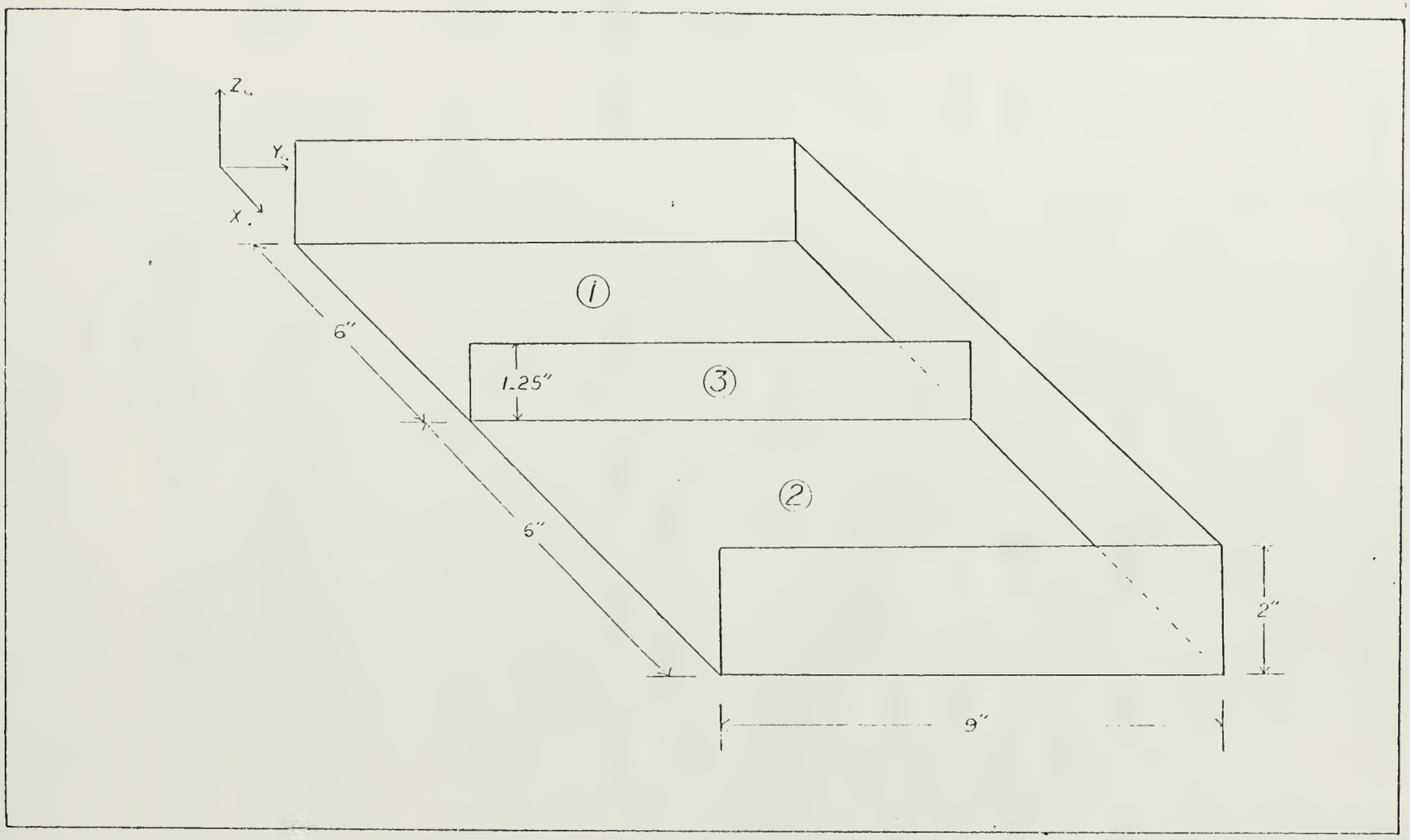

Figure 4.4 Shell Units for Rectangular-Stiffened Plate

necessitated by the use of a half-plate model instead of a quarter-plate set the total number of fluid elements beyond that number when the 0.6 inch element was used. Rectangular elements 1.2000 inches by 1.2857 inches were chosen for the base shells in order to allow strain gage placement at the center of each shell. Elements for the stiffener shell were 1.2857 inches by 0.6250 inch. This corresponded to 6 nodal rows and 8 nodal columns for shell units 1 and 2, and 3 rows and 8 columns for shell unit 3 (Fig. 4.5).

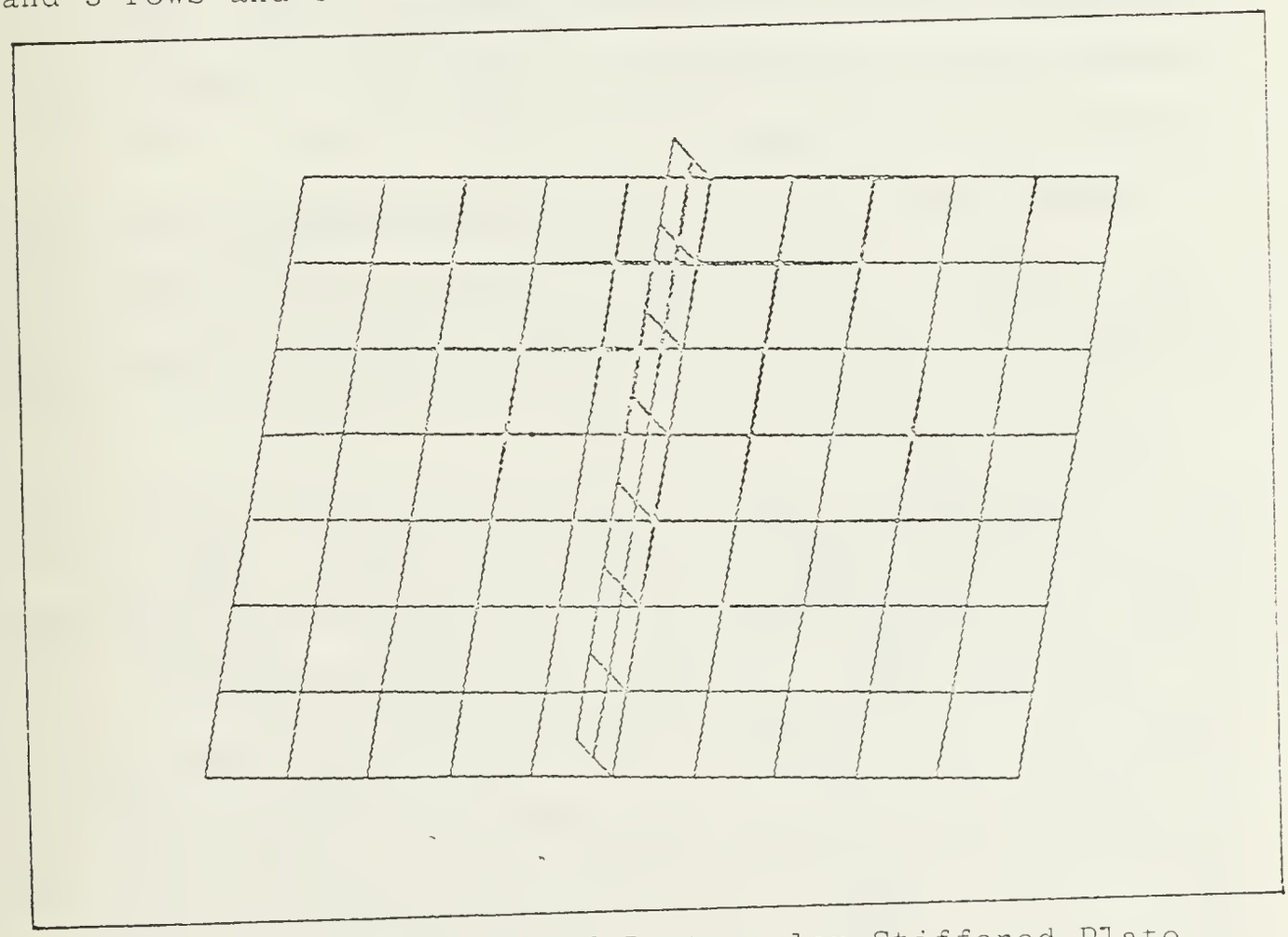

Figure 4.5 Half Model of Rectangular-Stiffened Plate

For the final model of both the tee-stiffened and rectangular-stiffened plates, the finite element mesh was placed at the mid-planes of the shell units. This was not

originally done. In an attempt to make the USA-STAGS output correspond directly to the strain gage outputs from underwater testing, the plates were modelled with the meshes placed on the surfaces of the plates which corresponded to the surface of strain gage mounting. The half-thickness of the plate was then input as the ECZ value on the M-5 record, thereby defining the true mid-plane for the code. This procedure worked extremely well for elastic runs. As stated in the previous section, however, the Gaussian quadrature that STAGS uses to calculate the plastic responses across the mesh surface is incapable of handling the integrations at any but the mid-plane.[25]

For each of the test plates, maximum advantage has been taken of geometric symmetries in order to reduce the size of the finite element model. For the tee-stiffened plate this

---

[25]This important point is reiterated here because it may not be immediately apparent from the STAGS run. The experence gained here seems to indicate that when a negative eccentricity is input to the code, perfectly reasonable (but wrong!) strain approximations are obtained. The first indication of error in this method for correlating STAGS and strain gage data arose when a run with a positive eccentricity was attempted. Under those conditions, STAGS produced no strain data at all. This inability of STAGS is not incapacitating, but it is inconvenient for it means that the data generated in the computer run will have to be converted to correspond to the strain gage information. In theory this is simply a matter of multiplying the plate half-thickness by the curvature calculated in the run and then adding or subtracting that from the mid-plane strain. Given the massive size of the STAGS output, however, this means that either special processors will have to be employed or a conversion program will have to be written.

presents no further complications since the resulting quarter model is non-symmetric. For the plate with the longitudinally oriented rectangular stiffener, however, the result of half plate modelling is that the stiffener itself lies on a plane of symmetry. This presents a problem for STAGS. Although deformations along the symmetric plane will be calculated, no lateral displacements will be recognized since, as far as STAGS is concerned, forces on either side are equal. This both affects the validity of the displacements that are calculated and causes a failure to indicate stiffener tripping. STAGS solves this problem by allowing the user to either input initial geometric imperfections in the shell reference surface or specify that the code generate random imperfections. As stated in the previous section, this is done by flagging the IWIMP and IRAMP variables on the M-5 record and then following the flow directions listed in the manual through the M-7A record. For the rectangularly stiffened plate used here, imperfections in the first three harmonics of 0.001 inch were specified.[26]

Finally, although not strictly related to plate discretization, there is one other point not mentioned in the STAGS user's manual, but which is essential if the computer code is to successfully compute plastic deformations. If

---

[26]See the STAGS1 inputs for the rectangular stiffened plate in Appendix C.

plasticity is to be included, the variable IPLST on the I-1 record must be set to some value between 0 and 4 to indicate which of four plastic strain theories should be used.[27] A non-zero positive value must also be specified for the variable NESP. This NESP value specifies the number of data points on a stress-strain curve for the plate material which will be input to the I-3 record. There are two points that the user's manual fails to make clear about these stress-strain points. First, this curve requires stress and engineering strains beyond the yield point. Second, the first point of the curve must correspond closely to the modulus of elasticity of the material specified in the I-2 record.[28] All the material and stress-strain characteristics for the 6061-T6 aluminum used to manufacture the test plates here were taken from the Military Standardization Handbook, Metallic Materials and Elements for Aerospace Vehicle Structures [Ref. 14: p. 3-184].

---

[27]The default value, 0, automatically triggers use of the White-Besseling theory, as does the set value 1.

[28]That is, the slope from the origin to the first point specified must be the modulus of elasticity. The White-Besseling theory will apply approximations to attempt a patch-up. If the discrepancy is large, however, continuity between the elastic and plastic responses will be lost and the resulting output will be in error.

V. TESTING THE CODE

A. MODAL TESTING

Determination of a structure's mode shapes and natural frequencies can provide a first test of a finite element code's ability to predict the dynamic responses of an excited system. Perhaps of even more importance to the purposes of this study, it can be an excellent check of the structural data input to the code. Failure to provide proper connectivity between shell units or inaccuracies in the input dimensions or material properties will show as gross discrepancies in the modal analysis.

The Naval Postgraduate School is fortunate to be one of the few institutions to have a Hewlett-Packard System 5451C Fourier Analyzer with modal testing capability.

The technique used by the H-P 5451C is in many ways similar to the solution processes used by the finite element codes themselves for it involves solving basically the same governing equation of motion [Ref. 15].

$$M\ddot{\chi} + C\dot{\chi} + K\chi + f = 0 \qquad \text{(eqn 5.1)}$$

Since both χ and f are functions of time, the transfer function, $h(\chi)$, may be found by taking the Laplace transform of Equation 5.1

$$B(s)X(s) = F(s) \qquad \text{(eqn 5.2)}$$

where,

$$B(s) = Ms^2 + Cs + K \qquad \text{(eqn 5.3)}$$

and,

$$H(s) = B(s)^{-1} \qquad \text{(eqn 5.4)}$$

If the exciting forces and displacements are known, H(s) may be readily found by solving the equation which results from substituting Equation 5.4 into Equation 5.2, namely

$$H(s)F(s) = X(s) \qquad \text{(eqn 5.5)}$$

For an oscillating system of order n, the transfer function will have 2n poles occurring in complex conjugate pairs. Each pair of poles will cause a mode of vibration in the structure. Each of these poles is a complex number which may be expressed as

$$P_k = -\sigma_k + \omega i_k \qquad \text{(eqn 5.6)}$$

where σ_k is the damping coefficient and ω_k the natural frequency for that mode.

Once σ_k and ω_k have been determined, the resonant frequency Ω_k (in radians per second) and the damping ratio ζ follow directly.

$$\Omega_k = \sigma_k^2 + \omega_k^2 \qquad \text{(eqn 5.7)}$$

$$\zeta = \frac{\sigma_k}{\Omega_k} \qquad \text{(eqn 5.8)}$$

The exciting forces and displacements that must be provided to the system may be found in a number of ways. The method chosen here was to excite the plate using a modally tuned impulse hammer.[29] An accelerometer[30] was attached to the plate to record the resulting accelerations, from which displacements were found by numerical integration.

The two fundamental assumptions of this test procedure [Ref. 15] are that:

1. Modal frequency and damping are constants for any transfer function taken from the structure.
2. Modes of vibration can be excited from anywhere on an elastic structure except at their node lines (where no excitation is possible).

It should therefore be possible to describe all modes of interest by simply choosing a sufficient number of excitation points on the structure and by placing these points close enough together to minimize the possibility of replication.

For the two plates used in these tests (the rectangular- and tee-stiffened test models), nine points of excitation

---

[29] PCB model 086B03.

[30] PCB model 302A07.

were chosen on the back of each plate.[31] Care was taken to avoid symmetric placements of the points.[32] The accelerometer was fixed at a single location arbitrarily chosen but spaced away from the clamped boundaries.

When any location was tapped with the modal hammer, the resulting forces were fed back through the hammer to the Fourier Analyzer; as were the accelerations from the accelerometer. The Fourier Analyzer then computed the displacements and solved the Laplace transform to create the plot shown in Figure 5.1. Each of the peaks in this representation corresponds to the poles of the transfer function for a single point of excitation. By then combining the plots for all points, an accurate representation of the system modes was obtained. It was then simply a matter of analyzing each of the poles in descending order of magnitude to whatever total number of modes is of interest to the user to determine the dominant modes of the system.

B. UNDERWATER SHOCK TESTING

Underwater explosion testing for all studies conducted in this series to date has been done at the West Coast Shock Test Facility (WCSF), located at the old Hunter's Point Naval Shipyard near San Francisco, California. This is a

---

[31] The plates were placed face downward upon a solid marble slab.

[32] The actual number and spacing of the excitation points seems to be primarily a matter of experience.

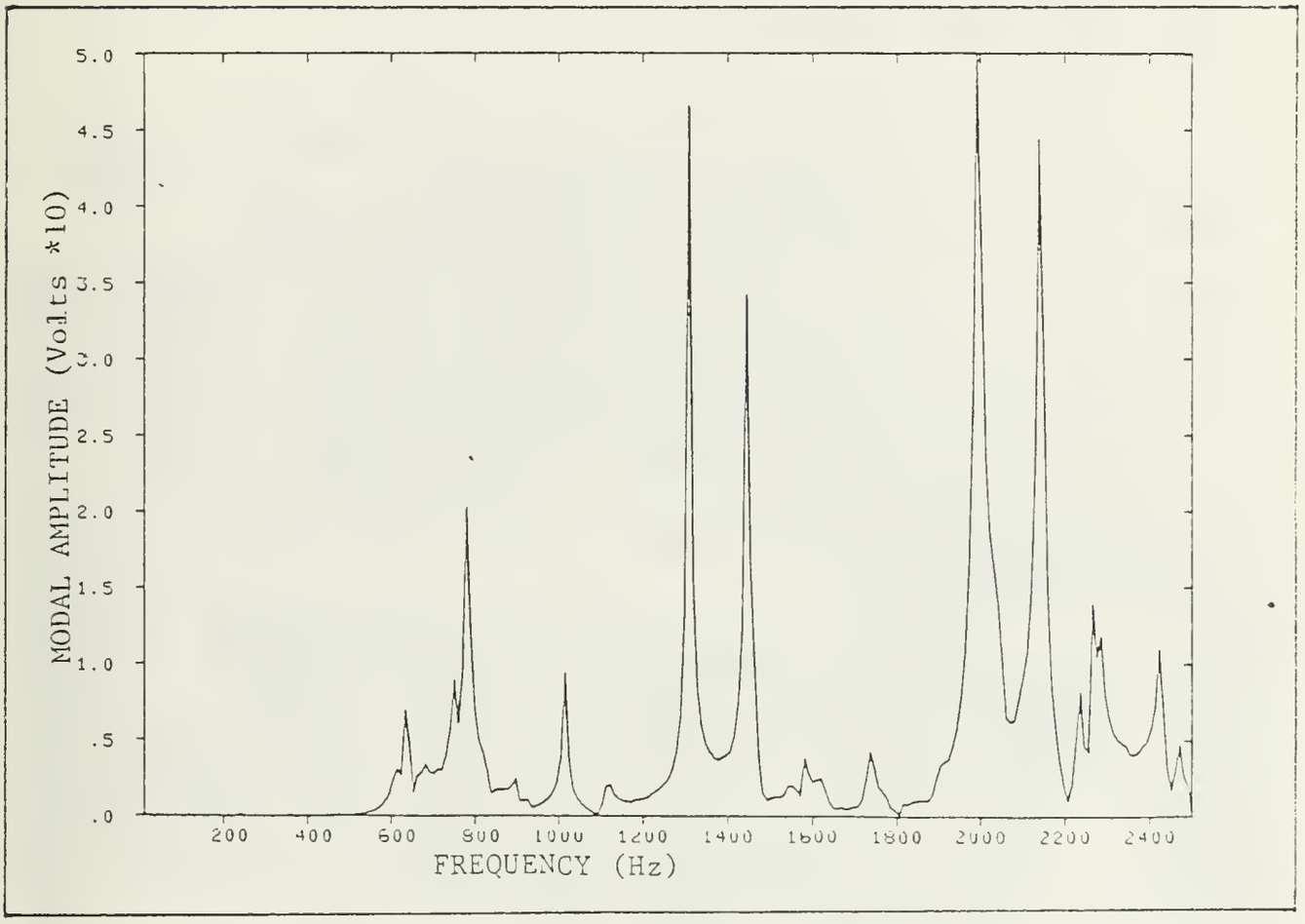

Figure 5.1 Typical Modal Test Plot

Navy activity reporting to the Supervisor for Shipbuilding, Conversion, and Repair, San Francisco. As the only licensed facility of its type on the West Coast, they have gained a considerable amount of experience in conducting underwater explosion testing; although most of it has been large scale work in support of the Navy's shock qualification program rather than experimentation.

1. The Test Platform

In order to provide the air backed condition that was required to simulate a ship's hull and to ensure rigidly clamped boundary conditions, the test plates used in this series of studies were securely bolted to a heavy steel backing structure (Fig. 5.2). This structure consisted of a box constructed of 1¼ inch thick A6 structural steel. A wide flange was welded around the open side of the box to which the edge of the plate was bolted. An O-ring gasket was fit into a channel machined into the surface of the flange to provide watertight integrity. Access to instrumentation on the inside of the box was allowed by a submarine style penetrator affixed through the bottom.[33]

To perform the actual testing, the plate and backing structure were suspended by heavy steel cables below two large pneumatic floats in the configuration developed in

---

[33]For a more complete description of this backing structure and the rationale used in designing it, see Reference 3, pp. 88-94.

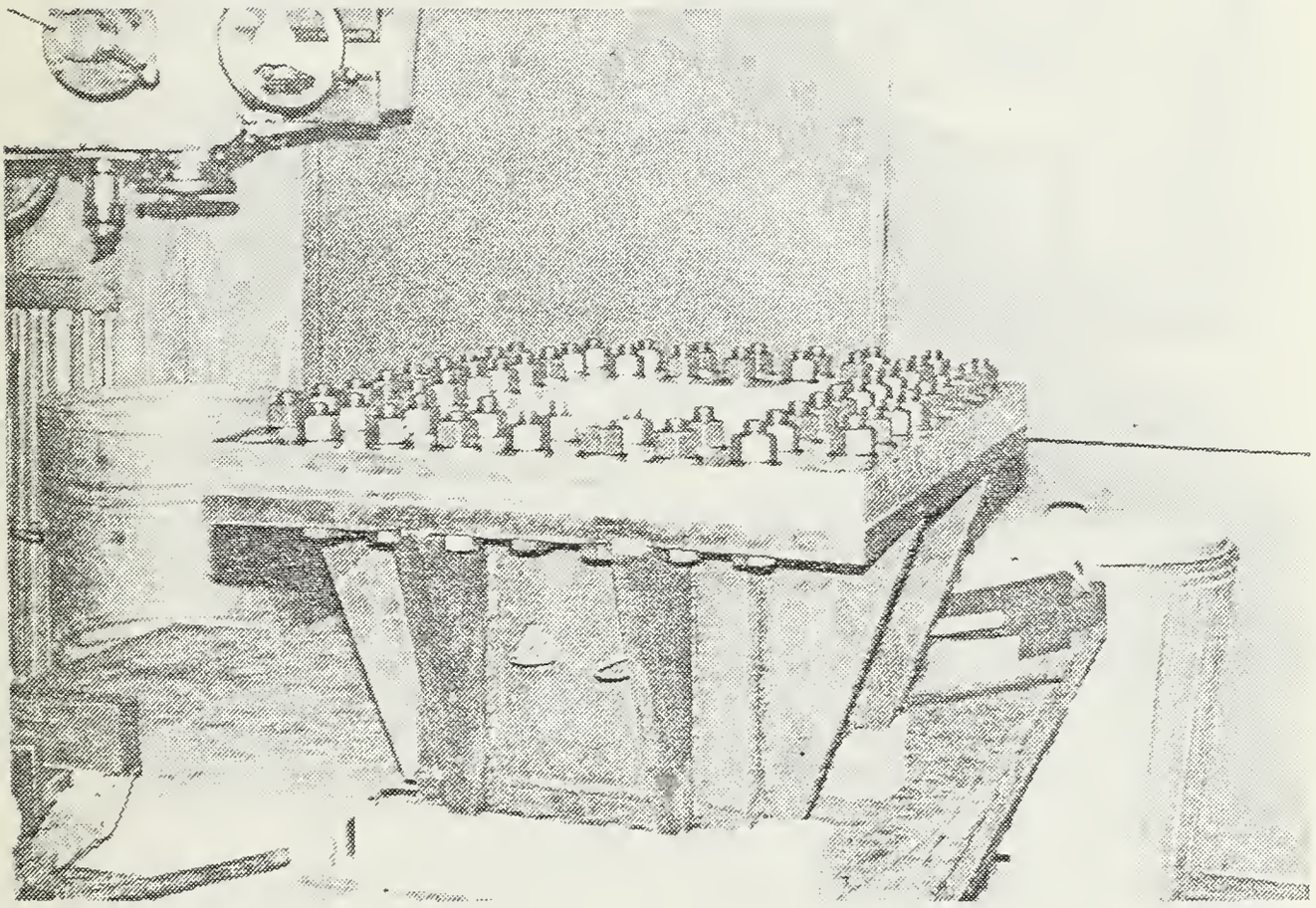

Figure 5.2 Test Plate and Backing Structure

Chapter 2 (Fig. 5.3). The cables were cut to length to assure that the nearest edges of the test panel stiffeners were maintained at depths as close to thirteen feet below the surface as possible. Once the entire apparatus had been towed into the bay, the explosive charge was lowered into position nine feet above the stiffeners in line vertically with the center of the plate.

2. Instrumentation

In his work, which has already been cited several times, LT Rentz outlined the basic theory governing the test of the flat plate and began developing the procedures which will be enlarged upon here.

Essentially, the information sought for comparison with the computer simulation codes being tested has been:

1. Fluid pressures at the plate and in the freefield.
2. Strain in the plate.
3. Final deflections in the plate.

Instrumentation used to gather this data was as follows:

a. Pressure Measurements

Three pressure gages were used in the tests conducted here. Two of these were located just as they had been in the previous study [Ref. 3: p. 46]. One was located one foot above the center of the plate and the other was clamped to the aluminum block bolted to the side of the plate. The forward edge of this second pressure gage was

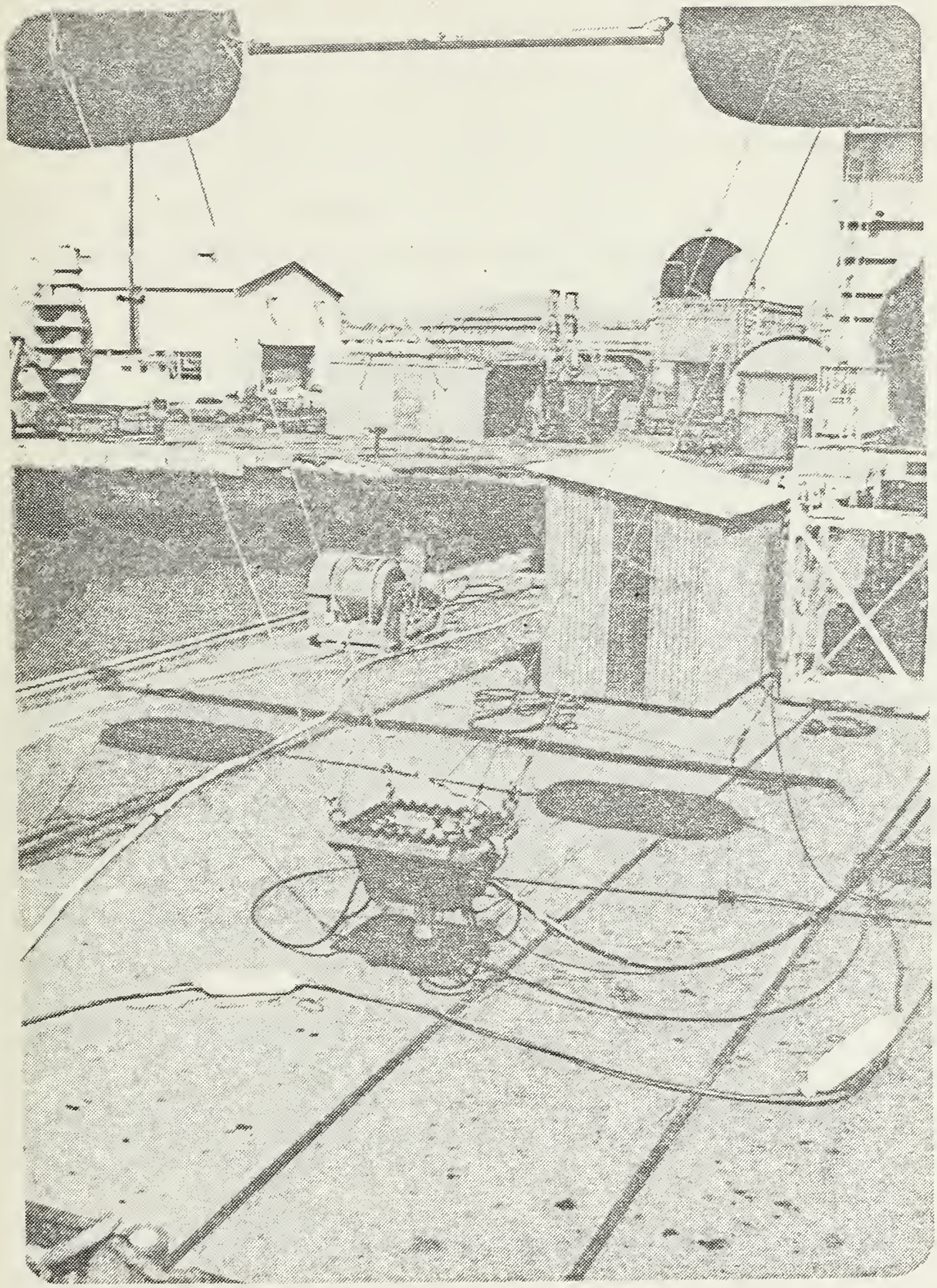

Figure 5.3 Test Platform

positioned so as to be on an arc of the same radius as the standoff distance.

The pressure recordings that had been obtained from these two gages had been so subject to interference from the plate structure and the rigging of the test platform that the futility of conducting further tests without a true free field pressure gage was readily obvious. Accordingly, although the first two gages were retained as backups, a third gage was positioned on an arc equal to the standoff distance but removed five feet from the centerline of the plate (Fig. 5.4). As will be discussed in the following chapter, the results obtained from this gage during the test shot on the tee-stiffened plate were excellent.

All tests in this series utilized one-quarter inch tourmaline crystal pressure gages rated to 10,000 psi. The response ratio,[34] R_p, is a function of the decay constant for the charge, θ, divided by the transit time of the shock wave across the gage, t_D [Ref. 16]. For the eight pound TNT charge chosen as the standard for these studies,

θ = 0.15 msec

---

[34]Defined as the ratio of the apparent peak pressure to the actual peak pressure.

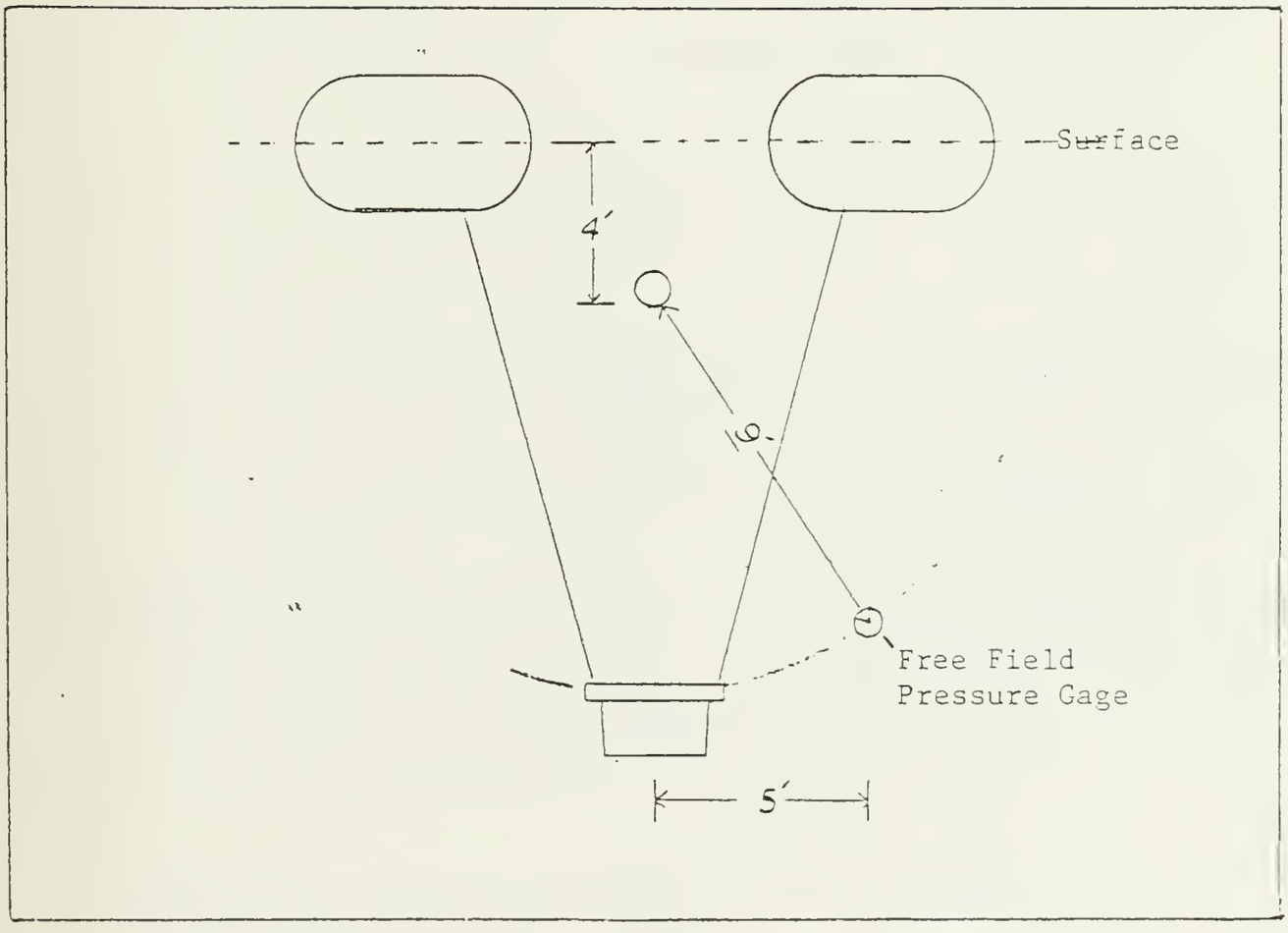

Figure 5.4 Location of Free Field Pressure Gage

For a quarter inch gage,

$$t_D = \frac{0.25 \text{ in}}{60{,}000 \frac{\text{in}}{\text{sec}}}$$

$$= 4.167 \times 10^{-6} \text{ sec}$$

Applying the correction factor for the oil-filled protective boot which surrounds the crystal,

$$1.5\ t_D = 6.25 \times 10^{-6} \text{ sec}$$

Thus,

$$\frac{\theta}{1.5\ t_D} = 24$$

From the chart on page 17 of Reference 16.

$$R_p = 0.9733$$

This indicates that a very good correlation can be expected between the actual and measured pressures, and is also the best indication that the correct gage size is being used.

b. Strain Measurements

Perhaps the single most critical aspect of obtaining successful data from underwater explosion testing of the type conducted here is the choice and application of the strain gages.

For the tee-stiffened plate, twenty SR-4 type FAE-25-12-S13ET strain gages [35] were attached as shown in Figure 5.5. These were the same type used in Reference 3; and, although rated to only 2000 microstrain, it had been demonstrated that their range could be extended sufficiently to provide useable data over the very earliest increments of the shock response. As in the earlier test, BLH's SR-4 Permabond 910 was used as the fixative, and the attached strain gages and their wiring was covered with PR-1422 A-1 Base Compound, manufactured by Products Research and Chemical Corporation of Glouster City, NJ.[36] This base compound was also used on the plate with the rectangular stiffener where 19 MX type PAHE-250BA-350EN strain gages[37] (Fig. 5.6) rated to approximately 200,000 microstrain were used in an attempt to increase the time span over which information could be gathered. Also, at the recommendation of the distributor, BLH type EPY-150 epoxy adhesive was used instead of the Bondo 910.[38]

---

[35] Manufactured by BLH Electronics of Waltham, MA.

[36] This was done to provide and smooth compliant covering that would keep the gages and wiring from being torn off with the passage of the shock wave, and to seal the gages from saltwater once the rig was submerged.

[37] Manufactured by Experimental Stress Analysis Products.

[38] In theory, the epoxy provides a stronger bond than does the Bondo, which is a contact-type adhesive.

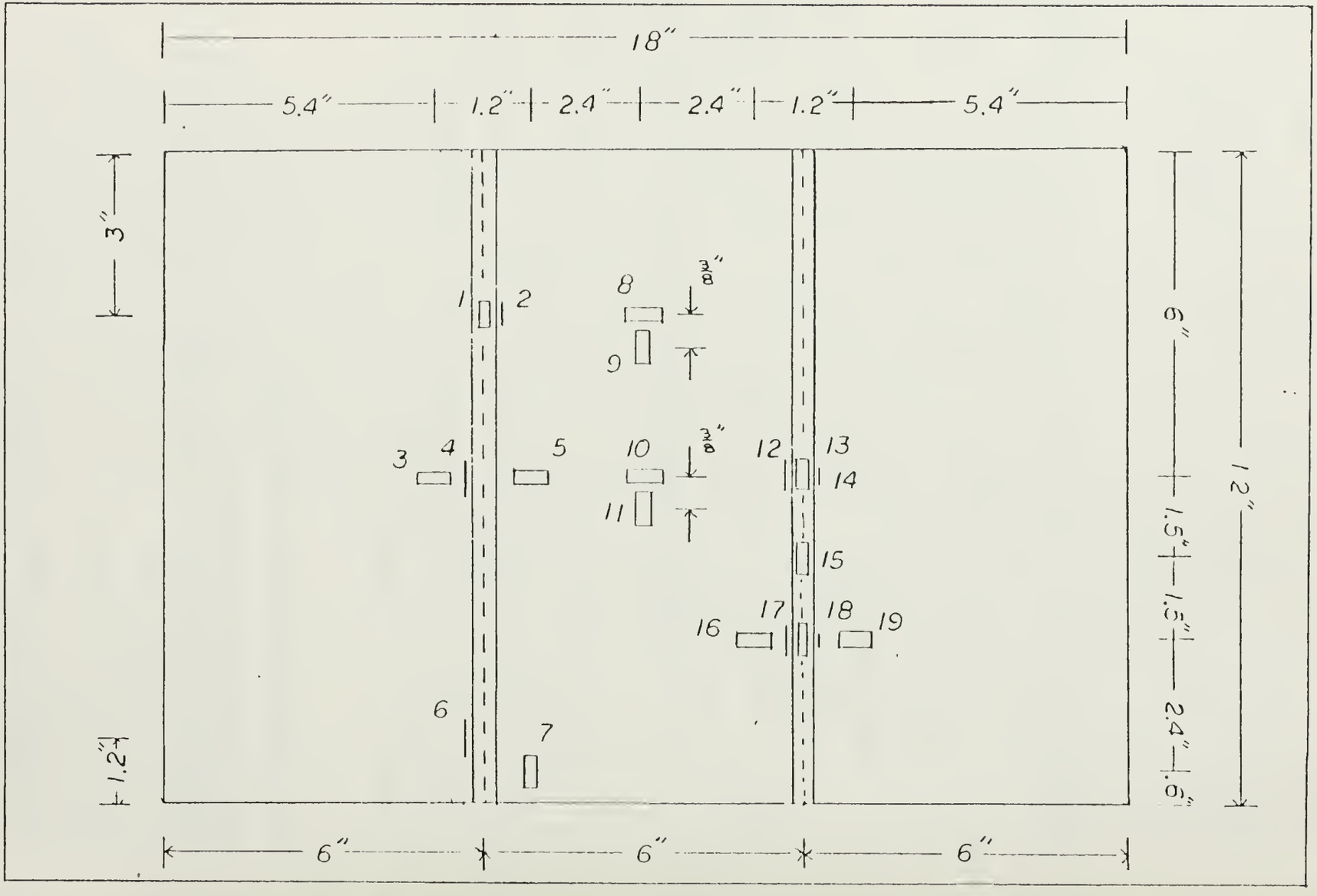

Figure 5.5 Strain Gage Placement on Tee-Stiffened Plate

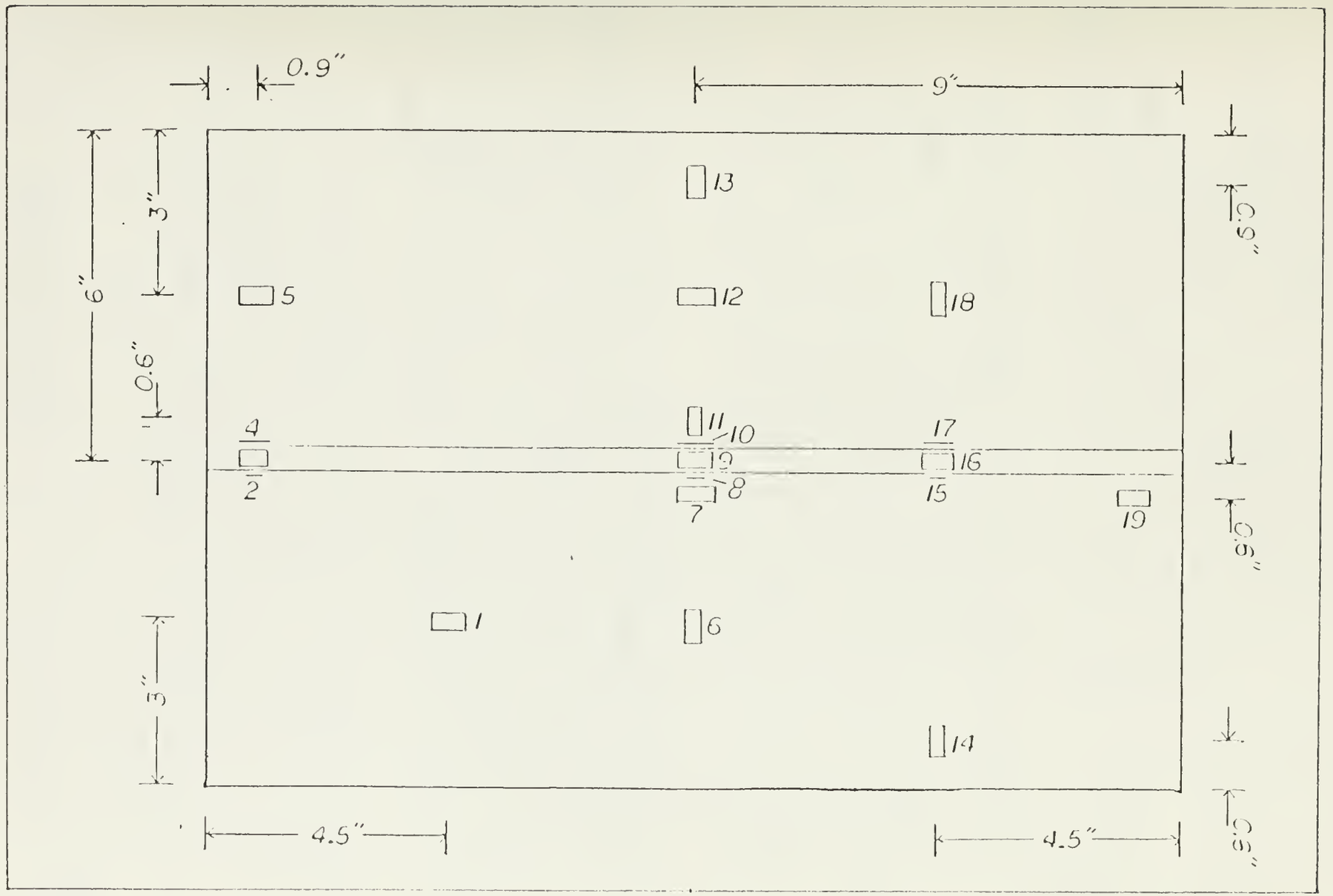

Figure 5.6 Strain Gage Placement on Rectangular-Stiffened Plate

In practice, although some useful data was obtained from each test, neither was a particularly successful source of strain information. The number of gages lost far exceeded the number that performed.

In recapitulation, a number of faults were found for which the following corrective measures have been proposed.

1. Although the MX type strain gages greatly exceed the strain requirements expected in these tests, their use is strongly recommended. Little or no loss of accuracy is experienced in the lower strain regions through use of the high-elongation gages, whereas mid-range gages tend to peak right at the strain ranges expected.
2. On any strain gage, the weakest points are the soldering tabs to which the gage wires are attached. These are brittle and will break if any bending stress is applied. All motion should be restricted to the plane of the gage. This means that the strain gage wires must be extremely flexible so that any bending motion, either during installation or as a result of plate deflections, is not transmitted to the gage tabs. Rated strain gage wire is recommended.[39]

---

[39]On the tee-stiffened plate, 28 gage wire made specifically for strain gages was used. This proved to be quite

3. Even with flexible strain gage wire, a determined force along the length of the wire, as would be experienced during plate deformation will break the tab, the wire, or the solder connection between the two. Although a plastic medium, the PRC Base Compound used to protect the gages and wires was not flexible enough to allow the wires to expand with the plate.[40] A suggested solution to this problem is to lay the gage wires with some s-curves to allow elongation as the plate deforms. The wires should not, of course, be otherwise affixed. A piping of Barrier WD, a tacky, semi-fluid substance manufactured by BLH which

---

satisfactory as far as the gages themselves were concerned, but presented definite problems on the human side of the equation. The wire was so fine that it was impossible to work with it. It also proved to be highly vulnerable to damage while the test structure was being transported or handled. For the following shot, the attempt was made to use 20 gage bell wire. This withstood handling magnificently, but was too stiff for the soldering tabs. Annealed 22 or 24 gage wire designed specifically for use with strain gages appears to be the best possible choice.

[40]This base compound seems to be an extremely protective medium. A couple of cautions should be issued governing its use, however. First, while the compound must be used within one hour of mixing base and accelerator, enough of that time should be dedicated to stirring to ensure that the compound is thoroughly mixed. Although this observation is not completely confirmed, it appears that insufficient mixing leaves a residual which can permeate wiring insulation and actually destroy very fine copper wires. Second, the compound is not compatible with the Gage Cote lacquer normally painted over strain gages as a sealant. If the base compound is to be applied directly to the strain gages, Gage Cote should not be used.

looks somewhat like a combination of beeswax and petroleum jelly, could then be applied over both gages and wires.[41] This piping of Barrier WD should then be covered by a layer of aluminum foil and then the whole overlayed by the usual PBC Base Compound. The net effect is an armored "tube" of Barrier WD through which the wires can run when the plate deforms.

4. The fixative used to attach the strain gages should, itself, be a subject for careful consideration. Even though the epoxy is supposed to be the stronger medium, experience gained here indicates that it is not as satisfactory as the Bondo for explosion testing. The postulated reason for this seeming discrepancy is that the epoxy places a thicker layer of adhesive between gage and plate material. Given the extremely rapid loadings experienced, intense shears are created in the thicker substance and the epoxy literally cracks and spalls off. The Bondo 910 therefore seems to be the preferable adhesive.[42]

---

[41] A bakers pastry tube works very nicely to do this.

[42] No failures due to loading were noted in the strain gages attached with Bondo. Therefore, Even if the cracking problem had not occurred in the epoxy, the greater separation between gage and plate material that the epoxy creates would argue in favor of the Bondo.

c. Plate Deflections

Plate deflections were by far the most reliable source of data that could be obtained as a result of testing since no electronics were involved. To get these, precise measurements were made at specified points on the plate both before and after the test shot. A jig was devised which took advantage of the rigid plate boundaries to provide a reference table for a dial indicator depth gage (Fig. 5.7). All measurements were made while the test plate was bolted onto the backing structure to ensure that plate warpage did not affect the readings.[43]

C. DATE RETRIEVAL

Signals from the gages mounted on and about the test plate were fed back through shielded cable to a common floating terminal box. From there, they were passed to an instrumentation shack located on one of the jetties defining the small bay in which the testing was conducted. A schematic of the setup is shown in Figure 5.8. Calibration levels were applied to all pressure signals by Endevco Model 4470 Signal Conditioners. These same signal conditioners were used to provide calibration for all but twelve

---

[43] Deflections have already been given for the rectangular stiffened plate in Figures 3.7 and 3.8. No post-shot measurements were made of the tee-stiffened plate because of the heavy damage which was inflicted when the plate was hit by one of the supporting cables.

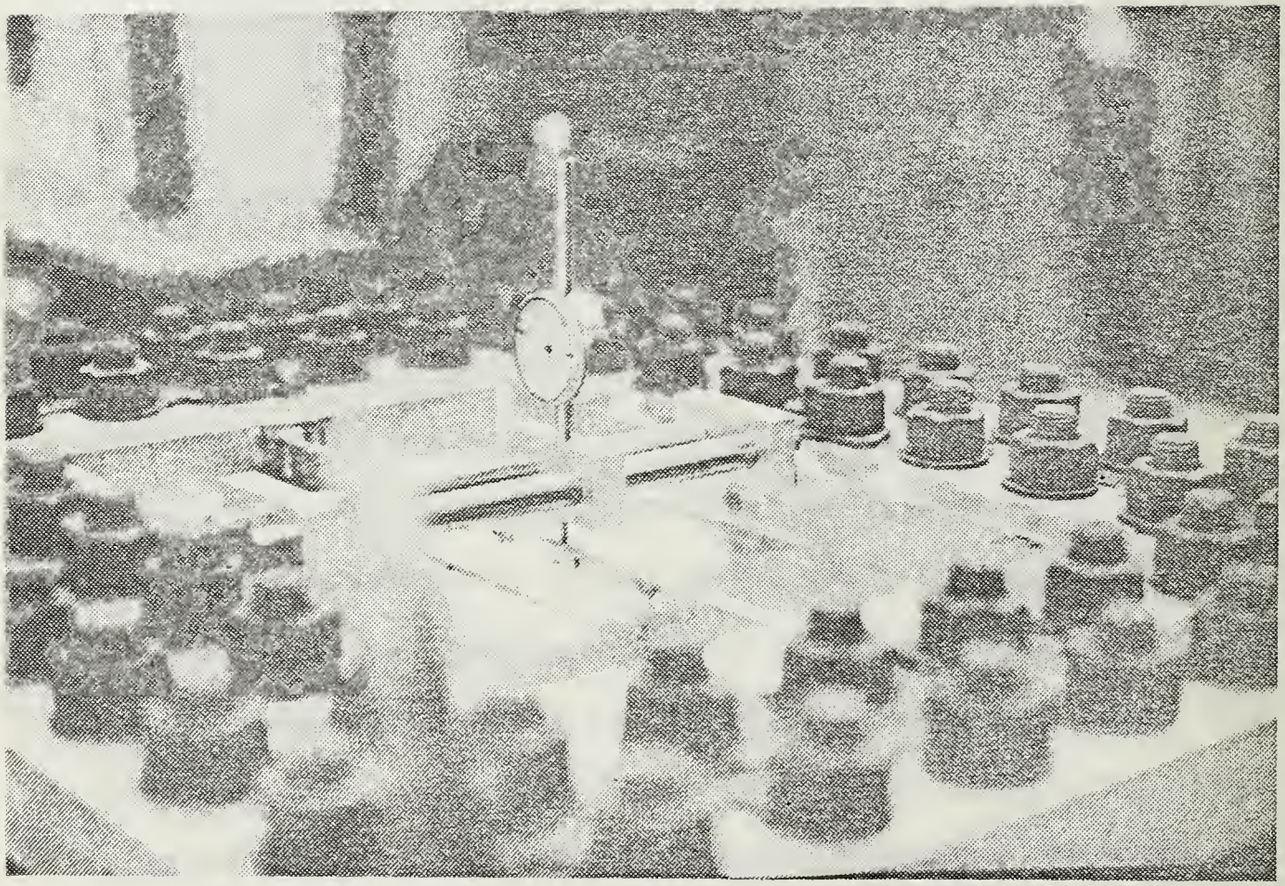

Figure 5.7 Jig Used to Measure Plate Deflections

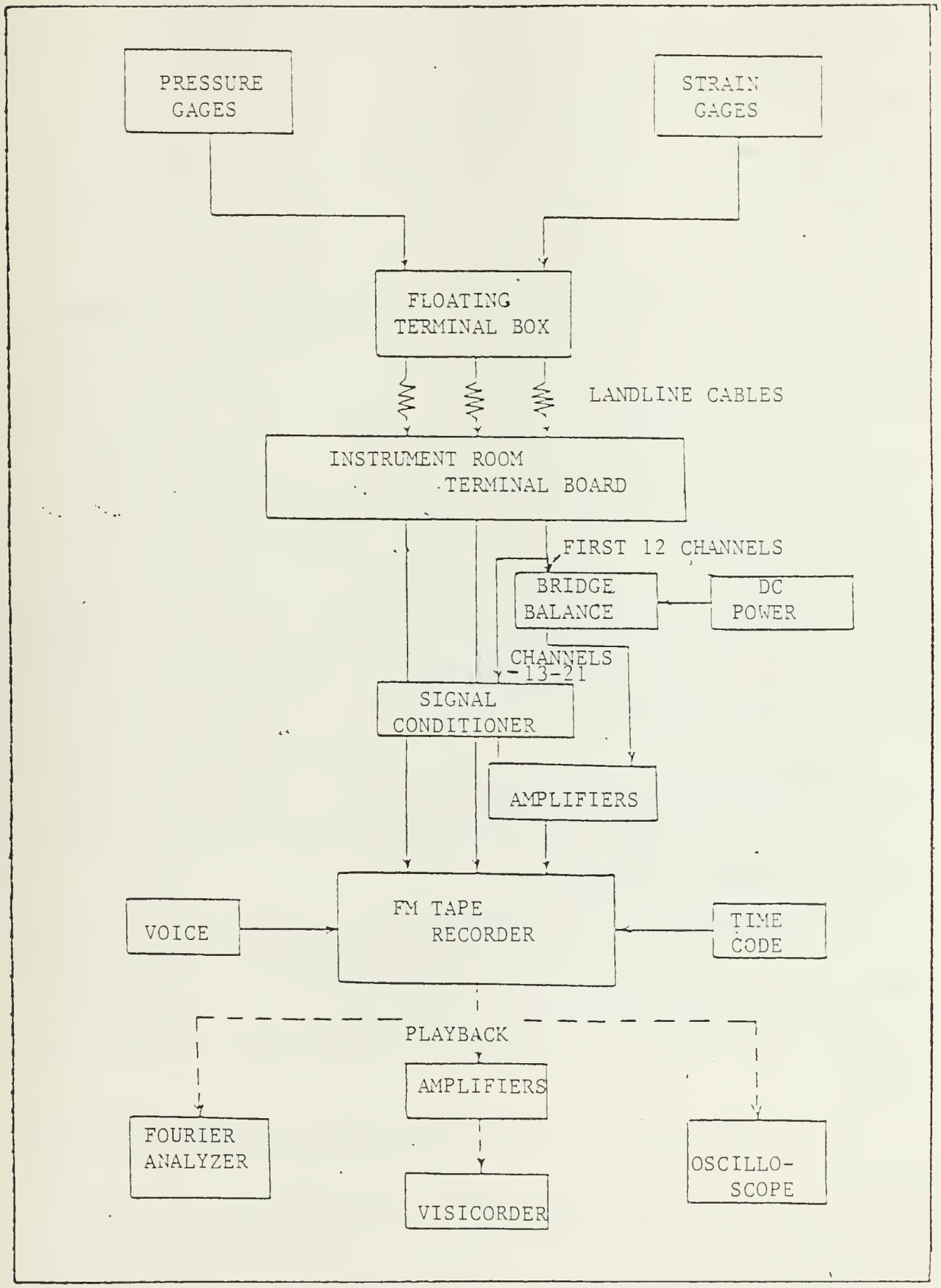

Figure 5.8 Flow Chart for Electronics Set-Up at WCSF

of the strain gage channels. Those remaining twelve channels were calibrated by two six-channel Honeywell Model B2-6 Universal Bridge Balance units. The strain gage signals were then amplified by Bell and Howell CEC 1-168 DC amplifiers before final recording. All signals were recorded on two twelve channel Ampex FR 1300 tape recorders.

Calibration levels for the tourmaline crystal pressure gages were all set at the 10,000 psi theoretical maximum. For the strain gages, however, attempts were made to use the computer codes to provide estimates of expected strains using the pressure and decay constant calculated from Equations 2.2 and 2.3. This was especially critical for the strain levels for the tee-stiffened plate where some of the strain gages were expected to be operating at or beyond their rated limits.

Unfortunately, difficulties encountered in learning to use the USA-STAGS code prevented runs from being made before the shot dates.[44]

Advantage could have been taken of earlier estimates used for the plate tested in Reference 3 if the charge weights had remained the same; however, such was not the case.

Since 8 pound TNT charges are listed as Navy standard stock items and order had been placed well in advance, no

---

[44] In fact no successful runs were made until long after all experimentation had been completed.

problems were anticipated in obtaining charges of this size. As the date of the first test neared, however, it became obvious that no 8 pound charges would be available. The nearest alternate that could be provided in time for the scheduled test was a 9½ pound TNT charge.

It can perhaps be appreciated that dimensional changes to the test platform are not simply a matter of moving the charge location. As charge weights are changed, the stand-off distance and the charge depth both must be changed; which involves cutting new supporting cables and recalibrating flotation depths. All of which is extremely time consuming. When the personnel at WCSF were contacted about the possibility of changing the configuration for a 9½ pound charge, they advised that it could not be done in time for the scheduled tests.

The choice for the first test was clear, either run the test with the existing platform and a 9½ pound charge, or abort the experiment. It was determined that more benefit could be gained from conducting the test.

The values for P_0 and θ found from Equations 2.2 and 2.3 for a 9½ pound charge are:

$$P_0 = 4081.7 \text{ psi}, \quad \theta = 0.161 \text{ msec}$$

This initial pressure was markedly higher than that for an 8 pound charge. The maximum bubble radius, too, was

much larger. From Equation 2.6, A_{max} = 14.03 ft. This gives a charge depth to bubble radius ratio of

$$\frac{4 \text{ ft}}{14.03 \text{ ft}} = 0.285$$

which implies that some pressure release will take place into the atmostphere.

For the second test shot, the problem was quite different. As was discussed in Chapter III, the tee-stiffened model appeared too rigid to successfully demonstrate stiffener tripping. The plate with the longitudinal rectangular stiffener was a largely tentative attempt to produce that action. It was desired to view the responses of the stiffener under a variety of loadings, beginning with small charges and concluding with ones in the 8 to 9½ pound range. Again use was made of what was available. In this case, the available charge weight was ½ pound.

For a ½ pound charge, the maximum bubble radius is 3.02 feet; which leads to a charge depth to bubble radius ratio of 1.33. This implies that bubble pulsation will be a problem. Fortunately, however, the time of the pulse is relatively late, t = 0.17 seconds. Thus, by limiting the period of study to early times the bubble pulse can be effectively neglected.

Calibration levels for the test shot on the tee-stiffened plate were determined by making an EPSA run on the plate model used in Reference 3 but with a 9½ pound charge

weight. As has already been stated, geometric similarities between these two plates permitted broad generalizations to be made between them even if exact comparisons could not be drawn. The results of that run are shown in Table III.

No similar comparisons could be made with the plate with the longitudinal rectangular stiffener. Strain gage calibrations were therefore arbitrarily set at a value at the higher end of the strain gage range which could be expected to exceed all requirements. In this case, that value was 150,000 microstrain.

The results of these tests will be discussed in the next chapter.

Table III

Calibration Data for Tee-Stiffened Plate

Gage	EPSA Strain*	Gage	EPSA Strain*
1	6210	11	76800
2	6210	12	7610
3	17600	13	7610
4	8500	14	8510
5	21700	15	7610
6	69400	16	21700
7	69400	17	6210
8	69400	18	6210
9	100000	19	17600
10	49500	20	58200

*All values in microstrain.

VI. RESULTS AND CONCLUSIONS

A. MODAL COMPARISONS

As stated in chapter four, the primary purpose of modal testing is to provide a check of the finite element model. A properly constructed model should exhibit substantially the same fundamental frequency as that determined by modal testing and should demonstrate close coincidence with other frequency values across the range tested. Exact concurrence cannot be expected since the computer code is analyzing an idealized model which will not be affected by the externalities inherent in the actual test. Also, the number of frequencies determined by the computer is a function of the number of iterations than can be made over a given time span. Certain economies in the use of computer time must therefore be observed. While the code might be able to calculate the frequencies for a large number of modes; such calculation will be purchased with a heavy expenditure in CPU time which is not really necessary for an adequate check.

Accordingly, the scheme followed here has been to limit the number of modal frequencies computed by the code to those that could be determined in two runs for each plate. Each of these runs can be performed entirely within the

combined STAGS1/STAGS2[45] processor without reference to the USA add-on. The first run simply specifies a broad range within which the computer can search for eigenvalues; the second uses one of the mid-range frequencies determined from the first run eigenvalues as a "seed" for further iterations in order to produce a refined product.[46] The actual performance of these functions is controlled by the D-2 and D-3 records ofthe STAGS input deck. Since the procedure is outlined clearly in Reference 13 and example input files are provided for both the tee-stiffened and rectangular stiffened plates in Appendix C, further elaboration will not be provided here.

Modal testing of the milled plates was conducted in the manner described in Section D of Chapter IV. The results of both that testing and the STAGS2 estimates are provided for comparison in Tables IV and V tee-stiffened and rectangular-stiffened plates, respectively.

It will be noted that, for each of these plates, the STAGS2 predicted values seem to correspond very well with

---

[45]Generally referred to here as a STAGS2 run.

[46]Since, in this case, modal testing of the milled plates was conducted prior to the computer runs, essentially the same frequency range was used for the computer runs as for the testing. Over this range, the first STAGS2 run will compute five modes with their corresponding natural frequencies. Although the user's manual states that calculation of up to twenty eigenvalues can be specified, and that all existing eigenvalues up to that number will be computed, five seems to be the true maximum. No increase in the

Table IV

Modal Comparisons for Tee-Stiffened Plate

Measured Resonant Frequency (Hz)	STAGS2 Predicted Modal Frequency (Hz)
629.7410	
653.2053	
721.1747	
772.3517	772.7611
793.0253	
1022.4708	957.8445
1310.2979	
1447.0071	
1448.4597	
1480.9890	
1499.5906	
1551.0845	
1556.0732	
1590.2947	
1747.9771	
1994.4626	
2143.0918	2043.4048
2236.9248	2200.9004
2259.6445	
2275.5000	
2430.0249	
2472.2305	
2571.7832	
	2629.4729

Table V

Modal Comparisons for Rectangular-Stiffened Plate

Measured Resonant Frequency (Hz)	STAGS2 Predicted Modal Frequecy (Hz)
516.5652	
804.2715	790.0587
924.8018	
980.5009	
981.1315	
1001.6130	
1118.0952	1115.3547
1204.4885	
1229.9939	
1365.3230	
1428.2920	
1651.2498	
1651.2747	
1852.1162	1812.0698
2040.0291	2048.0015
2154.0908	2176.5366
2368.5132	
2603.9736	
2725.8828	
	3039.6057

values from the modal testing, the greatest relative error (using the modal test value as a base) being 6.32% for the tee-stiffened plate and 2.16% for the rectangular-stiffened plate, and the average relative errors being 3.16% and 1.12% for the tee- and rectangular-stiffened plates, respectively.

Less promising is the seeming failure of the code to predict the fundamental frequency for either of the plates. It is suggested, however, that this is not due to any errors in the code or in the inputs to the code, but rather is attributable to the fact that the boundary conditions actually tested were not the clamped-clamped conditions specified in the STAGS inputs. The H-P 5451C Fourier Analyzer appears to be quite sensitive to relatively small changes in the boundary conditions. When the tests were conducted, the plates were laid face-downward upon a heavy marble slab. No attempt was made to further clamp the heavy aluminum frame into which the test plates are

---

amount of CPU time allowed for eigenvalue analysis (NSEC on the D-2 record) seems to affect that number. Computation of eigenvalues over a range without any seeding of known values is a slow process prone to convergence problems. It should therefore only be used to derive a value which can be used for the second run; or it can be eliminated altogether if one of the natural frequencies is already known. If such a frequency has been determined, it can be entered directly into the code and all frequencies closest to multiples of a fixed interval (SHIFT on the D-3 record) will be computed. This process is reasonably fast and will produce all existing frequencies up to the number (NEIG) specified.

milled, nor was it possible to ensure an absolutely flush mount between plate and slab.

When the tee-stiffened plate was tested, the bolt holes had already been drilled in the frame. These bolt holes seemed to cause reflections which were picked-up by the Fourier Analyzer as additional modes. These may be observed to some degree in Table IV in the repeated tendency for a group of frequencies to cluster about a single value. The effect was far more noticeable on the oscilloscope traces obtained as each of the excitation points on the plate was loaded.[47] When all of the variables are considered, it is believed that the actual correspondence between the modal test results and the STAGS2 prediction is quite good and provides adequate confirmation of both the code's ability to predict the natural frequencies of a simple structure and of the finite element models input to the code for this study.

B. COMPARISONS WITH UNDERWATER TEST RESULTS

As has already been stated in Chapter V, all underwater shock testing for this series of studies was conducted at the West Coast Shock Test Facility. The outputs from the

---

[47] It is strongly recommended that future modal testing be conducted before the bolt holes are drilled in the frame. An attempt might also be made to weight the frame with sandbags to simulate as nearly as possible the clamped boundary conditions input to the code.

pressure and strain gages used for the tests along with their associated calibration and time signals were recorded by two Ampex FR 1300 tape recorders. After each of the test shots, the data tapes and one of the tape recorders were transported to the Naval Postgraduate School where the tapes were played-back, filtered, and recorded on disk on the H-P 5451C Fourier Analyzer for later analysis and plotting.

As thorough a pretest analysis as was possible without actual disassembly was conducted upon the equipment at the West Coast Shock Test Facility before each shot. Calibration levels for all sensing devices were also checked using technicians and equipment provided by the Naval Postgraduate School. Despite these precautions, the quality of data obtained from the tests was highly problematical.

An excellent free-field pressure history was obtained from the test shot conducted on the tee-stiffened plate (Fig. 6.1); fully compensating the difficulties encountered in mounting the third pressure gage in a position where it would not be affected by interference. As can readily be observed, this curve displays all of the classical exponential decay characteristics predicted in Chapter II. Since this is so, the decay constant will correspond approximately to the time it takes for the pressure to drop to $\frac{1}{e}$ (about .36788) of its peak value. From Figure 6.1, the peak incident pressure was 3125 psi. Therefore,

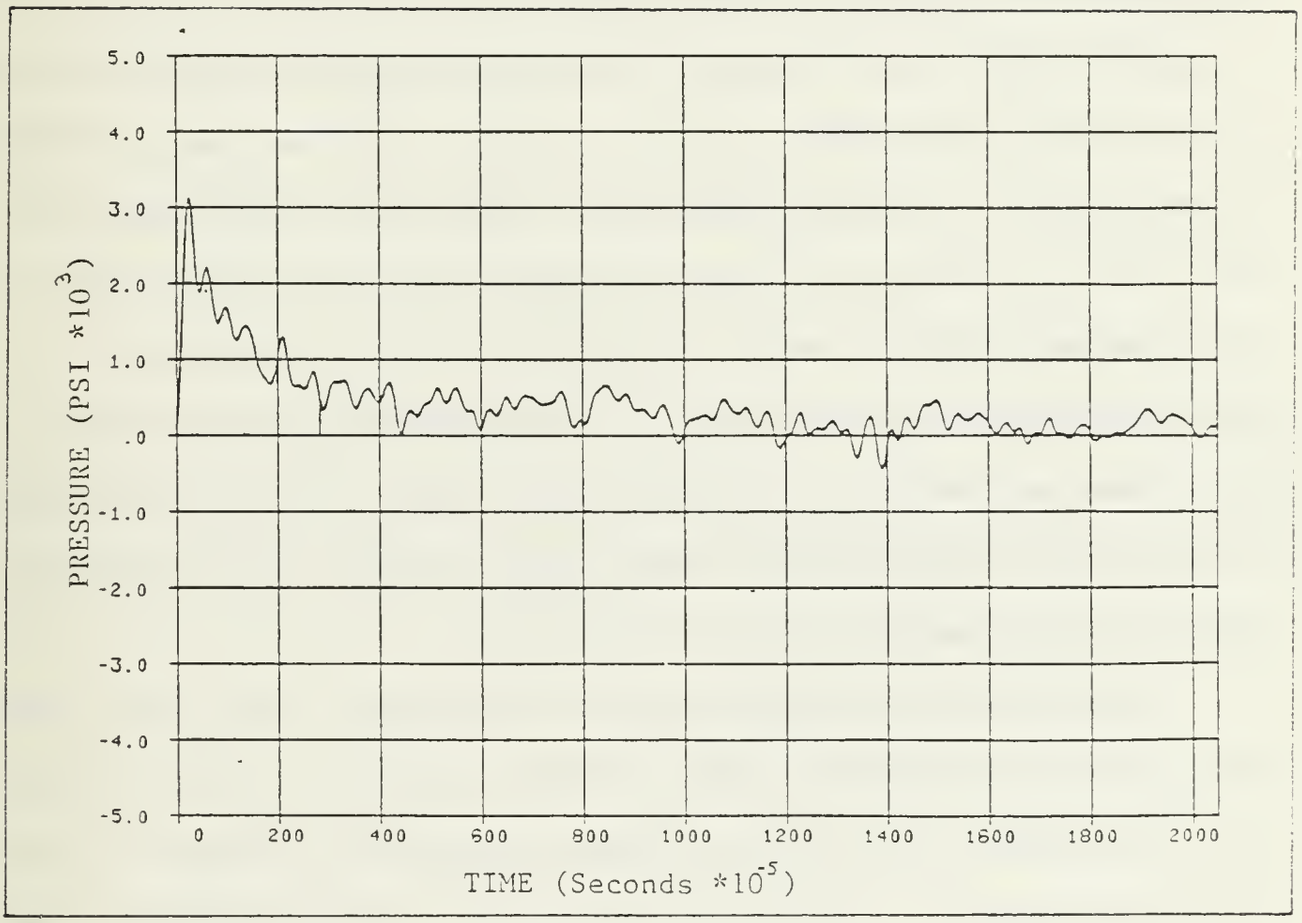

Figure 6.1 Freefield Pressure for Tee-Stiffened Plate

(3125 psi)(.36788) = 1149.6 psi

which occurs at about 1.56 milliseconds.

These values were input to the USA-STAGS code to conduct a post-shot analysis for comparison to test data.

The peak pressure and decay constant obtained from the test results are much smaller than those predicted by Equations 2.2 and 2.3. In retrospect, this is not particularly surprising. First, it will be recalled that Equations 2.2 and 2.3 are derived from empirical results and are therefore subject to wide variations. Even more pertinent, it was found in Chapter V that the ratio of the charge depth to the maximum bubble radius was much less than the .50 threshold for pressure loss. The decreased pressure and more gradual decay are exactly what would be expected from a charge that had vented a significant portion of its energy in the first moments after detonation.

Given the good results of the first shot, a high degree of optimism was established for the results of the pressure data from the second, the $\frac{1}{2}$ pound charge on the plate with the longitudinal rectangular stiffener. That optimism was not justified.

Upon playback of the data for the second shot, it became clear that the amplifiers from all three of the pressure gages had become totally saturated. This was surprising since the pressure gages were calibrated for 10,000 psi and

the peak pressure for a ½ pound TNT charge is far less than that.

The methods by which the two tests were conducted suggested a probable cause for the pressure gage saturation.

Once all wiring was connected and the gages tested, the test platform was lowered into the waters of the bay. Heavy halyards were attached to either end of the floats, one to be used as an outhaul and the other as an inhaul. Using these, the platform was positioned in the bay a safe distance from the jetties before the explosive charge was installed and the test conducted.

To conduct the test with the 9½ pound charge, the platform was centered in the bay to keep it as far away from the jetties as possible. There was a heavy wind blowing and when the cable used to carry the firing current to the explosive charge was taken out to the platform it was blown well away from the platform and the instrument cables. Since it was separated from the other instruments, the free-field pressure gage cable was farthest of all from the detonating cable.

When the test shot was conducted on the rectangular-stiffened plate, the charge was sufficiently small that the platform was kept much nearer pierside to make it easier to handle. All of the cabling was run out to the platform along the inhaul.

The voltage used to detonate the explosive charge is quite large (800 volts DC) and sets up a noticeable inductance on all electrical cabling in the vicinity. In fact, on the strain gages, which are very low impedance devices and therefore relatively insusceptible to inductive noise this was used as a convenient, if not very accurate, zero time mark.[48]

The pressure gages, on the other hand, are extremely high capacitance, high impedance gages and correspondingly are very much affected by induced currents. It is therefore believed that the close proximity of the detonation cable was the sole cause of the saturation observed on the pressure gages during the second test. Be that as it may, no pressure history was obtained for the rectangular-stiffened plate, making it necessary to use the peak pressure and decay constant calculated from Equations 2.2 and 2.3 in the subsequent USA-STAGS run.

The lack of a zero time signal was not the only deficiency noted on the strain gage histories. Three others should also be mentioned by way of warning for those conducting similar studies.

---

[48]This was a major deficiency in the way testing was conducted at WCSF. No accurate zero time was provided on any channel. The detonation signal was used as a best alternative, but since that typically covered a span of about one millisecond it was almost useless when only the first few milliseconds were being studied.

Before the test platform was placed in the water, all of the strain gage signals were balanced with their calibration resistors, setting their signals to zero. As soon as the platform was placed in the water, the change in temperature effected a corresponding change in the resistance of the strain gages. This in turn changed the balance of the bridge. This was an ongoing problem throughout the period of the tests; many of the strain gages never were brought into proper balance. The problem was exacerbated by the fact that the strain gage and its associated wiring formed an extremely long leg of the balance bridge which was subject to the environment of the bay. The balancing leg consisted of a calibration resistor located in the instrument shack; a very different environment from that outdoors.

The second of these three problems is one which is readily correctable by the experimenter if he is aware of it. When the test plate and backing structure were sent to the West Coast Shock Test Facility, all strain gage leads were connected to junctions in the terminal box located on the side of the backing structure. Connecting these leads through long cable runs was one of the many tasks that was performed by WCSF personnel between the time that the plate was delivered and the date of the test shot. Their experience was primarily with the Navy's shock test program, wherein the magnitudes of the strain outputs were of more value than the sign. Therefore, little attention was paid

to the polarity of the strain gage connections. Thus, the histories recorded can be the exact inverse of the true history. This can be especially debilitating when comparisons of the shapes of strain curves is of particular importance.

Even more debilitating, but far less obvious, was the last of the problems noted.

The amplifiers on the Ampex FR 1300 tape recorders used to record the strain signals are calibrated for a 40% deviation from a one volt rms input signal, peak-to-peak. The maximum signal deflection that is theoretically possible is about 1.4 volts in either the positive or negative direction. The calibration levels input to the system are based upon this maximum; signals greater than 1.4 volts will saturate the amplifier and the playback will simply be a straight line at the maxima. Yet on the recordings for virtually all of the strain gages which survived to produce intelligible records, the output was <u>greater</u> than the 1.4 volt limit, but no concurrent indication of amplifier saturation. Figures 6.2 and 6.3 are offered as typical representations of this phenomena for each of the two plates.

A number of possible sources for the strain gage error were considered:

1. The calibration signals were improperly set.
2. The signals were being altered either as they were being input to or output from the Fourier Analyzer.
3. The playback amplifiers on the tape recorders were out of calibration.

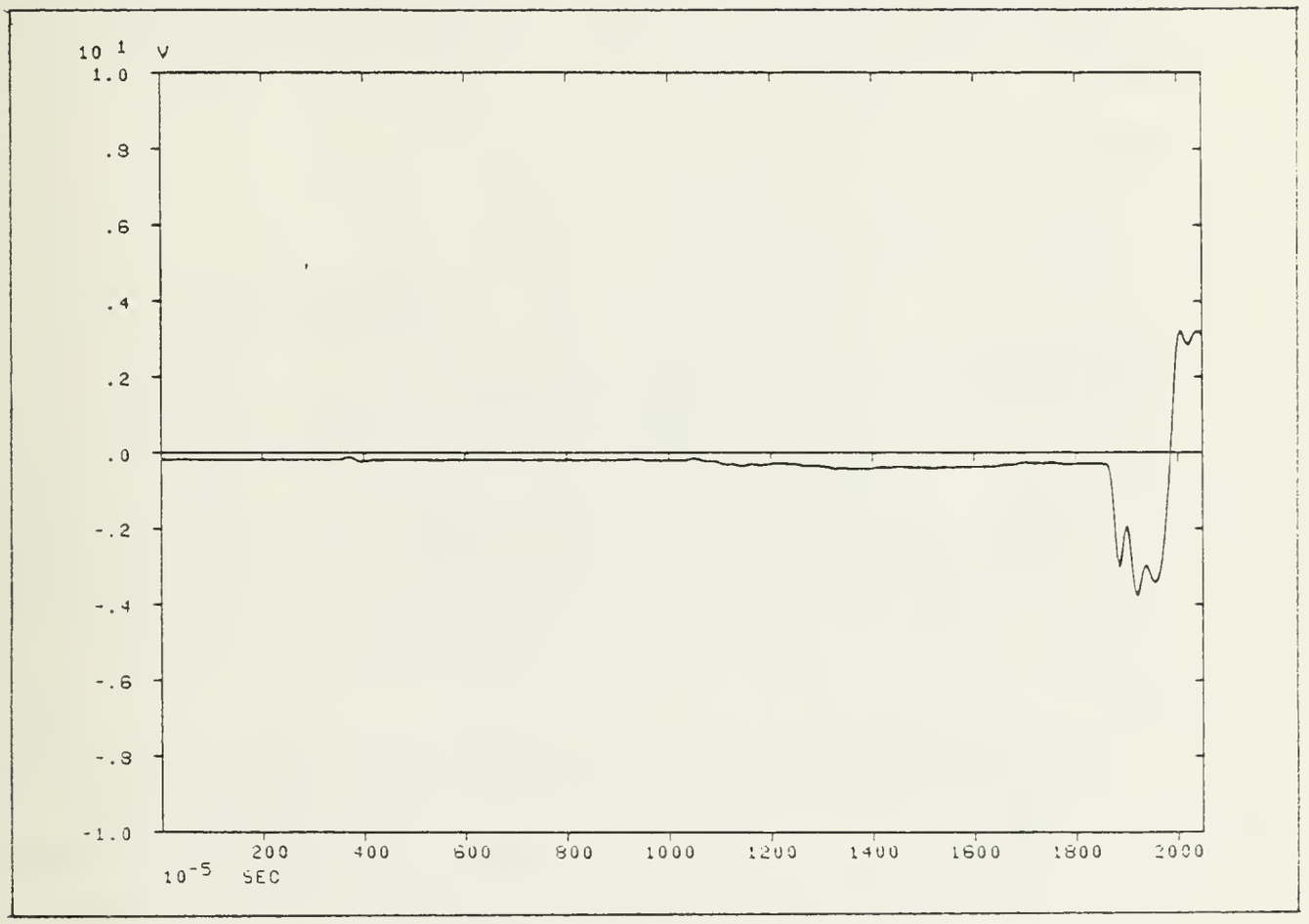

Figure 6.2 Untranslated Strain Output for Tee-Stiffened Plate (Gage 11).

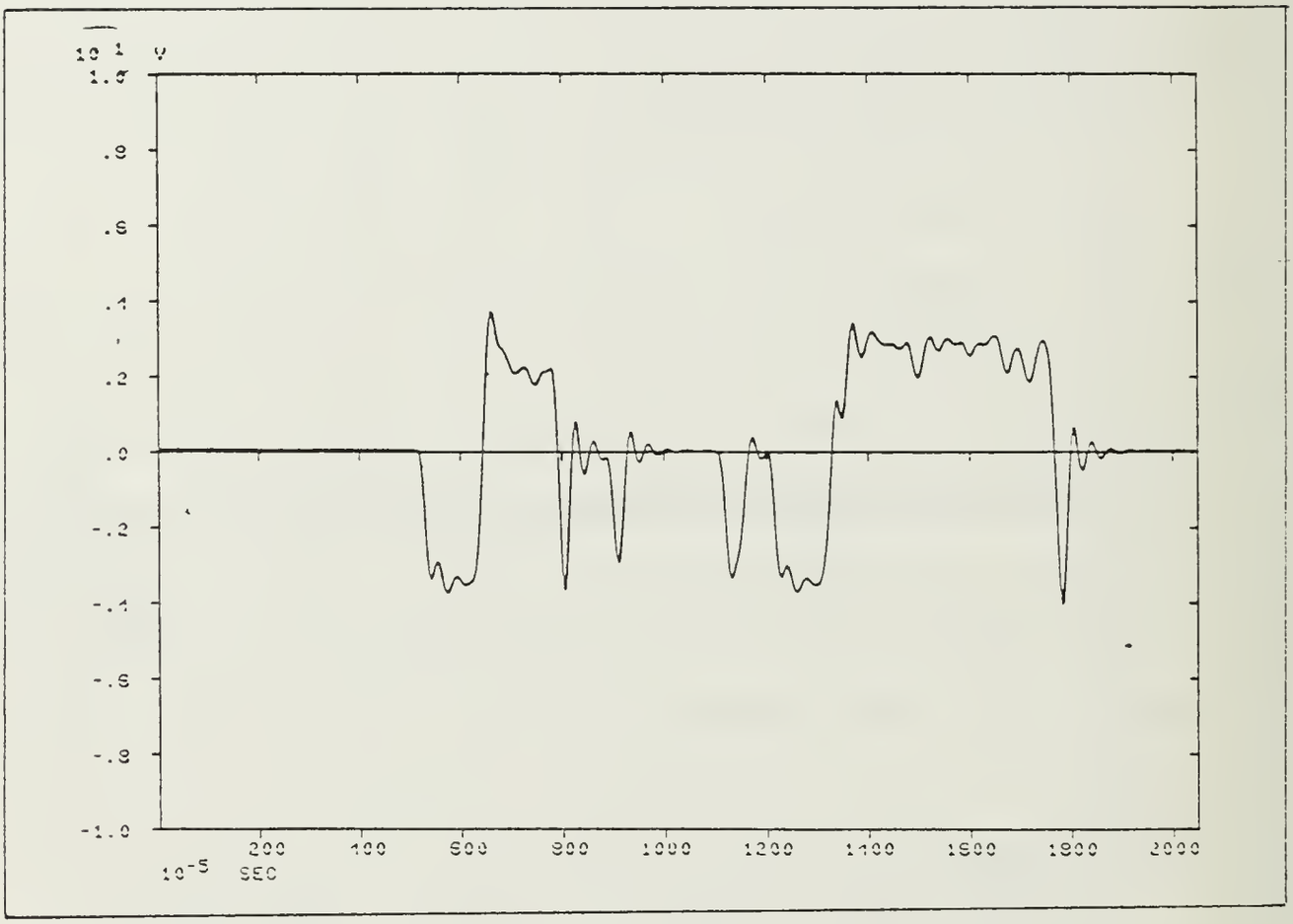

Figure 6.3 Untranslated Strain Output, Rectangular-Stiffened Plate (Gage 15).

4. The calibration signal was being input to the signal conditioners at the wrong location.

The first three of these postulated sources of error were readily discarded. The calibration signals recorded with the strain gage signals were precisely those set into the system prior to each shot; thus ruling out the possibility that either the calibration levels were incorrect or that the playback amplifiers were out of calibration. To check the second point, a series of calibrated sine waves were input to the Fourier Analyzer using the same connections and equipment settings used for the strain gage data recordings. These calibrated signals were recorded on disk and then output to the plotter in exactly the same manner as the strain gage signals had been. In no case did the Fourier Analyzer alter the calibration of the signal.

Whether the remaining suggested cause was, indeed, the source of error or whether the actual cause is something entirely different cannot be determined at this point. Whatever the actual cause, the effect remains the same; the strain magnitudes derived from the two underwater tests cannot be used for comparison with the results predicted by the USA-STAGS code.

Although the magnitudes of the test derived strain data are clearly unuseable, the general shape of the strain curves should be essentially unaffected. In an attempt to resurrect the comparative nature of this study, it was

determined that the shape of the curves from the tests should be contrasted with the strain curves predicted by the USA-STAGS code. This attempt, too, was doomed to frustration.

Figures 6.4, 6.6, and 6.8 are representative samples of the strain data calculated by USA-STAGS functioning as a post-shot analyzer of the tee-stiffened plate. Figures 6.5, 6.7, and 6.9 are the corresponding strain gage outputs.[49]

Similarly, Figures 6.10, 6.12, and 6.14 are USA-STAGS outputs for the rectangular-stiffened plate; and Figures 6.11, 6.13, and 6.15 are their corresponding strain gage histories.

While similarities exist at some points between the actual strain histories and the USA-STAGS predicted results, in general there is very little correlation.[50] This was unexpected since earlier discussions with personnel at Lockheed had indicated that extremely high degrees of correlation had been obtained when the code results had been compared to with tests conducted by the Defense Nuclear Agency and others.

---

[49]Unfortunately, after all of the problems encountered with the strain gages, there were not nearly as many of these as might have been desired.

[50]Once again it should be emphasized that the shapes alone of the curves can be compared. As already explained, the magnitudes of the strain gage records are not correct.

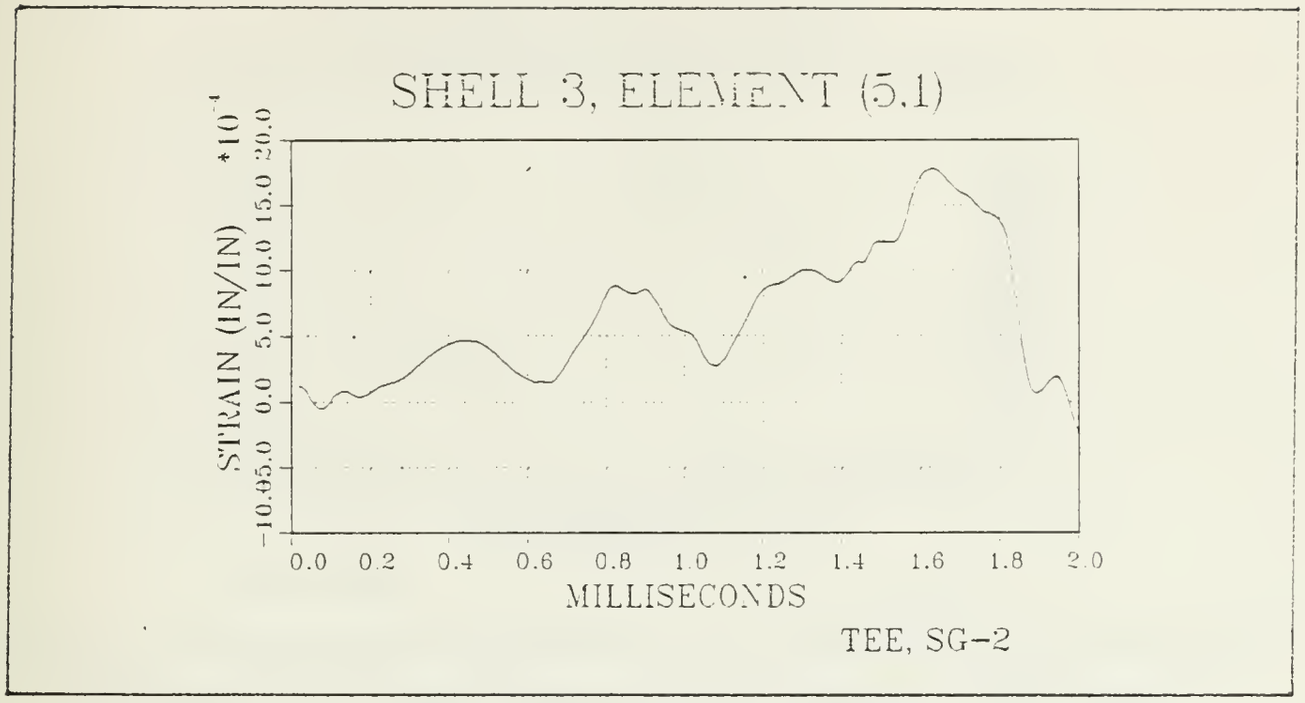

Figure 6.4 Tee-Stiffened Plate, Gage 2 (USA-STAGS)

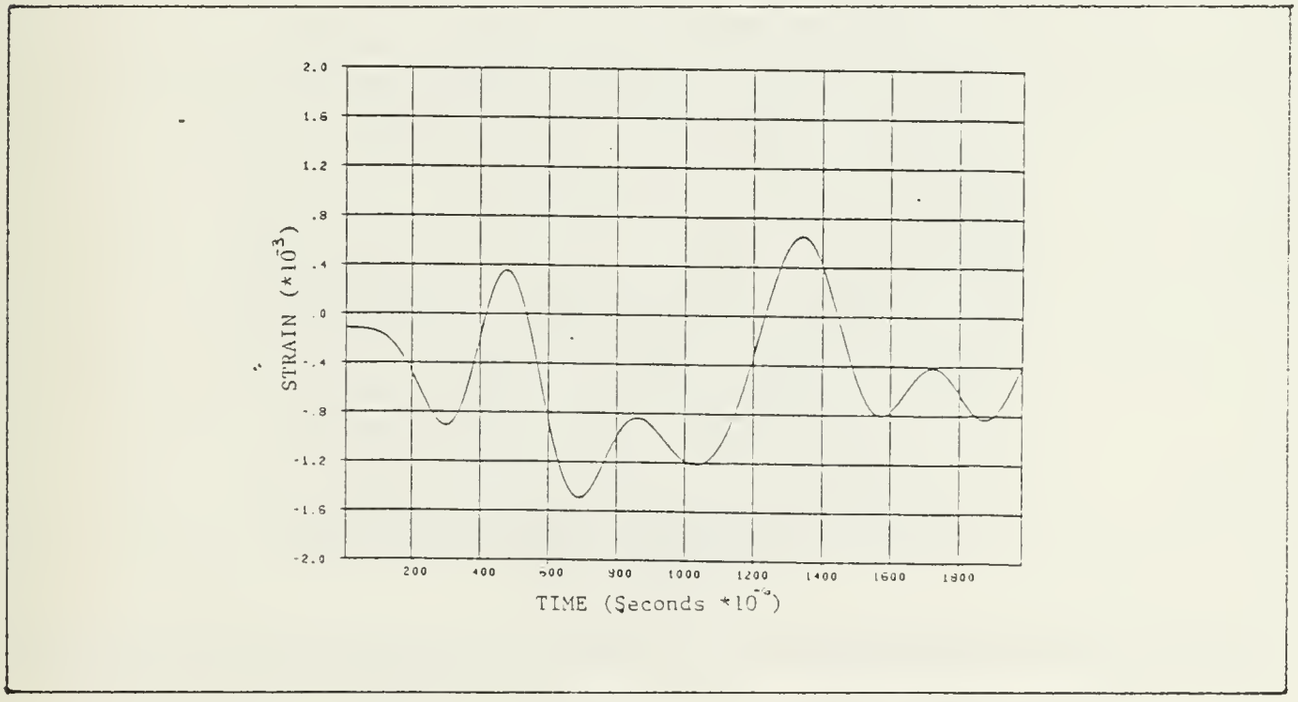

Figure 6.5 Tee-Stiffened Plate, Gage 2

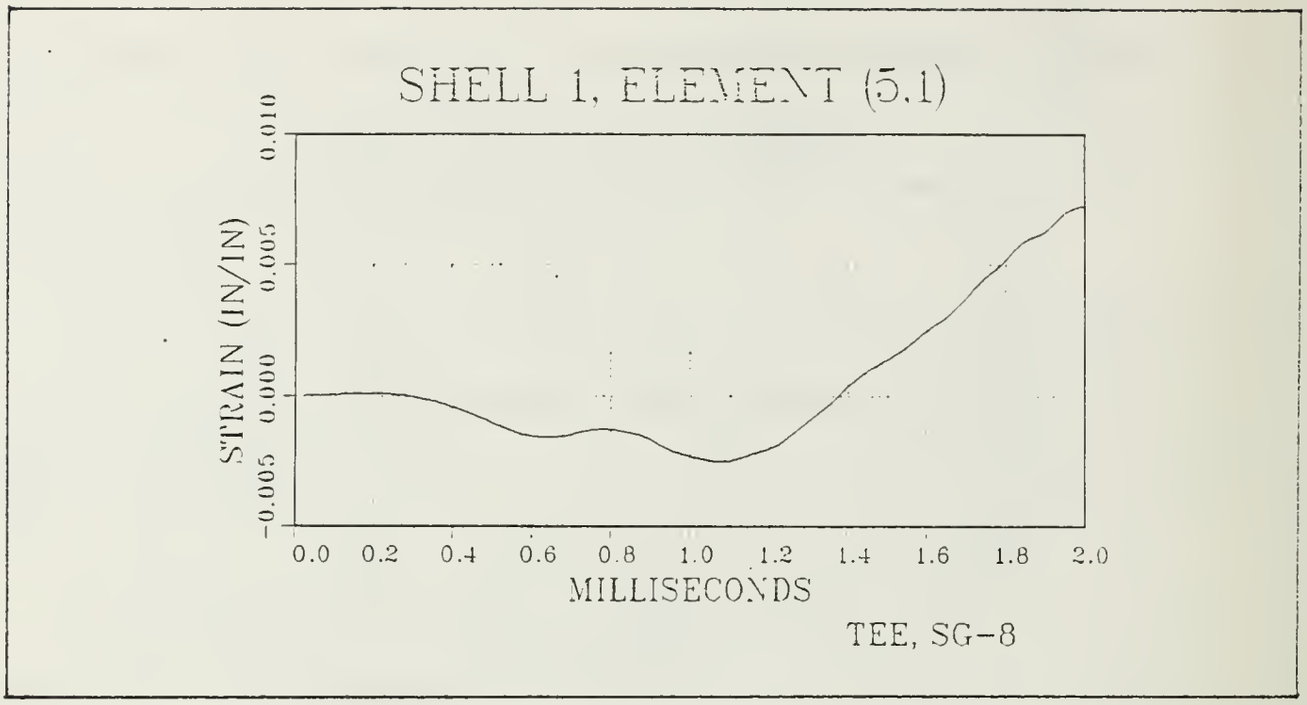

Figure 6.6 Tee-Stiffened Plate, Gage 8 (USA-STAGS)

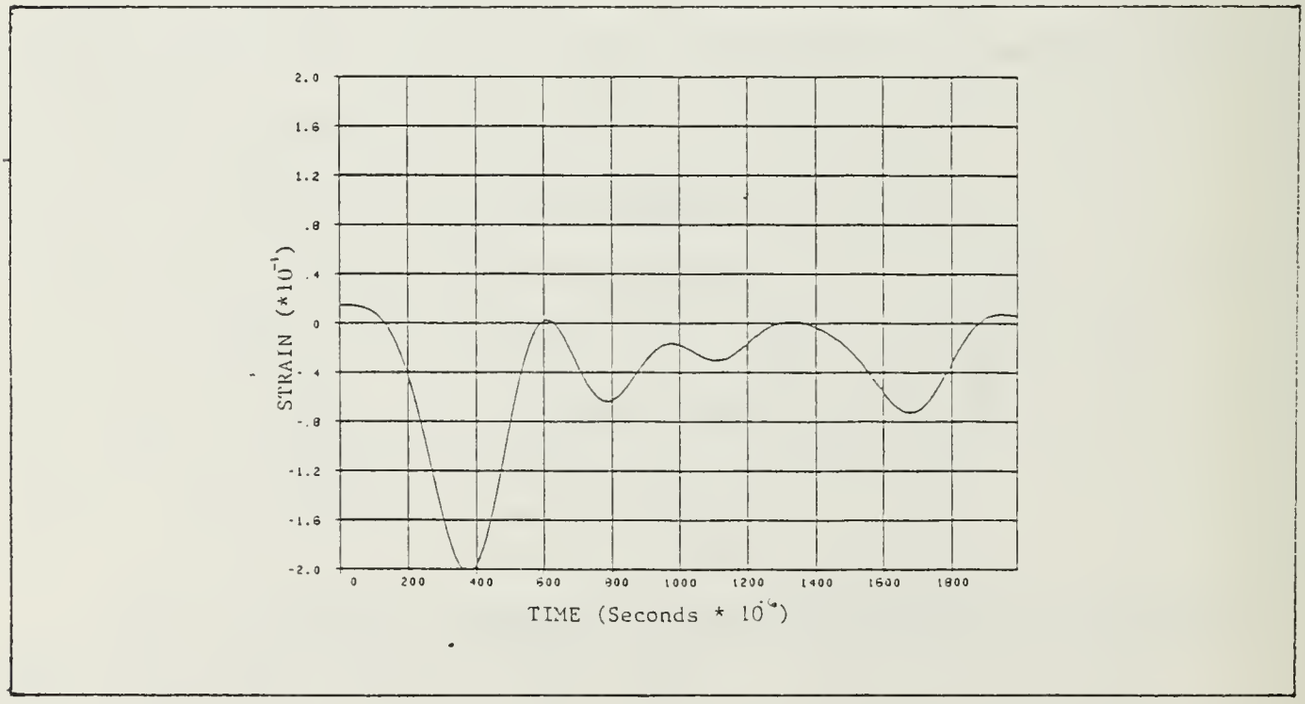

Figure 6.7 Tee-Stiffened Plate, Gage 8

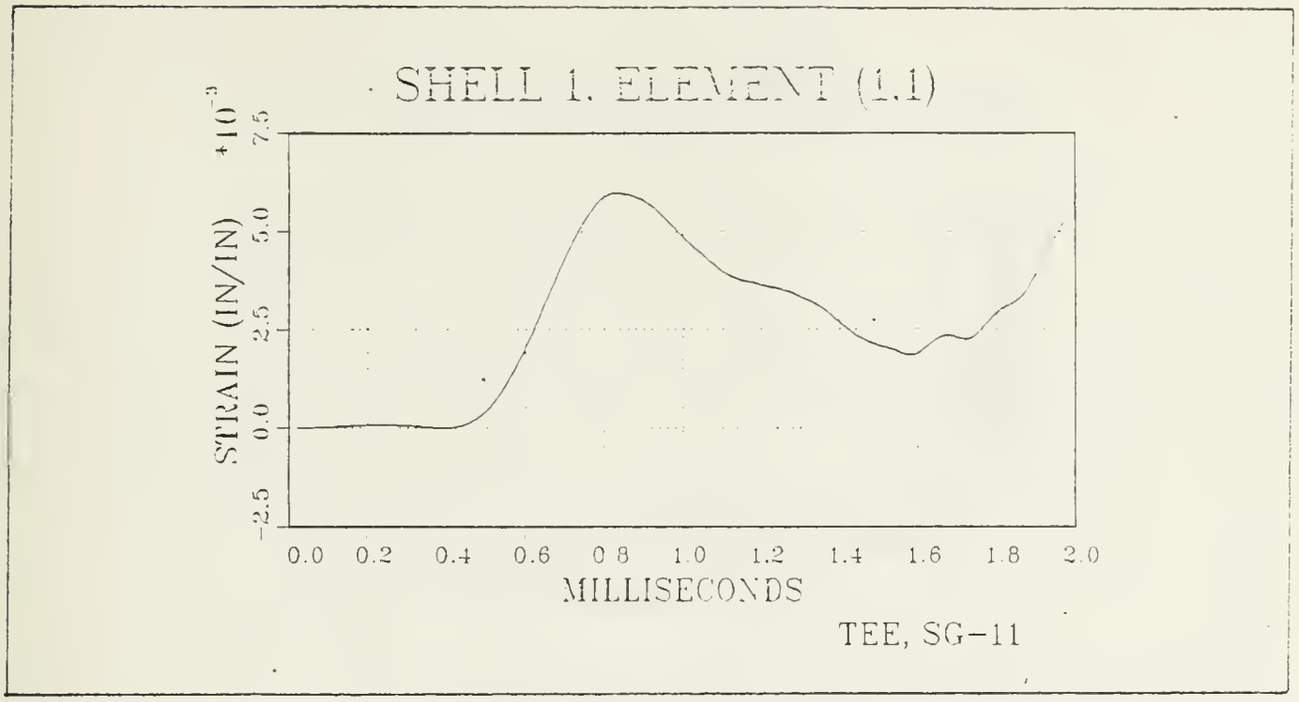

Figure 6.8 Tee-Stiffened Plate, Gage 11 (USA-STAGS)

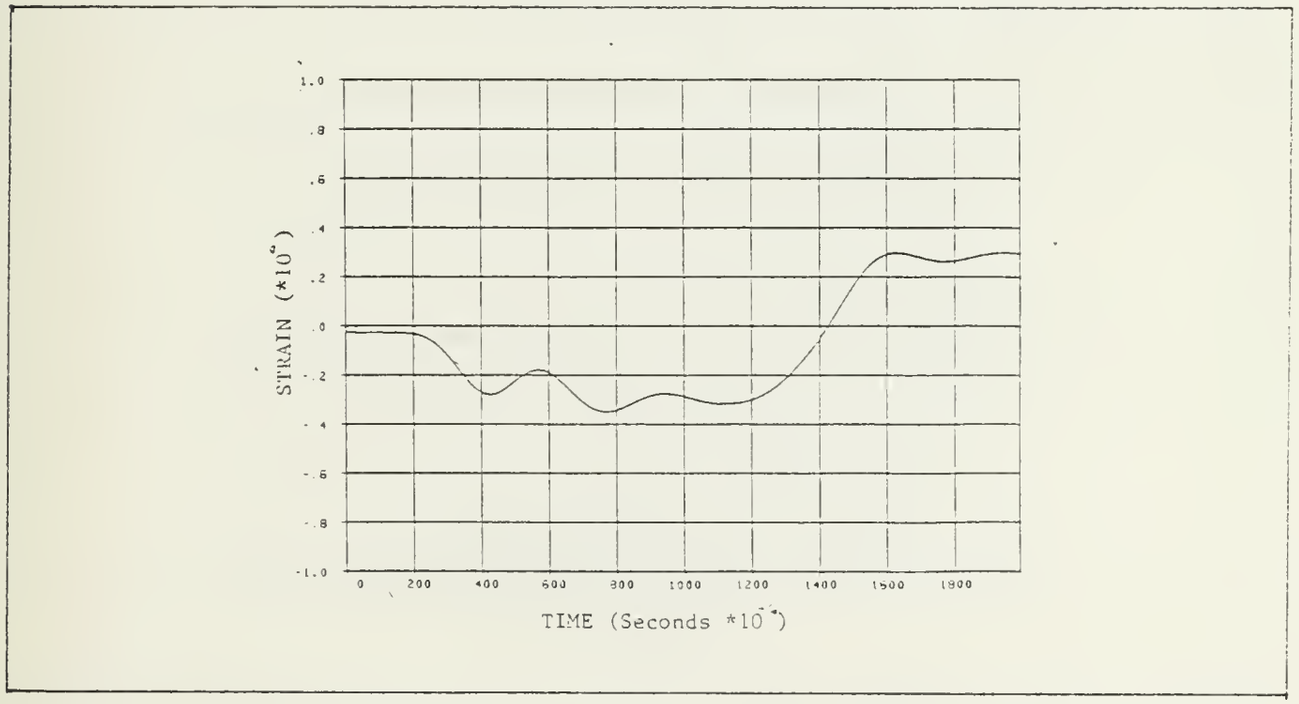

Figure 6.9 Tee-Stiffened Plate, Gage 11

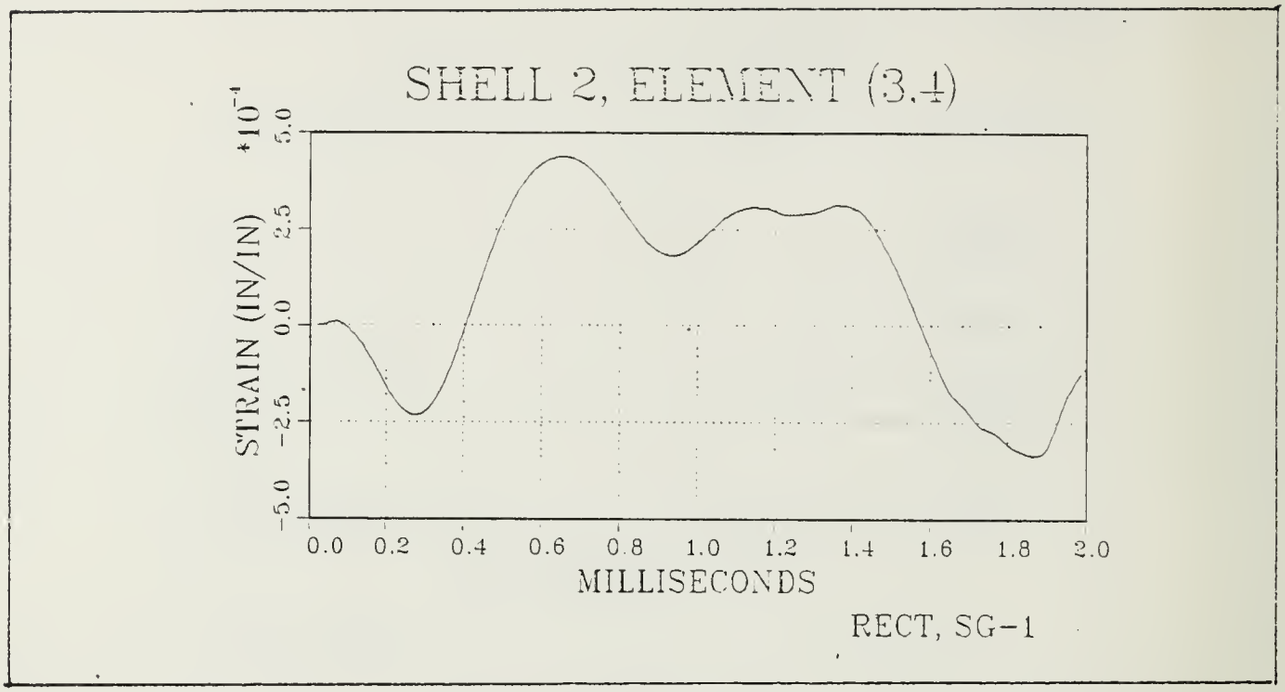

Figure 6.10 Rectangular-Stiffened Plate Gage 1 (USA-STAGS)

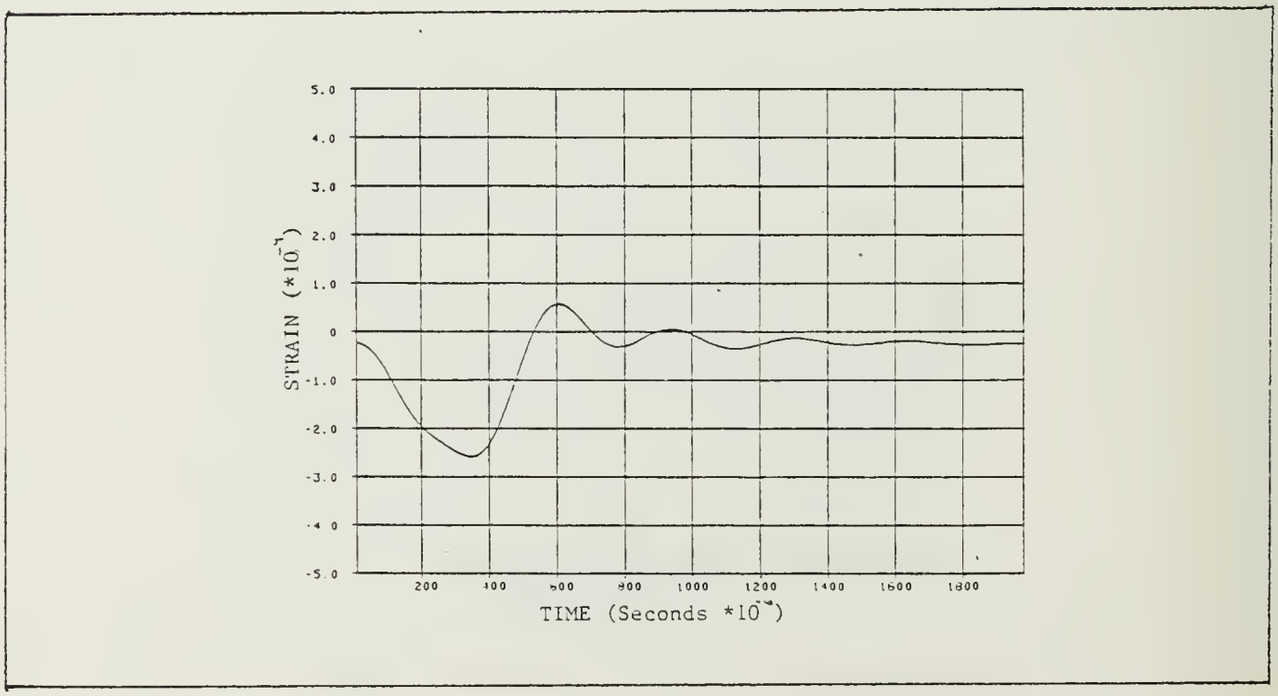

Figure 6.11 Rectangular-Stiffened Plate, Gage 1

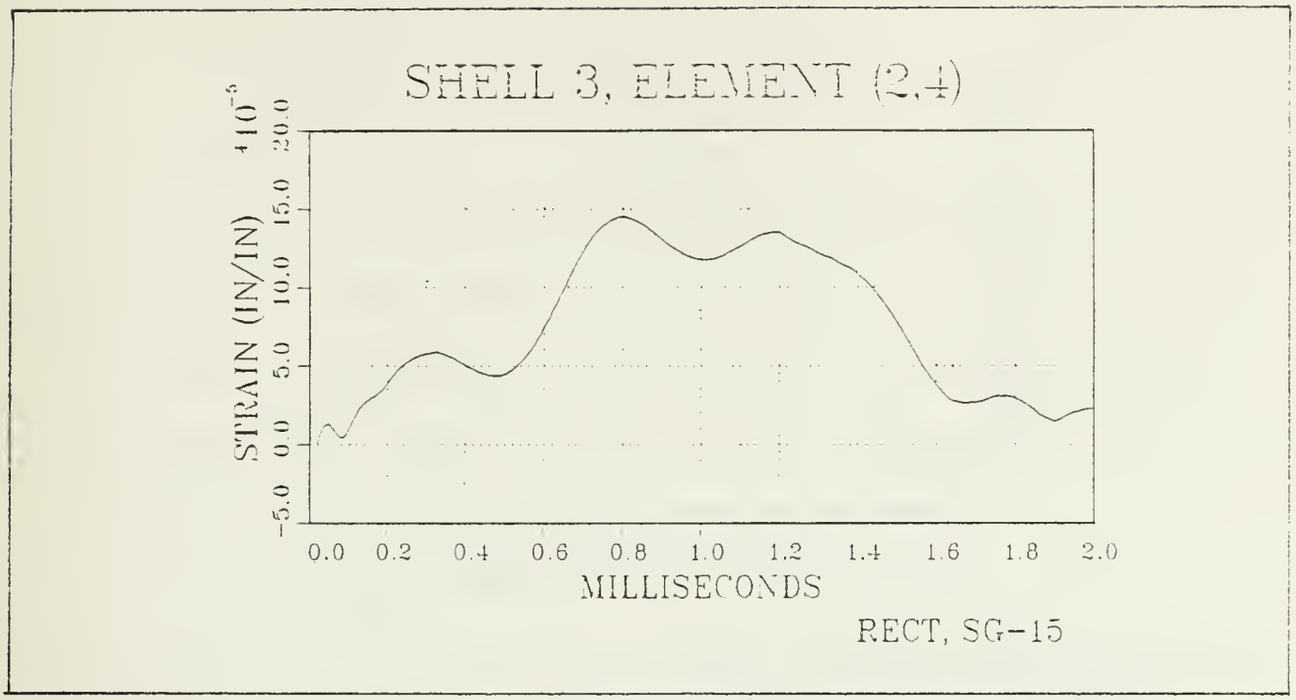

Figure 6.12 Rectangular-Stiffened Plate, Gage 15 (USA-STAGS)

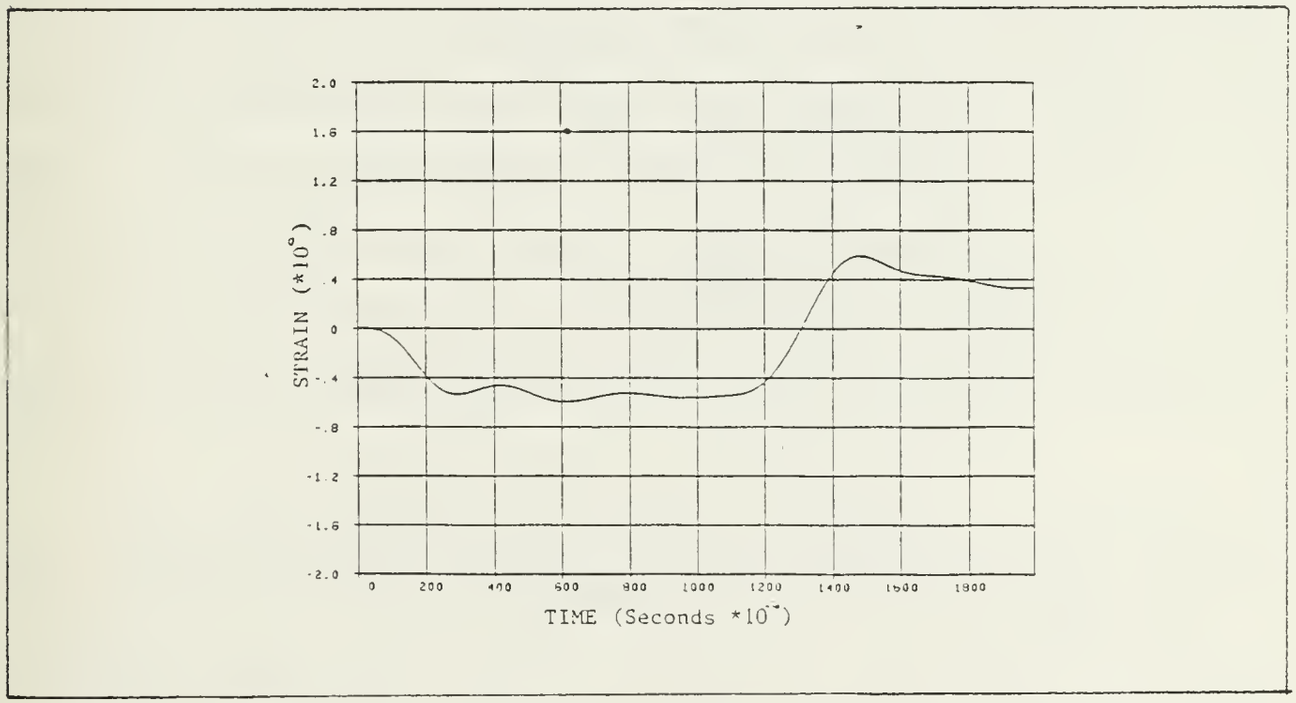

Figure 6.13 Rectangular-Stiffened Plate, Gage 15

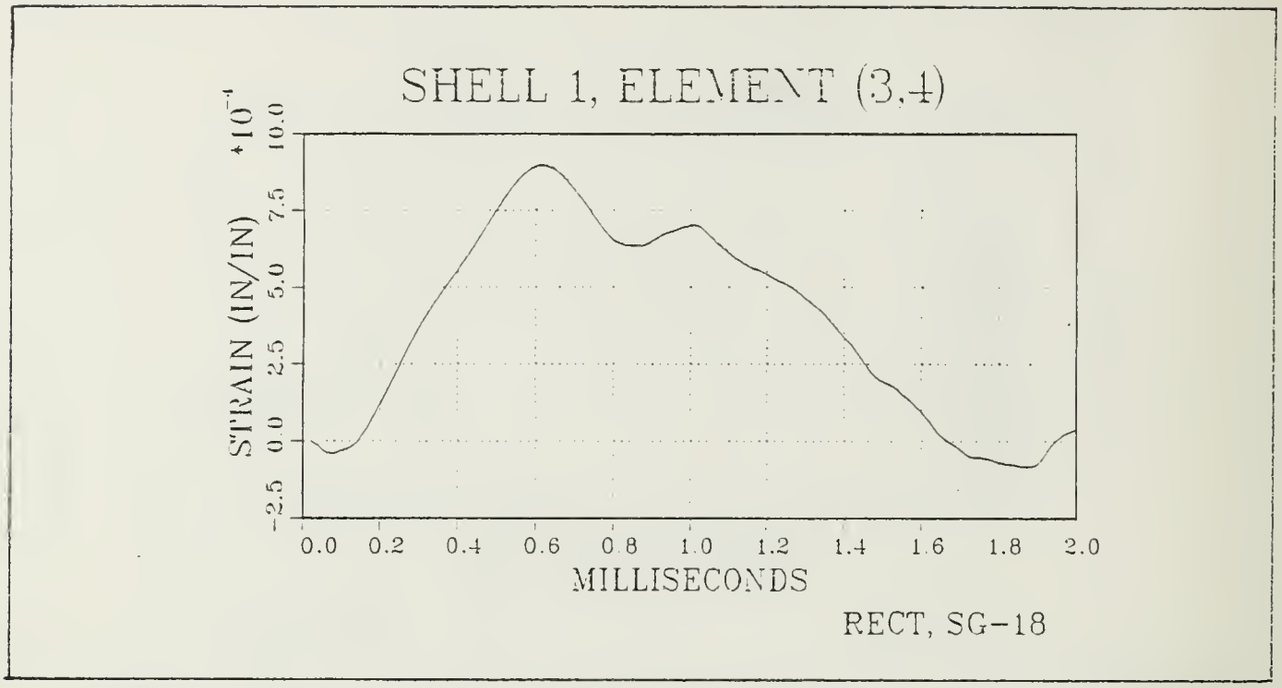

Figure 6.14 Rectangular-Stiffened Plate, Gage 18 (USA-STAGS)

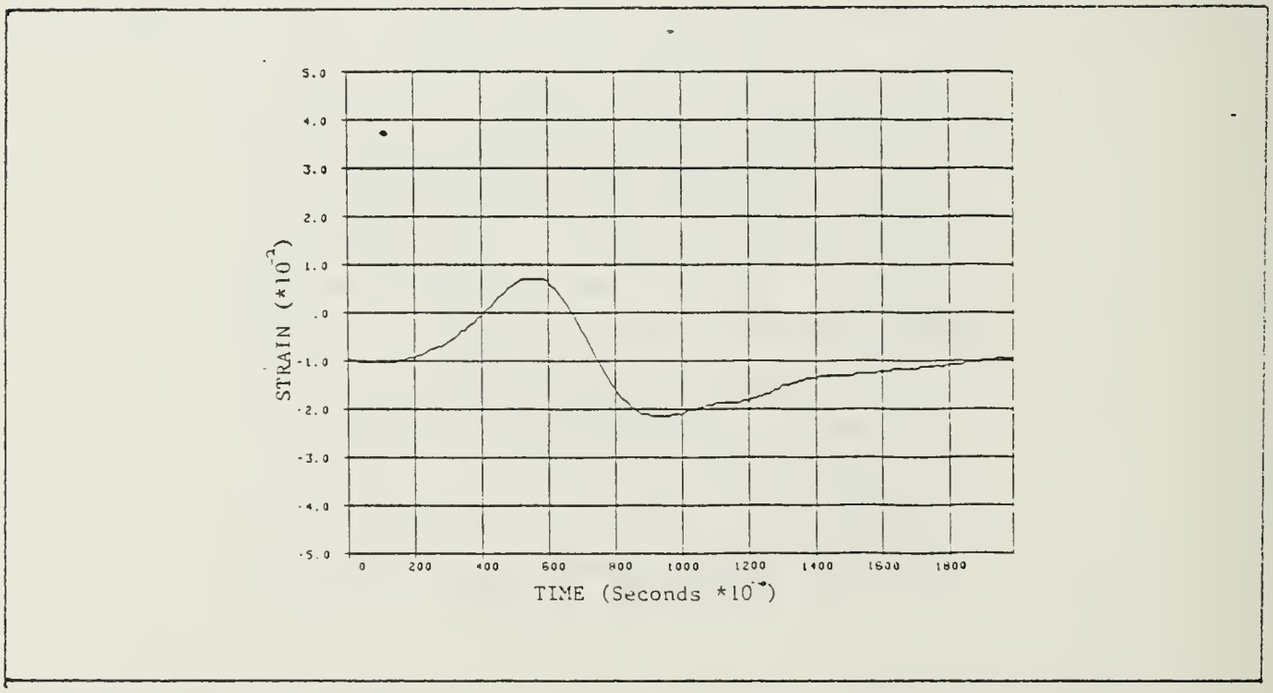

Figure 6.15 Rectangular-Stiffened Plate, Gage 18

Any number of possible solutions exist for this performance, of course; including the extremes of either USA-STAGS or the strain histories being totally wrong. In this case, however, utilizing the extended capabilities of the code itself may have provided the most plausible solution.

The USA postprocessor, POSTPR, has the capability of calculating the fluid pressures at the fluid structural interface. These results may then be displayed in either tabular or graphical form.[51] When this was done for the cases studied here, a very interesting result was obtained.

Figures 6.16 and 6.17 represent the predicted fluid pressures at the center of the tee-stiffened and rectangular-stiffened plated, respectively. As can be seen, USA-STAGS predicts that intense negative pressures will be generated within a very short time after the arrival of the shock wave. That is, USA-STAGS is predicting massive local cavitation across the faces of these plates.[52]

Viewed in that light, the reason for the seemingly poor performance of USA-STAGS in predicting the strain responses

---

[51] As noted earlier, no graphical capability exists on the VAX/VMS system at the Naval Postgraduate School. These post-shot analysis problems were run at Lockheed Research, Palo Alto. It was they who most generously provided the accompanying plots.

[52] In actuality, local cavitation would be marked by near zero pressures as the water flashed into steam to fill the void created by the sudden displacement of the plate. Since USA-STAGS assumes a homogeneous medium this must necessarily be represented by negative pressures.

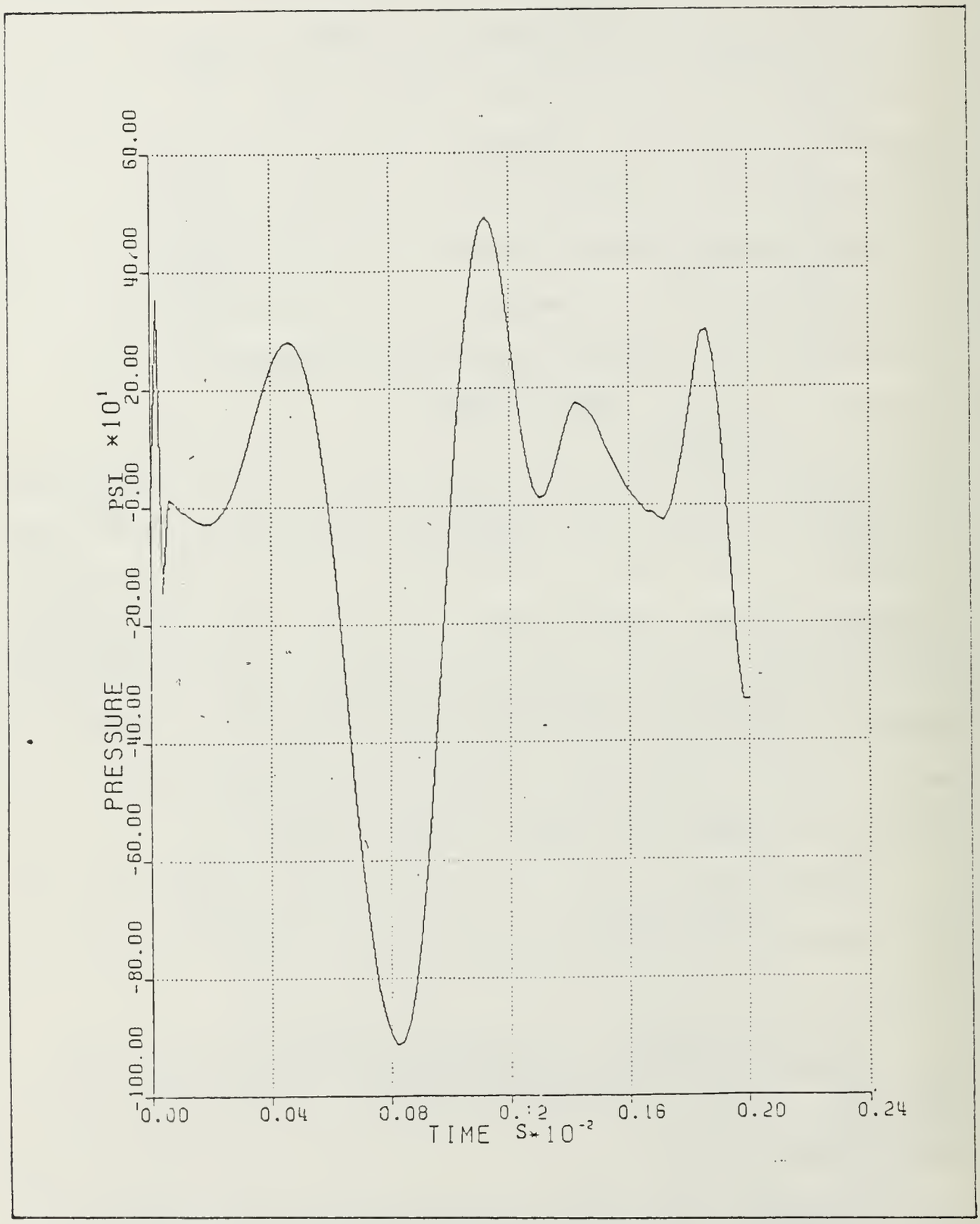

Figure 6.16 POSTPR Predicated Fluid Pressures for Tee-Plate

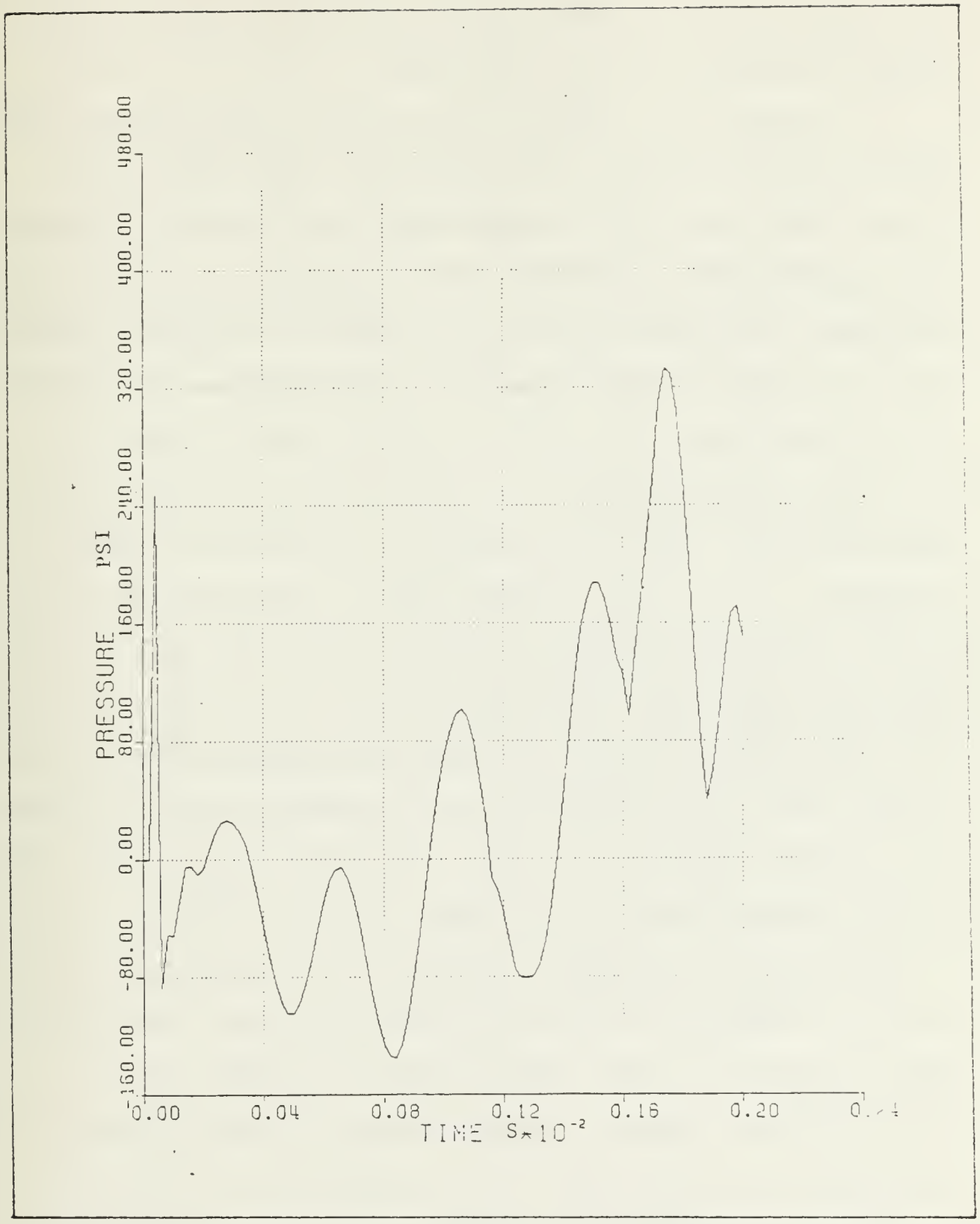

Figure 6.17 POSTPR Predicted Fluid Pressures for Rectangular-Stiffened Plate

can be better understood, and even the strain gage responses themselves become more understandable.

For example, in Figure 6.11 an initial compressive strain can be observed as the plate reacts to the incident pressure. This does not occur immediately but is delayed somewhat as the inertia of the plate is overcome. In this instance, the initial compressive strain is mimicked almost exactly by the response predicted by USA-STAGS. The strains then return to zero or become tensile as cavitation occurs. As would be expected, the responses predicted by the code are much more violent then those seen in the strain gage histories. This is so because they are activated by large values of assumed pressure rather than the actual zero pressure that would occur with cavitation.

The other plots seem to confirm this basic trend: Initial zero or compressive strain depending upon the location of the element/strain gage followed by a positive trend in the strain history as cavitation develops.[53]

The actual mechanisms involved in the results that seem to be indicated here are not fully understood. The implication, however, is that the velocity of the plate as it is being deformed is much greater than that of the fluid. A

---

[53] It is suggested that Figures 6.9 and 6.15 also adhere to this basic pattern, but are subject to the polarity problem mentioned earlier. It is believed that these plots should actually be inverted.

discontinuity is therefore being created in the fluid/structural interface. This discontinuity is manifested by the pressure drop which causes the local cavitation.

The strain gage histories seem to imply that local cavitation is indeed occurring. Whether that is in fact the case, or whether the cavitation predicted by USA-STAGS is simply a function of the way that the plates are modelled is something that must still be determined, however.

In these studies, the plate alone has been modelled. The structure that is "known" to the computer code can therefore be conceived as infinite in extent and must necessarily bear the full brunt of the pressure wave. In actuality, this is not so. The test plate is finite in size and pressure relief will occur around its boundaries. Since the breadth of the shock front is on the order of five feet for charges of the weight used in these tests (this is a function of the speed of sound in the fluid and the pressure decay, it will vary with charge weight), the entire assembly will be enveloped by the pressure front. This means that, almost instantaneously after the incident pressure is felt by the test plate, the pressure will begin to relieve around the edge of the plate and a negative pressure will be experienced on the backs of the flanges, and, soon after, on the rear of the backing structure.[54] Therefore the entire

---

[54]Complex interference patterns can also be expected.

force of the incident pressure wave may not, in fact, be impinging upon the test plate; since, while that wave is "pushing" on the front side of the structure, it is also "pulling" on the back.

Whether this decrease in force would be sufficient to eliminate cavitation is an open question. More testing must be done. For the USA-STAGS code to be able to predict this, however, it is not enough to model only the test panel. The entire assembly of test panel, milled edge, and backing structure must be included. If local cavitation is still predicted, then additional action will be required because Doubly Asymptotic Approximation which is the basis for the USA code is not valid where discontinuities such as cavitation exist between the fluid and the structural surface[55] [Ref. 17].

C. CONCLUSIONS AND SUGGESTIONS FOR FUTURE STUDY

Clearly, problems encountered both in conducting underwater testing and in using the USA-STAGS code have precluded any firm conclusions from being made about the predictive capabilities of the code. Thus, the primary objective of this study has not been met. It is in the fulfillment of

---

[55]Lockheed has developed a processor, USA-STAGS CFA (Cavitated Fluid Analyzer) which can be used to model the cavitated region. The process that must be followed is to model layers of fluid at increasing intervals from the plate until no further cavitation has been found. At that point, the standard DAA approximation may be applied.

the second objective presented in the introduction, that of providing guidelines for future study, that definite contributions can be made.

In the realm of underwater explosion testing, some specific problem areas were noted in the preceding chapters. Solutions to some of these (e.g., strain gage choice and attachment) were presented in the text of those chapters. Others of these problems are of a more fundamental nature and must be discussed separately.

First, a satisfactory plan of testing cannot be developed without an adequate source of appropriately sized explosive charges. The inability to match charge weight to test platform dimensions makes it impossible to use any computer code in its preshot capacity and impacts negatively upon the reproduceability of test results. Either the charge weight must be standardized or the test platform dimensions must be altered to accommodate changes in charge weight. In either case, the most apparent solution seems to be a carefully orchestrated test plan with long lead times before each test shot. If a match is not possible, it is suggested that the shot should probably be aborted. That valuable information was obtained from such mismatched conditions in this study is considered to be more a characteristic of a program in its developmental stages than of well-conceived experimental practice. Until more experience is gained, it appears that the rationale dictating use of

the eight pound TNT charge as the standard [Ref. 3] is still valid. It is therefore recommended that that weight charge be maintained if at all possible.

Second, the lack of adequate strain gage data has been an incapacitating flaw in the test results. Whether the poor quality of that data has been the result of errors in the equipment set-up at the West Coast Shock Test Facility, the interface between that equipment and the strain gages on the test plate, or some other cause is uncertain. What is certain is that the present arrangement of sending the test plate and backing structure to WCSF a few days before the test shot for attachment and then allowing only a few hours immediately before the shot for equipment testing is insufficient. Development of an in-house instrumentation capability at the Naval Postgraduate School is considered to be essential. This would permit the gages and electronic equipment to be integrated into a single system. Thorough testing could be conducted before the actual date of the test; and, equally important, responsibility for the outcome of the test would reside in a single organization.

Changes in the electronic instrumentation have already been recommended [Ref. 3]. Enactment of those changes would undoubtedly improve the data responses. A few other modifications suggested by the results of this study are considered equally important, however.

1. Rather than using calibration resistors, the strain gage bridge should be balanced using strain gages identical to those on the test plate. These should be attached to an aluminum plate in the terminal box. This has two effects: First, the balancing gages would be subjected to the same changes in temperature as the plate gages. Second, the balancing leg of the bridge would be of the same length as the measurement leg. Combined, these would make the bridge far less sensitive to environmental changes. A zero balance could be maintained and calibration fluctuations would be less likely.
2. A zero-time triggering signal should be superimposed upon all instrument channels. This would permit an exact assessment of the time of initial plate response to the incident wave.
3. Further shielding and grounding of the pressure gage cables should be attempted to prevent the saturation of the pressure gage amplifiers through currents induced by charge detonation.

From the results that have been explored in the preceding section of this chapter it is clear that certain questions need to be raised about the validity of the flat plate model that has been used here. These same questions should be asked about the ability of USA-STAGS or any other code to handle that model under the conditions imposed.

In particular the question of whether the local cavitation predicted by USA-STAGS is actually occurring or is simply a result of the choice of model must be addressed.

It is recommended that this study should be redone, but with the backing structure included as a part of the basic model. POSTPR could then be run to determine whether cavitation was still occurring across the plate. If cavitation was still being indicated, then either a new model would have to be found or the cavitated region would have to be modelled using a code capable of handling it.

Whatever the findings of continued tests, it may have to be recognized that increasing the scope of the models studied may put USA-STAGS beyond the reach of masters-level research at the Naval Postgraduate School. USA-STAGS is a diverse, highly capable code which has the reputation for high levels of accuracy. The price that is paid for such capability, however, is size and complexity. Given the limited time and computer resources available to most students at NPS, USA-STAGS may be beyond their capacity. If such research is undertaken, it is most emphatically recommended that a large block of time, weeks, perhaps, be spent at Lockheed Research in Palo Alto, California learning the code and perfecting models.

APPENDIX A

SOURCE DATA

This appendix contains the information listings supplied with the STAGS and USA source tapes. Section A is a full listing of the contents of the STAGS84 tape along with instructions for mounting the tape, command files for creating and linking executables, and sample command files for running the code. Section B contains similar listings for the USA source tape excepting that no command files are listed. USA places the link commands on the tape itself for immediate access. Command files for running the modules are identical in construction to those for STAGS and can be adapted from those in Section A.

A. THE STAGS84 SOURCE TAPE

VERSION AUGUST 1984

STAGS01 PROGRAM TAPE

VAX/VMS OPERATING SYSTEM

1 TAPE FORMAT

9-Track
1600 BPI
Labeled (STAG84)

2. TAPE CONTENTS

File	Name	Type	Description
1	INFO.VAX	Text	Table of contents, procedures
2	STAGSU.FOR	Source	FORTRAN programs for STAGS utility library
3	BLIOMF.MAR	Source	MACRO program for STAGS utility library
4	JOBSTA.MAR	Source	MACRO program for STAGS utility library.
5	STAGS1.FOR	Source	FORTRAN programs forSTAGS1 library
6	MOUNTEL.FOR	Source	FORTRAN programs for the MOUNT elements
6	STAGS2.FOR	Source	FORTRAN programs for STAGS2 library
8	STAPL.FOR	Source	FORTRAN programs for STAPL library
9	POSTP.FOR	Source	FORTRAN programs for POSTP library.
10	STAGS1.OLB	Library	Library of STAGS1 programs
11	STAGS2.OLB	Library	Library of STAGS2 programs.
12	STAGSU.OLB	Library	Library of STAGS utility routines.
13	POSTP.OLB	Library	Library of POSTP programs
14	STAPL.OLB	Library	Library of STAPL plot programs.
15	NICE.OLB	Library	
16	TP.FOR	Source	Thurston Processor.
17	TP.OBJ	Object	Thurston Processor.
18	ZSYS.FOR	Source	Z-system utilities (for TP).
19	RES.FOR	Source	Reduced Equation Solver
20	RES.OBJ	Object	Reduced Equation Solver
21	ZSYS.OLB	Library	Z-system utilities object library
22-36	CASE*.*.*	List	Input and output for 5 sample cases

3. LOADING FROM TAPE

Use the following control cards to copy all files to disc.

```
$ MOUNT MTA0: STAG84 TAPE
$ COPY TAPE:*.*.* []
```

Files may also be read indidually from tape with the following control cards (e.g., to load STAGS1.OLB).

```
$ COPY TAPE:STAGS1.OLB []
```

Complete sample case output may be obtained as follows

```
$ PRINT/HEAD CASE* *.*
```

4 PROCEDURES

A. LIBR COM (Compile programs and create libraries)

```
$ FOR STAGSU FOR/NOLIST
$ LIBRARY/CREATE STAGSU OLB STAGSU
$ MACRO BLIOMF MAR
$ MACRO JOBSTA MAR
$ LIB STAGSU BLIOMF,JOBSTA

$ FOR STAGS1.FOR/NOLIST
$ LIBRARY/CREATE STAGS1 OLB STAGS1
$ FOR MOUNTEL FOR/NOLIST
$ LIB STAGS1 MOUNTEL

$ FOR STAGS2 FOR/NOLIST
$ LIBRARY/CREATE STAGS2 OLB STAGS2
$ FOR MOUNTEL.FOR/NOLIST
$ LIB STAGS2 MOUNTEL

$ FOR STAPL FOR/NOLIST
$ LIBRARY/CREATE STAPL.OLB STAPL

$ FOR POSTP FOR/NOLIST
$ LIBRARY/CREATE POSTP OLB POSTP

$ FOR TP FOR/NOLIST
$ FOR ZSYS FOR/NOLIST
$ LIB/CREATE ZSYS ZSYS

$ FOR RES.FOR/NOLIST
```

B. LSTAGS1.COM (Load STAGS1)

```
$ LINK/MAP=STAGS1/BRIEF/EXECUTABLE=STAGS1-
      STAGS1 OLB/LIB/INCLUDE=MAIN1,-
      STAGSU.OLB/LIB
```

C. LSTAGS2.COM (Load STAGS2)

```
$ LINK/MAP=STAGS2/BRIEF/EXECUTABLE=STAGS2-
      STAGS2.OLB/LIB/INCLUDE=MAIN2,-
      STAGSU OLB/LIB
```

D. LSTAPL.COM (Load STAPL)

```
$ LINK/MAP=STAPL/BRIEF/EXECUTABLE=STAPL-
      STAPL.OLB/LIB/INCLUDE=STAPL,-
      STAGSU.OLB/LIB,-
      (File containing local plot routines)
```

E. LPOSTP COM (Load POSTP)

```
$ LINK/MAP=POSTP/BRIEF/EXECUTABLE=POSTP-
      POSTP OLB/LIB/INCLUDE=POSTP,-
      STAGS1 OLB/LIB,STAGS2 OLB/LIB,-
      STAGSU OLB/LIB,NICE.OLB/LIB
```

F. STAGS1.COM (Execute STAGS1)

```
$ ASSIGN CASE1 INP FOR005
$ ASSIGN CASE1 OUT FOR006
$ ASSIGN CASE1 MOD FOR021
$ RUN STAGS1.EXE
$ PRINT CASE1.OUT
```

G. STAGS.COM (Execute STAGS1 and STAGS2)

```
$ ASSIGN CASE1 INP FOR005
$ ASSIGN CASE1.OUT FOR006
$ ASSIGN CASE1 MOD FOR021   (optional if modal plots desired)
$ RUN STAGS1.EXE
$ ASSIGN CASE1 RST FOR020   (previous solution data, reqd for restart)
$ ASSIGN CASE1 SOD FOR022   (optional if solution data should be saved)
$ RUN STAGS2.EXE
$ PRINT CASE1.OUT
```

H. POSTP.COM (Execute STAGS1 and POSTP)

```
$ ASSIGN CASE4 INP FOR005
$ ASSIGN CASE4 OUT FOR006
$ RUN STAGS1.EXE            (May be omitted if FOR002.DAT saved)
$ ASSIGN CASE4 PPN FOR005
$ ASSIGN CASE4 POP FOR006
$ ASSIGN CASE4 RST FOR020   (previous solution data from CASE4 SOD)
$ ASSIGN CASE4 SOD FOR022
$ RUN POSTP.EXE
$ DEL FOR009.DAT
```

I. STAPL.COM (Execute STAPL)

```
$ ASSIGN CASE1 PIN FOR005
$ ASSIGN CASE1 RST FOR020
$ ASSIGN CASE1 MOD FOR021
$ ASSIGN CASE1.OUT FOR006
$ RUN STAPL.EXE
$ (Execute plot file on local plot device)
```

B. THE USA SOURCE TAPE

UNDERWATER SHOCK ANALYSIS (USA-

VAX TAPE LOADING INSTRUCTIONS

This tape contains symbolics, include procedures, object libraries executables, and manuals for a number of USA processors. All files have been created with COPY commands and can be retrieved in the same manner with only a few lines of input at the terminal. Examination of the tape directory will reveal that the files have various cycle numbers and this is the key to keeping those files together that belong to a particular processor. The following table contains this identification code

USA PROCESSOR	CYCLE
FLUMAS	1
AUGMAT	2
TIMINT	3
POSTPR	4
MODLIB	5

To load the TIMINT files, for example, go to the directory where they are to reside and simply do a COPY TAPE *.*;3 [] command where TAPE is the internal name that has been assigned to the magnetic tape unit. This process is simply repeated until all desired directories have been loaded

The 3 character 'extension' on the file names denotes the type of file according to the following table

EXTENSION	TYPE
.PDP	INCLUDE PROCEDURES
.INC	INCLUDE PROCEDURES
.VAX	SYMBOLICS
.OLB	OBJECT LIBRARIES
.COM	LINK STATEMENTS
.EXE	EXECUTABLES
.UAL	MANUALS

For example, AUGMAN.UAL is a file containing the AUGMAT manual while LINKUSAS.COM is the LINK statement for USA-STAGS. It should be noted that all LINK statements must be modified slightly as the directories referenced in them reflect names that are in use here at Lockheed and contain users names that will not exist at other VAX installations

Directory WRITE.[]

```
ADMASS.EXE;1              57/57     6-SEP-1984 00:00
AMDATA.PDP;1               1/1     17-MAY-1984 00:00
AMGE01.PDP;1               1/1      4-JUN-1984 00:00
AMGE02.PDP;1               1/1      4-JUN-1984 00:00
AMGE03.PDP;1               1/1     19-JUL-1982 00:00
AMGE04.PDP;1               1/1      4-JUN-1984 00:00
FLOLIB.OLB;1              69/69     6-SEP-1984 00:00
FLOMAN.UAL;1              37/37     6-SEP-1984 00:00
FLOMAS.FOR;1              74/74     6-SEP-1984 00:00
LINKFLO.COM;1              1/1      6-SEP-1984 00:00
NAMFLO.PDP;1               1/1     22-APR-1982 00:00
AMGE01.PDP;2               1/1      4-JUN-1984 00:00
AMGE03.PDP;2               1/1     22-JUL-1982 00:00
AUGLIB.OLB;2              25/25     6-SEP-1984 00:00
AUGMAN.UAL;2              12/12    13-MAY-1982 00:00
AUGMAT.FOR;2              23/23     6-SEP-1984 00:00
FILDAT.PDP;2               1/1     23-MAY-1984 00:00
LINKAUG.COM;2              1/1      6-SEP-1984 00:00
NAMAUG.PDP;2               1/1     22-APR-1982 00:00
PREPROC.EXE;2             42/42     6-SEP-1984 00:00
TRANSF.PDP;2               1/1     29-MAY-1984 00:00
CHGDAT.PDP;3               1/1     30-MAR-1984 00:00
COMADD.PDP;3               1/1     30-MAR-1984 00:00
CSWFAC.INC;3               1/1     29-MAR-1984 00:00
DATFIL.PDP;3               1/1     15-JUN-1984 00:00
DATINT.PDP;3               1/1     30-MAR-1984 00:00
INTLIB.OLB;3              53/53     6-SEP-1984 00:00
INTMAN.UAL;3              22/22     3-NOV-1982 00:00
LINKUSA.COM;3              1/1      6-SEP-1984 00:00
NAMINT.PDP;3               1/1     30-MAR-1984 00:00
TIMINT.FOR;3              58/58     6-SEP-1984 00:00
UNWASH.EXE;3              70/70     6-SEP-1984 00:00
COMADD.PDP;4               1/1     30-MAR-1984 00:00
DATFIL.PDP;4               1/1     30-MAR-1984 00:00
LINKPOS.COM;4              1/1     30-MAR-1984 00:00
NAMINT.PDP;4               1/1     30-MAR-1984 00:00
POSLIB.OLB;4              38/38    30-MAR-1984 00:00
POSMAN.UAL;4              15/15    27-MAR-1984 00:00
POSPRO.FOR;4              41/41    29-MAR-1984 00:00
POSTPR.EXE;4              61/61    30-MAR-1984 00:00
CHGDAT.PDP;5               1/1      5-APR-1983 00:00
COMADD.PDP;5               1/1     18-MAR-1983 00:00
DATFIL.PDP;5               1/1     15-JUN-1984 00:00
DATINT.PDP;5               1/1     15-JUL-1982 00:00
LINKUSAS.COM;5             1/1      6-SEP-1984 00:00
MODLIB.FOR;5              10/10     6-SEP-1984 00:00
MODLIB.OLB;5               9/9      6-SEP-1984 00:00
NAMINT.PDP;5               1/1     22-APR-1982 00:00
USAS.EXE;5              223/223     6-SEP-1984 00:00
USTLIB.OLB;5               7/7      6-SEP-1984 00:00
USTSYM.FOR;5              11/11     6-SEP-1984 00:00
BIOSUP.MAR;8               9/9     15-AUG-1981 00:00
CC.FOR;8                   1/1      9-SEP-1982 00:00
CGMERR.PRC;8               1/1      6-JAN-1982 00:00
DMGASP.FOR;8              18/18     8-JAN-1982 00:00
DMGASP.OBJ;8              12/12     8-JAN-1982 00:00
```

```
IOMCOF PRC;8              1/1      6-JAN-1982 00:00
IOMCOM PRC;8              1/1      6-JAN-1982 00:00
IOMDAT PRC;8              1/1      6-JAN-1982 00:00
IOMDEF PRC;8              1/1      6-JAN-1982 00:00
IOMSOV PRC;8              1/1      6-JAN-1982 00:00
NICE OLB;8              2e5/2e5    10-AUG-1982 00:00
OUCH TES;8                1/1      21-NOV-1980 00:00
SYMBIO PRC;8              1/1      6-JAN-1982 00:00
SYMBOL PRC;8              2/2      6-JAN-1982 00:00
SYMDAT PRC;8              1/1      6-JAN-1982 00:00
TESTGASP TES;8            1/1      6-JAN-1982 00:00
SKYLINE FOR;9            12/12     2-AUG-1982 00:00
SKYLINE OLB;9             9/9      10-AUG-1982 00:00
CYL DAA;11                3/3      30-MAR-1984 00:00
CYL FLU;11                3/3      30-MAR-1984 00:00
CYL GEO;11                2/2      30-MAR-1984 00:00
CYL POS;11              161/161     1-APR-1984 00:00
CYL PRE;11                5/5      30-MAR-1984 00:00
CYL RST;11               20/20      1-APR-1984 00:00
CYL USC;11                1/1      13-JAN-1984 00:00
CYL USD;11                2/2      13-JAN-1984 00:00
CYLAUG INP;11             1/1      17-FEB-1983 00:00
CYLAUG OUT;11            32/32     30-MAR-1984 00:00
CYLFLU INP;11             1/1      4-JAN-1984 00:00
CYLFLU OUT;11            39/39     30-MAR-1984 00:00
CYLINT INP;11             1/1      1-APR-1984 00:00
CYLINT OUT;11            80/80      1-APR-1984 00:00
CYLPOS INP;11             1/1      1-APR-1984 00:00
CYLPOS OUT;11           113/113     1-APR-1984 00:00
CYLSTG INP;11             1/1      4-JAN-1984 00:00
CYLSTG OUT;11            13/13      1-APR-1984 00:00
FOR002 DAT;11           120/120     1-APR-1984 00:00
FOR022 DAT;11            15/15      1-APR-1984 00:00
BEAM DAA;15               3/3      3-JAN-1984 00:00
BEAM GEO;15               1/1      3-JAN-1984 00:00
BEAM PRE;15               2/2      3-JAN-1984 00:00
BEAM.USC;15               1/1      3-JAN-1984 00:00
BEAM USD;15               1/1      3-JAN-1984 00:00
BEAMAUG.INP;15            1/1      3-JAN-1984 00:00
BEAMFLU.INP;15            1/1     24-JAN-1984 00:00
BEAMINE INP;15            1/1      3-JAN-1984 00:00
BEAMINS.INP;15            1/1      3-JAN-1984 00:00
BEAMPSE.INP;15            1/1      3-JAN-1984 00:00
BEAMPSS INP;15            1/1      3-JAN-1984 00:00
BEAMSTG.INP;15            1/1      3-JAN-1984 00:00

Total of 101 files, 1954/1954 blocks.
```

APPENDIX B

BASIC SHELL TYPES FOR USE WITH STAGS

This appendix contains a detailed listing of the eleven basic shell types used with the STAGS code. Drawings are included to show numbering conventions for edges and corners. This information can be particularly useful for discretizing the shell unit and specifying compatibilities with adjoining shells. (All figures from Reference 13.)

ISHELL = 2 RECTANGULAR PLATE

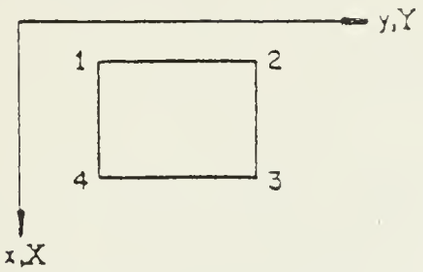

PROP(1) = X_1
PROP(2) = X_4
PROP(3) = Y_1
PROP(4) = Y_2

Subscripts refer to corner number.

ISHELL = 3 QUADRILATERAL PLATE:

$f_1 = (1-X)\cdot(1-Y)$, $f_2 = X(1-Y)$, $f_3 = XY$, $f_4 = X(1-Y)$

$$x(X,Y) = \sum_{i=1}^{4} f_i X_i$$

$$y(X,Y) = \sum_{i=1}^{4} f_i Y_i$$

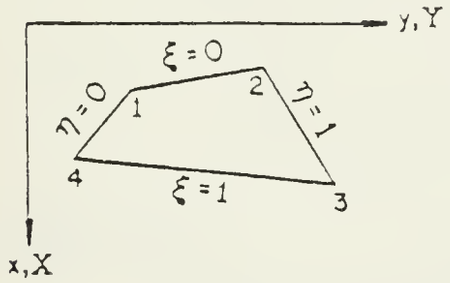

PROP(1) = X_1
PROP(2) = Y_1
PROP(3) = X_2
PROP(4) = Y_2
PROP(5) = X_3
PROP(6) = Y_3
PROP(7) = X_4
PROP(8) = Y_4

ISHELL = 4 ANNULAR PLATE:

$$y^2 + z^2 = r^2 = X^2$$
$$x = f(X, Y) = 0$$
$$y = g(X, Y) = X \sin Y$$
$$z = h(X, Y) = X \cos Y$$

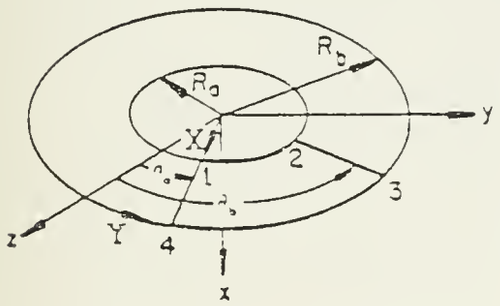

PROP(1) = R_a
PROP(2) = R_b
PROP(3) = θ_a
PROP(4) = θ_b

Lateral displacement positive up (negative x)!

ISHELL = 5

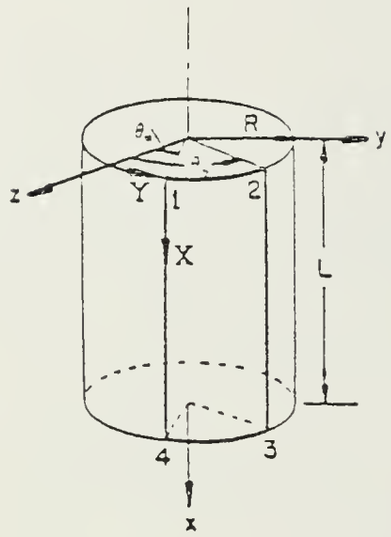

CYLINDER:

$y^2 + z^2 = R^2$

$x = f(X, Y) = X - X_1$

$y = g(X, Y) = R \sin Y$

$z = h(X, Y) = R \cos Y$

PROP(1) = X_1
PROP(2) = X_4
PROP(3) = $Y_1 = \vartheta_a$
PROP(4) = $Y_2 = \vartheta_b$
PROP(5) = R

$L = X_4 - X_1$.

ISHELL = 6

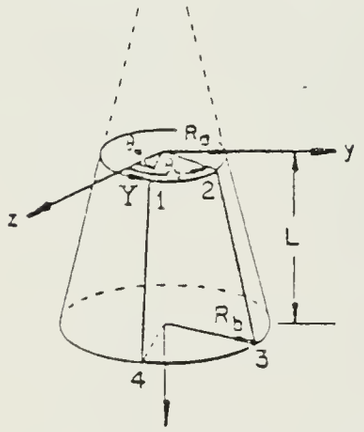

CONE:

$y^2 + z^2 = r^2 = ((X - X_1) \cdot \tan\varphi + R_a)^2$

$\tan\varphi = (R_b - R_a) / (X_4 - X_1)$

$x = f(X, Y) = X - X_1$

$y = g(X, Y) = ((X - X_1) \cdot \tan\varphi + R_a) \cdot \sin Y$

$z = h(X, Y) = ((X - X_1) \cdot \tan\varphi + R_a) \cdot \cos Y$

PROP(1) = X_1
PROP(2) = X_4
PROP(3) = $Y_1 = \vartheta_a$
PROP(4) = $Y_2 = \vartheta_b$
PROP(5) = R_a
PROP(6) = R_b

R_a may be > R_b

ISHELL = 7

SPHERE:

$x^2 + y^2 + z^2 = R^2$
$x = f(X, Y) = -R \cos X$
$y = g(X, Y) = R \sin X \sin Y$
$z = h(X, Y) = R \sin X \cos Y$

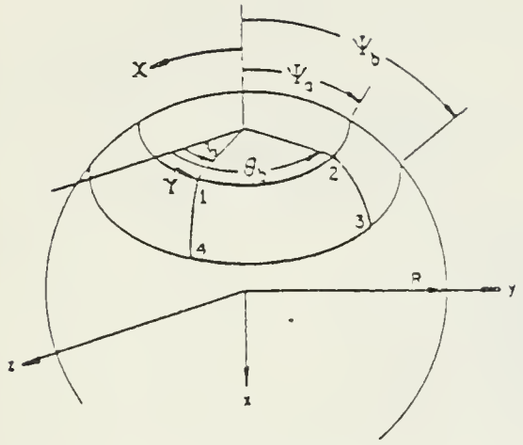

PROP(1) = $X_1 = \gamma_a$
PROP(2) = $X_2 = \gamma_b$
PROP(3) = $Y_1 = \vartheta_a$
PROP(4) = $Y_2 = \vartheta_b$
PROP(5) = R

ISHELL = 8

TORUS:

$x = f(X, Y) = -R_b \cos X$
$y = g(X, Y) = (R_a - R_b \sin X) \sin Y$
$z = h(X, Y) = (R_a - R_b \sin X) \cos Y$

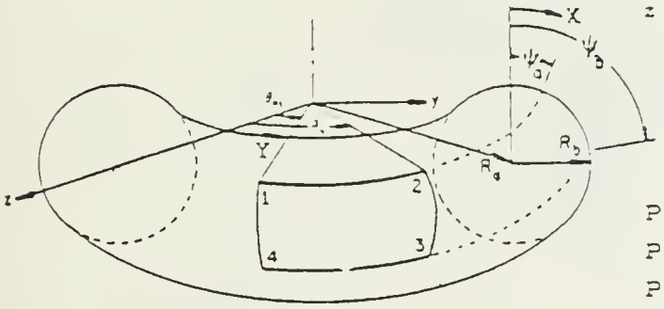

PROP(1) = $X_1 = \gamma_a$
PROP(2) = $X_2 = \gamma_b$
PROP(3) = $Y_1 = \vartheta_a$
PROP(4) = $Y_2 = \vartheta_b$
PROP(5) = R_a
PROP(6) = R_b

ISHELL = 9

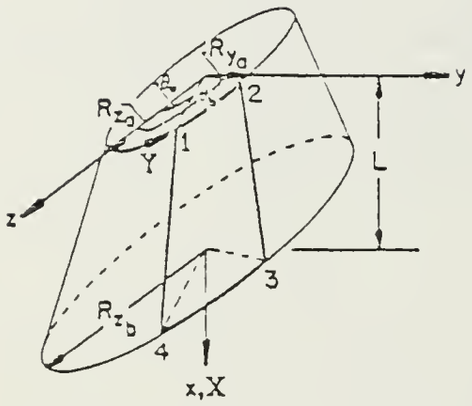

ELLIPTIC CONE/CYLINDER:

$$\frac{y^2}{r_y^2} + \frac{z^2}{r_z^2} = 1$$

$$r_z = (X - X_1) \cdot \tan\vartheta + R_{za}$$

$$\tan\vartheta = (R_{zb} - R_{za})/(X_4 - X_1)$$

$$r_y = (X - X_1) \cdot \tan\gamma = \tan\vartheta \cdot R_{ya}/R_{za}$$

$$x = f(X, Y) = X - X_1$$
$$y = g(X, Y) = r_y \sin Y^e$$
$$z = h(X, Y) = r_z^y \cos Y^e$$

$$Y^e = \arctan(\tan Y \cdot R_{za}/R_{ya})$$

PROP(1) = X_1
PROP(2) = X_4
PROP(3) = $Y_1 = \vartheta_a$
PROP(4) = $Y_2 = \vartheta_b$
PROP(5) = R_{za}
PROP(6) = R_{ya}
PROP(7) = R_{zb}

R_{za} may be > R_{zb}.

ISHELL = 10

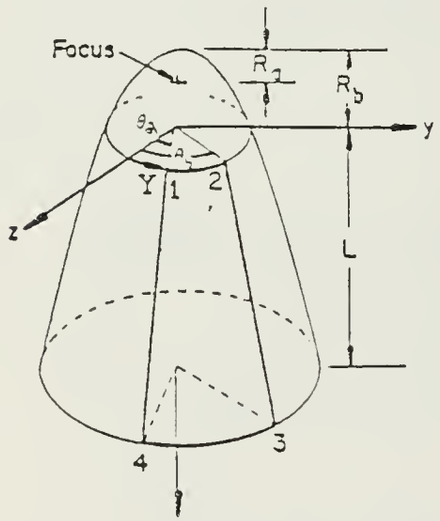

PARABOLOID:

$$y^2 + z^2 = r^2 = 4R_a \cdot (x + R_b)$$

$$x = f(X, Y) = X - X_1$$
$$y = 2\sqrt{R_a (X + R_b)} \cdot \sin Y$$
$$z = 2\sqrt{R_a (X - R_b)} \cdot \cos Y$$

PROP(1) = X_1
PROP(2) = X_4
PROP(3) = $Y_1 = \vartheta_a$
PROP(4) = $Y_2 = \vartheta_b$
PROP(5) = R_a
PROP(6) = R_b

x,X (Axis of revolution)

ISHELL = 11

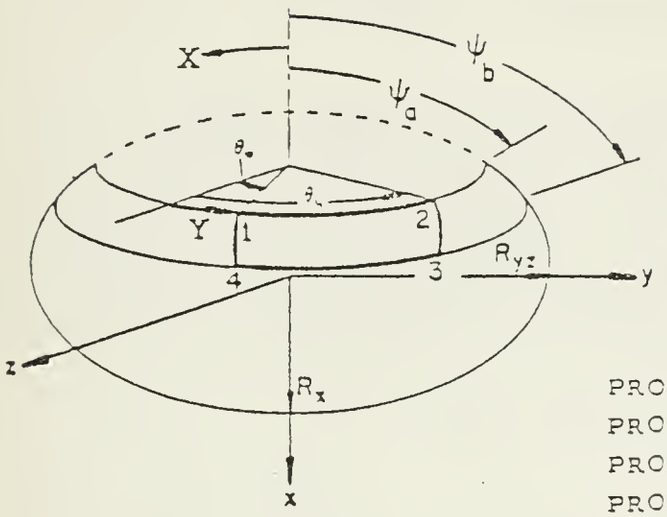

ELLIPSOID:

$$\frac{y^2 + z^2}{R_{yz}^2} + \frac{x^2}{R_x^2} = 1$$

$$x = f(X, Y) = -R_x \cos X^e$$

$$y = g(X, Y) = R_{yz} \sin X^e \sin Y$$

$$z = h(X, Y) = R_{yz} \sin X^e \cos Y$$

$$X^e = \arctan(\tan X \cdot R_{yz}/R_x)$$

PROP(1) = $X_1 = \psi_a$
PROP(2) = $X_4 = \psi_b$
PROP(3) = $Y_1 = \theta_a$
PROP(4) = $Y_2 = \theta_b$
PROP(5) = R_x
PROP(6) = R_{yz}

ISHELL = 12

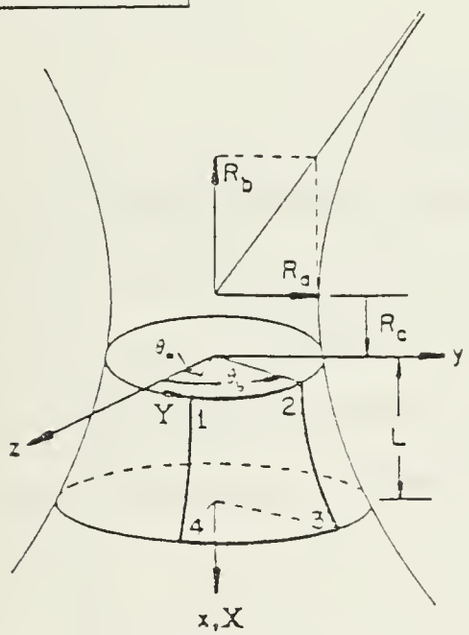

(Axis of revolution)

HYPERBOLOID:

$$\frac{y^2 + z^2}{R_a^2} - \frac{(x - R_c)^2}{R_b^2} = 1$$

$$x = X - X_1$$

$$y = (R_a/R_b)\sqrt{R_b^2 - (X - X_1 - R_c)^2} \cdot \sin Y$$

$$z = (R_a/R_b)\sqrt{R_b^2 - (X - X_1 - R_c)^2} \cdot \cos Y$$

PROP(1) = X_1
PROP(2) = X_4
PROP(3) = $Y_1 = \theta_a$
PROP(4) = $Y_2 = \theta_b$
PROP(5) = R_a
PROP(6) = R_b
PROP(7) = R_c

APPENDIX C

USA-STAGS INPUT FILES

This appendix contains the input files used for the complete USA-STAGS runs for both the tee-stiffened and rectangular-stiffened plates. These are listed in the order in which they would normally be run:

- STAGS2 (Modal Analysis) Input File
- STAGS1 Input File
- Fluid Mass Input
- Augmented Matrix Input
- Time Integrator Input
- USA postprocessor (POSTPR) Input

The input files for the tee-stiffened plate include an example of STAPL input. The files for the rectangular-stiffened plate contain an example of POSTP input file. Since these last files are readily generalized, it was not considered necessary to provide examples for each case.

```
TEESTAGS2.INP;10                          9-SEP-1984 10:58

STAGS2 DATA FOR TRANSVERSE TEE STIFFENER (MODAL ANALYSIS)
2 0 0 0 0 0 1 0 0 $ B-1
5 0 0 4 $ B-2
1 0 2 $ B-3
0. $ C-1
1 0 10000 $ D-2
12 200. 0. 2600. $ D-3
11 6 11 11 11 3 11 3 11 3 $ F-1
1 2 2 4 $ G-1-1 COMPATABILITY 1-2
1 2 3 4 $ G-1-2 COMPATABILITY 1-3
3 2 4 4 $ G-1-3 COMPATABILITY 3-4
3 2 5 2 $ G-1-4 COMPATABILITY 3-5
1 0 $ I-1
10.E6 .3 0. .098 $ I-2 MATERIAL PROPERTIES
1 1 1 $ K-1-1 FLOOR SHELLS
1 .1875 $ K-2-1
2 1 1 $ K-1-2 STIFFENER SHELLS
1 .125 $ K-2-2
2 0 $ M-1-1
0. 6. 0. 3. $ M-2A-1
1 0 0. -.0938 $ M-5-1
410 $ N-1-1
4 6 2 4 $ P-1-1 BOUNDS 1
0 $ Q-1-1
0 $ R-1-1
2 0 $ M-1-2
0. 6. 3. 9. $ M-2A-2
1 0 0. -.0938 $ M-5-2
410 $ N-1-2
4 2 2 6 $ P-1-2 BOUNDS 2
0 $ Q-1-2
0 $ R-1-2
2 2 $ M-1-3
0. 6. 0. .7813 $ M-2A-3
1 3 0. 3. .7813 $ M-3-3
2 0 90. 0. $ M-5-3
410 $ N-1-3
4 6 2 6 $ P-1-3 BOUNDS 3
0 $ Q-1-3
0 $ R-1-3
2 2 $ M-1-4
0. 6. 3. 3.3594 $ M-2A-4
1 3 0. 3.3594 .7813 $ M-3-4
2 0 0. .0625 $ M-5-4
410 $ N-1-4
4 3 2 6 $ P-1-4 BOUNDS 4
0 $ Q-1-4
0 $ R-1-4
2 2 $ M-1-5
0. 6. 2.6406 3. $ M-2A-5
1 1 0. 2.6406 .7813 $ M-3-5
2 0 0. .0625 $ M-5-5
410 $ N-1-5
4 6 2 3 $ P-1-5 BOUNDS 5
0 $ Q-1-5
0 $ R-1-5
```

```
STAGS1 DATA FOR TRANSVERSE TEE STIFFENER (PLASTIC)
6 1 1 1 0 0 1 0 1 $ B-1
5 0 0 4 $ B-2
1 0 2 $ B-3
0. $ C-1
0 1000 1 1 $ D-1
0  2.E-3 20 E-6 $ E-1
0 4 $ E-2
11 6 11 11 11 3 11 3 11 3 $ F-1
1 2 2 4 $ G-1-1 COMPATABILITY 1-2
1 2 3 4 $ G-1-2 COMPATABILITY 1-3
3 2 4 4 $ G-1-3 COMPATABILITY 3-4
3 2 5 2 $ G-1-4 COMPATABILITY 3-5
1 3 1 $ I-1
10.E6 .3 0. .098 $ I-2 MATERIAL PROPERTIES
.0041 41.E3 .06 45.E3 1.  47.E3 $ I-3 PLASTICITY
1 1 1 5 $ K-1-1 FLOOR SHELLS
1  1875 0.  2 $ K-2-1
2 1 1 5 $ K-1-2 STIFFENER SHELLS
1 .125 0.  2 $ K-2-2
2 0 $ M-1-1
0.  6.  0.  3.  $ M-2A-1
1 0 0.  0.  0 1 $ M-5-1
410 $ N-1-1
4 6 2 4 $ P-1-1 BOUNDS 1
0 $ Q-1-1
0 $ R-1-1
2 0 $ M-1-2
0.  6.  3.  9  $ M-2A-2
1 0 0  0.  0 1 $ M-5-2
410 $ N-1-2
4 2 2 6 $ P-1-2 BOUNDS 2
0 $ Q-1-2
0 $ R-1-2
2 2 $ M-1-3
0  6.  0  .9375 $ M-2A-3
1 3 0.  3.  9375 $ M-3-3
2 0 90  0.  0 1 $ M-5-3
410 $ N-1-3
4 6 2 6 $ P-1-3 BOUNDS 3
0 $ Q-1-3
0 $ R-1-3
2 2 $ M-1-4
0  6.  3  3.3594 $ M-2A-4
1 3 0.  3.3594 .9375 $ M-3-4
2 0 0  0  0 1 $ M-5-4
410 $ N-1-4
4 3 2 6 $ P-1-4 BOUNDS 4
0 $ Q-1-4
0 $ R-1-4
2 2 $ M-1-5
0  6  2.6406 3  $ M-2A-5
1 1 0  2.6406  9375 $ M-3-5
2 0 0  0.  0 1 $ M-5-5
410 $ N-1-5
4 6 2 3 $ P-1-5 BOUNDS 5
0 $ Q-1-5
0 $ R-1-5
```

```
FLUID MASS DATA FOR TRANSVERSE TEE STIFFENER
0 242 150 0 0
1.152E-3 59 83
T T F T
T F F T
F F T F
F F T F
F T F F
F T
TEE.FLU TEE.GEO TEE.COR
10
1. 1. 1. 1.
MESH
1 4 0 0 0
1 7 8 2
2 4 0 0 0
2 8 9 3
3 4 0 0 0
3 9 10 4
4 4 0 0 0
4 10 11 5
5 4 0 0 0
5 11 12 6
6 4 0 0 0
7 13 14 8
7 4 0 0 0
8 14 15 9
8 4 0 0 0
9 15 16 10
9 4 0 0 0
10 16 17 11
10 4 0 0 0
11 17 18 12
11 4 0 0 0
13 19 20 14
12 4 0 0 0
14 20 21 15
13 4 0 0 0
15 21 22 16
14 4 0 0 0
16 22 23 17
15 4 0 0 0
17 23 24 18
16 4 0 0 0
19 25 26 20
17 4 0 0 0
20 26 27 21
18 4 0 0 0
21 27 28 22
19 4 0 0 0
22 28 29 23
20 4 0 0 0
23 29 30 24
21 4 0 0 0
25 31 32 26
22 4 0 0 0
26 32 33 27
23 4 0 0 0
27 33 34 28
24 4 0 0 0
```

28 34 35 29
25 4 0 0 0
29 35 36 30
26 4 0 0 0
31 37 38 32
27 4 0 0 0
32 38 39 33
28 4 0 0 0
33 39 40 34
29 4 0 0 0
34 40 41 35
30 4 0 0 0
35 41 42 36
31 4 0 0 0
37 43 44 38
32 4 0 0 0
38 44 45 39
33 4 0 0 0
39 45 46 40
34 4 0 0 0
40 46 47 41
35 4 0 0 0
41 47 48 42
36 4 0 0 0
43 49 50 44
37 4 0 0 0
44 50 51 45
38 4 0 0 0
45 51 52 46
39 4 0 0 0
46 52 53 47
40 4 0 0 0
47 53 54 48
41 4 0 0 0
49 55 56 50
42 4 0 0 0
50 56 57 51
43 4 0 0 0
51 57 58 52
44 4 0 0 0
52 58 59 53
45 4 0 0 0
53 59 60 54
46 4 0 0 0
55 61 62 56
47 4 0 0 0
56 62 63 57
48 4 0 0 0
57 63 64 58
49 4 0 0 0
58 64 65 59
50 4 0 0 0
59 65 66 60
51 4 0 0 0
6 12 77 67
52 4 0 0 0
67 77 78 68
53 4 0 0 0
68 78 79 69
54 4 0 0 0
69 79 80 70

```
55 4 0 0 0
70 80 81 71
56 4 0 0 0
71 81 82 72
57 4 0 0 0
72 82 83 73
58 4 0 0 0
73 83 84 74
59 4 0 0 0
74 84 85 75
60 4 0 0 0
75 85 86 76
61 4 0 0 0
12 18 87 77
62 4 0 0 0
77 87 88 78
63 4 0 0 0
78 88 89 79
64 4 0 0 0
79 89 90 80
65 4 0 0 0
80 90 91 81
66 4 0 0 0
81 91 92 82
67 4 0 0 0
82 92 93 83
68 4 0 0 0
83 93 94 84
69 4 0 0 0
84 94 95 85
70 4 0 0 0
85 95 96 86
71 4 0 0 0
18 24 97 87
72 4 0 0 0
87 97 98 88
73 4 0 0 0
88 98 99 89
74 4 0 0 0
89 99 100 90
75 4 0 0 0
90 100 101 91
76 4 0 0 0
91 101 102 92
77 4 0 0 0
92 102 103 93
78 4 0 0 0
93 103 104 94
79 4 0 0 0
94 104 105 95
80 4 0 0 0
95 105 106 96
81 4 0 0 0
24 30 107 97
82 4 0 0 0
97 107 108 98
83 4 0 0 0
98 108 109 99
84 4 0 0 0
99 109 110 100
85 4 0 0 0
```

```
100 110 111 101
86 4 0 0 0
101 111 112 102
87 4 0 0 0
102 112 113 103
88 4 0 0 0
103 113 114 104
89 4 0 0 0
104 114 115 105
90 4 0 0 0
105 115 116 106
91 4 0 0 0
30.36 117 107
92 4 0 0 0
107 117 118 108
93 4 0 0 0
108 118 119 109
94 4 0 0 0
109 119 120 110
95 4 0 0 0
110 120 121 111
96 4 0 0 0
111 121 122 112
97 4 0 0 0
112 122 123 113
98 4 0 0 0
113 123 124 114
99 4 0 0 0
114 124 125 115
100 4 0 0 0
115 125 126 116
101 4 0 0 0
36 42 127 117
102 4 0 0 0
117 127 128 118
103 4 0 0 0
118 128 129 119
104 4 0 0 0
119 129 130 120
105 4 0 0 0
120 130 131 121
106 4 0 0 0
121 131 132 122
107 4 0 0 0
122 132 133 123
108 4 0 0 0
123 133 134 124
109 4 0 0 0
124 134 135 125
110 4 0 0 0
125 135 136 126
111 4 0 0 0
42 48 137 127
112 4 0 0 0
127 137 138 128
113 4 0 0 0
128 138 139 129
114 4 0 0 0
129 139 140 130
115 4 0 0 0
130 140 141 131
```

116 4 0 0 0
131 141 142 132
117 4 0 0 0
132 142 143 133
118 4 0 0 0
133 143 144 134
119 4 0 0 0
134 144 145 135
120 4 0 0 0
135 145 146 136
121 4 0 0 0
48 54 147 137
122 4 0 0 0
137 147 148 138
123 4 0 0 0
138 148 149 139
124 4 0 0 0
139 149 150 140
125 4 0 0 0
140 150 151 141
126 4 0 0 0
141 151 152 142
127 4 0 0 0
142 152 153 143
128 4 0 0 0
143 153 154 144
129 4 0 0 0
144 154 155 145
130 4 0 0 0
145 155 156 146
131 4 0 0 0
54 60 157 147
132 4 0 0 0
147 157 158 148
133 4 0 0 0
148 158 159 149
134 4 0 0 0
149 159 160 150
135 4 0 0 0
150 160 161 151
136 4 0 0 0
151 161 162 152
137 4 0 0 0
152 162 163 153
138 4 0 0 0
153 163 164 154
139 4 0 0 0
154 164 165 155
140 4 0 0 0
155 165 166 156
141 4 0 0 0
60 66 167 157
142 4 0 0 0
157 167 168 158
143 4 0 0 0
158 168 169 159
144 4 0 0 0
159 169 170 160
145 4 0 0 0
160 170 171 161
146 4 0 0 0

```
161 171 172 162
147 4 0 0 0
162 172 173 163
148 4 0 0 0
163 173 174 164
149 4 0 0 0
164 174 175 165
150 4 0 0 0
165 175 176 166
MASS
EIGEN
EXIT
```

```
AUGMENTED MATRIX DATA FOR TRANSVERSE TEE STIFFENER
TEE MAS TEE.FLU TEE GEO TEE BSE
F T F F
F F F F
T T F F
0
242 1452 6 3
1
0 1 150 1
```

```
TEETIM INP.1                          19-OCT-1994 15:26

TIME INTEGRATOR DATA FOR TRANSVERSE TEE STIFFENER
TEE.PRE TEE.POS
TEE RST
0  0  108.78
0.  2  64  .9375
T F F F
F
101
1
 2E-4
3125 0 1.56E-3
1
0  20 E-6
2.E-3
1 20
0 0 0 0
F F
F
```

```
TEEPOST.INP;1                    23-OCT-1984 12:04

USA POST-PROCESSOR DATA FOR TRANSVERSE TEE STIFFENER
1
101
TEE PRE
TEE POS
F T F F F
F F F F
F F T
0 0 2
3 1 6 1
3 67 76 1
0 0 2
3 1 6 1
3 67 76 1
0 2
1 6 1
61 69 1
F
1 0
F F F F
```

```
TESSTAB51 MODEL PLOT
9 1 11  0
0 0 0 0
 7 23  23  23
0
- 7 23  23. 23
1 0 0 0 1 100 0 0
 7 23  23. 23  3
2 1 0 0 6 100 0 1 0 0
.7 23. 23. 23. 10. 10
2 1 0 0 6 100 0 2 0 0
 7 23  23  23  10. 10
2 1 0 0 6 100 0 3 0 0
.7 23. 23. 23  10. 10
2 2 0 0 6 100 0 1 0 0
 7 23  23  23  10. 10
2 2 0 0 6 100 0 2 0 0
 7 23  23. 23  10. 10
2 2 0 0 6 100 0 3 0 0
.7 23. 23. 23. 10. 10
```

```
RECSTAGS2.INP;10                          9-SEP-1984 10:58

STAGS2 DATA FOR LONGITUDINAL RECTANGULAR STIFFENER (MODAL ANALYSIS)
2 0 0 0 0 0 1 0 0 $ B-1
3 0 0 2 $ B-2
1 0 1 $ B-3
0. $ C-1
1 0 10000 $ D-2
12 200. 0. 2600. $ D-3
6 8 6 8 3 8 $ F-1
1 3 2 1 $ G-1-1 COMPATABILITY 1-2
1 3 3 1 $ G-1-2 COMPATABILITY 1-3
1 0 $ I-1
10.0E6 .3 0. .098 $ I-2 MATERIAL PROPERTIES
1 1 1 $ K-1
1 .25 $ K-2
2 0 $ M-1-1
0. 6. 0. 9. $ M-2A-1
1 0 0. -0.125 $ M-5-1
410 $ N-1-1
2 2 6 4 $ P-1-1 BOUNDS 1
0 $ Q-1-1
0 $ R-1-1
2 0 $ M-1-2
6. 12. 0. 9. $ M-2A-2
1 0 0. -0.125 $ M-5-2
410 $ N-1-2
6 2 2 4 $ P-1-2 BOUNDS 2
0 $ Q-1-2
0 $ R-1-2
2 2 $ M-1-3
0. 1.25 0. 9. $ M-2A-3
3 1 6. 0. 1.25 $ M-3-3
1 0 90. 0. $ M-5-3
410 $ N-1-3
6 2 3 4 $ P-1-3 BOUNDS 3
0 $ Q-1-3
0 $ R-1-3
```

```
STAGS1 DATA FOR LONGITUDINAL RECTANGULAR STIFFENER (PLASTIC)
6 1 1 1 0 0 1 0.1 $ B-1
3 0 0 2 $ B-2
1 0 1 $ B-3
0. $ C-1
0 1000 1 1 $ D-1
0 2.E-3 20 E-6 $ E-1
0 4 $ E-2
6 8 6 8 3 8 $ F-1
1 3 2 1 $ G-1-1 COMPATABILITY 1-2
1 3 3 1 $ G-1-2 COMPATABILITY 1-3
1 3 1 $ I-1
10.0E6 .3 0. .098 $ I-2 MATERIAL PROPERTIES
.0041 41.E3 .06 45.E3 1. 47.E3 $ I-3 PLASTICITY
1 1 1 5 $ K-1
1 .25 0. 2 $ K-2
2 0 $ M-1-1
0. 6. 0. 9. $ M-2A-1
1 0 0. 0. 0 1 $ M-5-1
410 $ N-1-1
2 2 6 4 $ P-1-1 BOUNDS 1
0 $ Q-1-1
0 $ R-1-1
2 0 $ M-1-2
6 12. 0. 9. $ M-2A-2
1 0 0. 0. 0 1 $ M-5-2
410 $ N-1-2
2 2 2 4 $ P-1-2 BOUNDS 2
0 $ Q-1-2
0 $ R-1-2
2 2 $ M-1-3
0. 1.375 0 9 $ M-2A-3
3 1 6. 0. 1.375 $ M-3-3
1 3 90 0. 0 1 $ M-5-3
1 0. 0 9 001
0 0 0 4 5 .0005
0 0 0. 2.25 .00025
410 $ N-1-3
2 2 3 4 $ P-1-3 BOUNDS 3
0 $ Q-1-3
0 $ R-1-3
```

```
FLUID MASS DATA FOR LONGITUDINAL RECTANGULAR STIFFNER
0 104 70 0 0
1.152E-3 59 0E3
T T F T
T F T F
F F T F
F F T F
F T F F
F T
REC.FLU REC.GEO REC.COR
10
1. 1.
0. 0. -1. 0.
MESH
1 4 0 0 0
1 9 10 2
2 4 0 0 0
2 10 11 3
3 4 0 0 0
3 11 12 4
4 4 0 0 0
4 12 13 5
5 4 0 0 0
5 13 14 6
6 4 0 0 0
6 14 15 7
7 4 0 0 0
7 15 16 8
8 4 0 0 0
9 17 18 10
9 4 0 0 0
10 18 19 11
10 4 0 0 0
11 19 20 12
11 4 0 0 0
12 20 21 13
12 4 0 0 0
13 21 22 14
13 4 0 0 0
14 22 23 15
14 4 0 0 0
15 23 24 16
15 4 0 0 0
17 25 26 18
16 4 0 0 0
18 26 27 19
17 4 0 0 0
19 27 28 20
18 4 0 0 0
20 28 29 21
19 4 0 0 0
21 29 30 22
20 4 0 0 0
22 30 31 23
21 4 0 0 0
23 31 32 24
22 4 0 0 0
25 33 34 26
23 4 0 0 0
26 34 35 27
```

```
24 4 0 0 0
27 35 36 28
25 4 0 0 0
28 36 37 29
26 4 0 0 0
29 37 38 30
27 4 0 0 0
30 38 39 31
28 4 0 0 0
31 39 40 32
29 4 0 0 0
33 41 42 34
30 4 0 0 0
34 42 43 35
31 4 0 0 0
35 43 44 36
32 4 0 0 0
36 44 45 37
33 4 0 0 0
37 45 46 38
34 4 0 0 0
38 46 47 39
35 4 0 0 0
39 47 48 40
36 4 0 0 0
41 49 50 42
37 4 0 0 0
42 50 51 43
38 4 0 0 0
43 51 52 44
39 4 0 0 0
44 52 53 45
40 4 0 0 0
45 53 54 46
41 4 0 0 0
46 54 55 47
42 4 0 0 0
47 55 56 48
43 4 0 0 0
49 57 58 50
44 4 0 0 0
50 58 59 51
45 4 0 0 0
51 59 60 52
46 4 0 0 0
52 60 61 53
47 4 0 0 0
53 61 62 54
48 4 0 0 0
54 62 63 55
49 4 0 0 0
55 63 64 56
50 4 0 0 0
57 65 66 58
51 4 0 0 0
58 66 67 59
52 4 0 0 0
59 67 68 60
53 4 0 0 0
60 68 69 61
54 4 0 0 0
```

```
61 69 70 62
55 4 0 0 0
62 70 71 63
56 4 0 0 0
63 71 72 64
57 4 0 0 0
65 73 74 66
58 4 0 0 0
66 74 75 67
59 4 0 0 0
67 75 76 68
60 4 0 0 0
68 76 77 69
61 4 0 0 0
69 77 78 70
62 4 0 0 0
70 78 79 71
63 4 0 0 0
71 79 80 72
64 4 0 0 0
73 81 82 74
65 4 0 0 0
74 82 83 75
66 4 0 0 0
75 83 84 76
67 4 0 0 0
76 84 85 77
68 4 0 0 0
77 85 86 78
69 4 0 0 0
78 86 87 79
70 4 0 0 0
79 87 88 80
MASS
EIGEN
EXIT
```

```
AUGMENTED MATRIX DATA FOR LONGITUDINAL RECTANGULAR STIFFNER
REC MAS REC.FLU REC.GEO REC.PRE
F T F F
F F F F
T T F F
0
104 624 6 3
1
0 1 63 1
```

```
TIME INTEGRATOR DATA FOR LONGITUDINAL RECTANGULAR STIFFENER
REC PRE REC POS
REC RST
6.  0.  109 25
6  0.  1.25
T F F F
F
101
1
.2E-4
1389.22  0737E-3
1
0.  20.E-6
2.E-3
1 20
0.0 0 0
F F
F
```

```
USA POST-PROCESSOR DATA FOR LONGITUDINAL RECTANGULAR STIFFENER
1
101
REC PRE
REC POS
F T F F F
F F F F
F F T
0 0 1
3 42 48 1
0 0 1
3 42 48 1
0 1
29 35 1
F
1 0
F F F F
```

```
TEST POST, RECSTIFF
100
1 2 3 4 5 6 7 8 9 10 11 12 13 14 15 16 17 18 19 20,
21 22 23 24 25 26 27 28 29 30 31 32 33 34 35 36 37 38 39 40,
41 42 43 44 45 46 47 48 49 50 51 52 53 54 55 56 57 58 59 60,
61 62 63 64 65 66 67 68 69 70 71 72 73 74 75 76 77 78 79 80,
81 82 83 84 85 86 87 88 89 90 91 92 93 94 95 96 97 98 99 100
0 0 0 0 0 0 0 0
0 0  0 0 0 0 0 0
0 0  0 0 0 0 0 2
1 1
5 1
0 0 0 0 0 0
0 0 0 0 0 0
```

LIST OF REFERENCES

1. Till, Geoffrey, Maritime Strategy and the Nuclear Age, p. 175, St. Martin's Press, 1982.

2. NRL Memorandum Report 1396, Interim Design Values for Shock Design of Shipboard Equipment, by G. J. O'Hara and R. O. Belsheim, February 1963.

3. Rentz, T. R., An Experimental Investigation into the Dynamic Response of a Stiffened Flat Plate Loaded Impulsively by an Underwater Shockwave, Master's Thesis, Naval Postgraduate School, Monterey, California, June 1984.

4. Rentz, T. R. and Shin, Y. S., "On the Field Experience of UNDEX Testing On the Field Experience of UNDEX Testing for a Stiffened Flat Plate," paper presented at the Shock and Vibration Conference, Dayton, Ohio, 24-29 October 1984.

5. Cole, Robert H., Underwater Explosions, Princeton University Press, 1948.

6. Sartori, Leo, "Effects of Nuclear Weapons," Physics Today, v. 36, no. 3, pp. 32-8, March 1983.

7. Naval Surface Weapons Center Report TR 80-299, Similitude Equations for Explosives Fired Underwater, by R. S. Price, Confidential, November 16, 1979.

8. Daddazio, R. P., Weidlinger Associates, Inc., in private communication with Dr. Y. S. Shin, November 1983.

9. David W. Taylor Naval Ship Research Center Report 79/064, Design Equations for Tripping of Stiffeners Under Inplane and Lateral Loads, by John C. Adamchak, October 1979.

10. Lockheed Palo Alto Research Laboratory, User's Manual for STAGS, v. 1, March 1978.

11. Bathe, Klaus-Jurgen, Finite Element Procedures in Engineering Analysis, pp. 96-102, Prentice-Hall, Inc., 1982.

12. DeRuntz, J. A. and Brogan, F. A., Underwater Shock Analysis of Nonlinear Structures, A Reference Manual for the USA-STAGS Code (Version 3), Lockheed Missiles and Space Co., Inc., 9 December 1980.

13. Amroth, B. O., Brogan, F. A., and Stanley, G. M., Structural Analysis of General Shells, v. 2, Lockheed Missiles and Space Co., Inc., December 1982.

14. Wright-Patterson AFB Report MIL-HDBK-5B, Military Standardization Handbook, Metallic Materials and Elements for Aerospace Vehicle Structures, September 1971.

15. Hewlett-Packard, Modal Analysis Options 402, 403, 404 Fourier Analyzer System, March 1981.

16. Naval Surface Weapons Center Report S2-294, Accuracy and Response of Tourmaline Gages for Measurement of Underwater Explosion Phenomena, by Ronald B. Tussing, 1 July 1982.

17. Geers, T. L., Lockheed Research, Palo Alto, in private communication, October 1984.

BIBLIOGRAPHY

Butt, L. T., Naval Ship Shock Design Analysis, lecture notes presented at N.P.S. for Naval Ship Shock Course, January 1984.

DeRuntz, J. A., AUGMAN.UAL, Lockheed Missiles and Space Co., Inc., December 1982.

DeRuntz, J. A., FLUMAN.UAL, Lockheed Missiles and Space Co., Inc., December 1982.

DeRuntz, J. A., INTMAN.UAL, Lockheed Missiles and Space Co., Inc., December 1982.

DeRuntz, J. A., POSMAN.UAL, Lockheed Missiles and Space Co., Inc., December 1982.

INITIAL DISTRIBUTION LIST

		No. Copies
1.	Defense Technical Information Center Cameron Station Alexandria, Virginia 22314	2
2.	Library, Code 0142 Naval Postgraduate School Monterey, California 93943	2
3.	Professor Y. S. Shin, Code 69Sb Department of Mechanical Engineering Naval Postgraduate School Monterey, California 93943	3
4.	Department Chairman, Code 69 Department of Mechanical Engineering Naval Postgraduate School Monterey, California 93943	1
5.	R. Daddazio Weidlinger Associates 333 Seventh Avenue New York, New York 10001	1
6.	T. L. Geers Lockheed Missile and Space Company 3251 Hanover Street Palo Alto, California 94304	1
7.	LCDR James White, SSPS Defense Nuclear Agency Washington, D.C. 20305	1

199.69

Thesis
K4491
c.1

King
Underwater shock-induced responses of stiffened flat plates: an investigation into the predictive capabilities of the USA-STAGS code.

thesK4491
Underwater shock-induced responses of st
3 2768 000 60966 3
DUDLEY KNOX LIBRARY